1-1-1978

Preparation, characterization, and theoretical comparisons of polystyrene latexes prepared with the inogenic monomer 2-acrylamido-2-methylprcpane sulfonic acid.

Richard Lewis Schild

PREPARATION, CHARACTERIZATION, AND THEORETICAL COMPARISONS OF POLYSTYRENE LATEXES PREPARED WITH THE IONOGENIC MONOMER 2-ACRYLAMIDO-2-METHYLPROPANE SULFONIC ACID

by

Richard Lewis Schild

A Thesis

Presented to the Graduate Committee

of Lehigh University

in Candidacy for the Degree of

Master of Science

in

Chemical Engineering

Lehigh University

1978

CERTIFICATE OF APPROVAL

This thesis is accepted and approved in partial fulfillment of the requirements for the degree of Master of Science in Chemical Engineering.

9/15/78
Date

Professor in Charge

Chairman of Department

ACKNOWLEDGEMENTS

I would like to express my sincere appreciation and gratitude to Dr. Mohamed El-Aasser with whose guidance, suggestions, discussions, assistance and patience this work was completed. I would also like to thank Dr. Gary Poehlein who first introduced me to latex technology and conceived of this work and to Dr. John Vanderhoff for his help, advice and readiness for discussion.

I would like to thank my fellow graduate students for their positive encouragement and help in the laboratory. Special thanks go to Syed Ahmed and Tina Vital who critically proofread this manuscript.

I would like to thank Ellen Raber who helped draw many of the figures and drawings in this work.

I am gratuitous for financial support from Lehigh University for a University Fellowship, the Proctor and Gamble Company for fellowship support, and to the Emulsion Polymers Institute. Part of this work was funded by the Nation Science Foundation, Grant No. SMI 76-03330, during an NSF undergraduate summer research program.

This work was first presented at an AIChE student paper contest and later at the 51st National Colloid Symposium in Buffalo, New York. Part of this work will be published in late 1978 in the book "Emulsions, Latices, and Dispersions" edited by P. Beecher and M. Yudenfreund.

TABLE OF CONTENTS

		Page
Abstract		1
Chapter I	INTRODUCTION	3
Chapter II	THEORETICAL AND EXPERIMENTAL DETAILS	7
	Materials	7
	Latex Preparation	11
	Particle Size	13
	Surface Characterization by Conductometric Titration	14
	Ultracentrifuge	15
	Coagulation Rate Studies	16
	Molecular Weight Determination	25
Chapter III	RESULTS AND DISCUSSION	28
	Coagulum	28
	Particle Size	30
	Surface Characterization	32
	Ultracentrifugation	40
	Latex Stability	40
	Molecular Weight Analysis	59
Chapter IV	SUMMARY AND CONCLUSIONS	70
References		73
	APPENDICES	75
Appendix I	Results of Conductometric Titrations	76
Appendix II	Results of Stability Analysis	86
Appendix III	Results of Molecular Weight Analysis	107
Vita		119

LIST OF TABLES

Table		Page
I	Latex Recipes	8
II	Particle Size and Dispersity	33
III	Titration Results for AMPS(H^+) Series	35
IV	Titration Results for AMPS(Na^+) Series	36
V	Expected and Experimental Amounts of Strong Acid Surface Charge	41
VI	Results of Stability Analysis	48
VII	Hamaker Constant and Stern Potential	54
VIII	Degree of Dissociation	55
IX	Scattering Cross-Sections	57
X	Fast Coagulation Rate Constant	58
XI	Molecular Weight Analysis	66
XII	Incorporation of AMPS	68

LIST OF FIGURES

Figure		Page
1.	Schematic diagram of potential of interaction of two spheres.	18
2.	Schematic diagram of Cary 14 Spectrophometer.	21
3.	Percent coagulum versus AMPS concentraction.	29
4.	Variation of particle diameter with AMPS concentration.	31
5.	Electron micrograph of Latex SA-28.	34
6.	Conductometric titration for SA-27.	37
7.	Conductometric titration for SA-10.	39
8.	Electron micrograph of polyelectrolyte film.	42
9.	Electron micrograph of polyelectrolyte film.	43
10.	Electron micrograph of polyelectrolyte film.	44
11.	Optical density-time curve for SA-2.	45
12.	Stability curve for SA-2.	47
13.	Stability curves for AMPS(H^+) series.	50
14.	Stability curves for AMPS(Na^+) series.	51
15.	Schematic representation of surface functional groups on a latex particle.	52
16.	GPC calibration curve for polystyrene in THF at 2 ml/min.	60
17.	Normalized chromatogram of SA-27 before and after ion exchange.	61
18.	Differential molecular weight distribution of SA-27 before and after ion exchange.	62
19.	Normalized chromatogram of SA-10 before and after ion exchange.	64

APPENDIX I

Figure		Page
I-A.1	Conductometric Titration of SA-2.	77
I-A.2	Conductometric Titration of SA-1.	78
I-A.3	Conductometric Titration of SA-13.	79
I-A.4	Conductometric Titration of SA-14.	80
I-A.5	Conductometric Titration of SA-28.	81
I-A.6	Conductometric Titration of SA-29.	82
I-A.7	Conductometric Titration of SA-30.	83
I-A.8	Conductometric Titration of SA-31.	84
I-A.9	Conductometric Titration of SA-32.	85

APPENDIX II

II-A.1	Optical density-time curve for SA-10.	87
II-A.2	Optical density-time curve for SA-1.	88
II-A.3	Optical density-time curve for SA-13.	89
II-A.4	Optical density-time curve for SA-14.	90
II-A.5	Optical density-time curve for SA-27.	91
II-A.6	Optical density-time curve for SA-28.	92
II-A.7	Optical density-time curve for SA-29.	93
II-A.8	Optical density-time curve for SA-30.	94
II-A.9	Optical density-time curve for SA-31.	95
II-A.10	Optical density-time curve for SA-32.	96

Figure		Page
II-A.11	Stability curve for SA-10.	97
II-A.12	Stability curve for SA-1.	98
II-A.13	Stability curve for SA-13.	99
II-A.14	Stability curve for SA-14.	100
II-A.15	Stability curve for SA-27.	101
II-A.16	Stability curve for SA-28.	102
II-A.17	Stability curve for SA-29.	103
II-A.18	Stability curve for SA-30.	104
II-A.19	Stability curve for SA-31.	105
II-A.20	Stability curve for SA-32.	106

APPENDIX III

III-A.1	Normalized chromatogram of SA-28 before and after ion exchange.	108
III-A.2	Normalized chromatogram of SA-29 before and after ion exchange.	109
III-A.3	Normalized chromatogram of SA-30 before and after ion exchange.	110
III-A.4	Normalized chromatogram of SA-31 before and after ion exchange.	111
III-A.5	Normalized chromatogram of SA-32 before and after ion exchange.	112
III-A.6	Cumulative molecular weight distribution of SA-10 before and after ion exchange.	113
III-A.7	Cumulative molecular weight distribution of SA-28 before and after ion exchange.	114

Figure		Page
III-A.8	Cumulative molecular weight distribution of SA-29 before and after ion exchange.	115
III-A.9	Cumulative molecular weight distribution of SA-30 before and after ion exchange.	116
III-A.10	Cumulative molecular weight distribution of SA-31 before and after ion exchange.	117
III-A.11	Cumulative molecular weight distribution of SA-32 before and after ion exchange.	118

ABSTRACT

Two series of polystyrene latexes were prepared with the ionogenic monomer 2-acrylamido-2-methylpropane sulfonic acid (AMPS). In the AMPS(Na^+) series, the pH was controlled at 7.5, while in the AMPS(H^+) series, the pH varied from 2.1 to 7.5. The effects of increasing the concentration of ionogenic monomer on the coagulum, particle size and distribution, surface charge density, electrolyte stability and molecular weight distribution were investigated.

Particle size was found to decrease and then increase slightly with increasing concentration of AMPS. The latexes prepared were monodisperse with a uniformity ratio range of 1.001 to 1.048. The level of coagulum followed a trend similar to particle size.

Characterization of cleaned latex by conductometric titration found strong and weak acid groups on all latexes prepared with AMPS(H^+). The AMPS(Na^+) had strong acid groups only. The surface charge density was found to increase with charged AMPS concentration. The number of strong acid groups per polymer molecule increased from 3.3 to 25.2 as AMPS concentration increased. The degree of dissociation calculated from the critical coagulation concentration ranged from 0.8 to 7.1%.

Latex stability as determined by coagulation kinetics, showed a general increase with increasing AMPS concentration. Deviations in these trends were attributed to the particle surface being a poor model for the DLVO theory and to superposition of electro-

static and steric stabilizing effects. The rate constant for fast coagulation was determined to be $(2.923 \pm 1.086)\times10^{-12}$ cm^3/particle-second and in agreement with theory.

The molecular weight distribution was found to be considerably broader than predicted by Smith-Ewart Case II kinetics. The weight average molecular weight was found to increase with AMPS concentration. Ion exchange was found to be adequate in removing low molecular weight polyelectrolyte adsorbed on the particle surface.

CHAPTER I

INTRODUCTION

Ionogenic monomers (also referred to as functional monomers, ionic comonomers, comonomeric emulsifiers, or polymerizable surfactants) can be used in small quantities to modify or incorporate certain properties into the polymer latex. The ionogenic monomer consists of a 4-8 carbon chain backbone with a double bond at one end and a functional group at the other end. Ionogenic monomers with sulfonate functional groups are often used in emulsion polymerization to improve the stability of a latex during or after polymerization. Latexes copolymerized with sulfonated vinyl monomers are stable to coagulation over a wide range of acidic and basic pH's.[1]

The use of ionogenic monomers in emulsion polymerization in place of traditional surfactants offers several advantages. Upon polymerization, the ionogenic monomer provides a source of constant, chemically bound charge at the polymer particle surface. The hydrophilic nature of the functional group tends to keep it oriented at the water/polymer interface. Consequently, the physical properties of the latex cannot be altered by an adsorption/desorption cycle which would occur if traditional surfactants were used in the polymer latex system. Since the source of the constant charge is chemically bound to the particle surface, a smaller amount of func-

tional monomer is required to provide the same stability as an adsorbed surfactant molecule. The amount of functional monomer used to modify the polymer is usually less than 1% of the base monomer, which is favorable from an economic viewpoint.

Ionogenic monomers, in addition to their stabilizing function, can be used to modify or control certain latex properties. Films produced from latexes using functional monomers can be made to be redispersable or water-resistant depending on the amount of functional monomer used. Latexes produced with functional monomers have found applications in paints, paper coatings, leather treatment, foams and adhesives.[1]

The properties of the latex for applications in different technologies are controlled by the surface properties and the interactions that occurs at the water/polymer interface during their application. The polystyrene latex is also well suited as a model colloid because of its nondeformable nature, the ability to control its particle size and size distribution and because it has a hydrophobic surface.

Probably, the most important colloidal property of a latex is its stability or resistance to coagulation. All latexes are required to remain stable during polymerization. After polymerization, many latexes are stored for days or years, while some are flocculated for recovery of the polymer. The stability of the latex system is controlled by the concentration of electrolyte,

the amount of charge present on the particle surface, and the temperature. The resistance to shear is also important in determining the mechanical stability of a latex. The two mechanisms controlling the latex stability are electrostatic and steric stabilization.

A major concern in the use of a functional monomer is to determine the location of the functional groups after polymerization. It is important to maximize the incorporation of the ionogenic monomer such that a majority of the functional groups are located at the water/polymer interface. The functional monomer can enter into the emulsion polymerization reaction in several ways:

1. Itmay copolymerize at the particle surface so that it is incorporated or chemical bound into the polymer matrix.
2. It may copolymerize or homopolymerize inside the particle.
3. It may homopolymerize or copolymerize in the aqueous phase as polyelectrolyte or surface active oligomer. The presence of polyelectrolyte can cause particle flocculation because of its large number of adsorption sites. This also makes it difficult to remove.
4. It may not polymerize at all, remaining in the aqueous phase.

The purpose of this investigation is to correlate, in terms of colloid theory and polymerization kinetics, the surface and physical properties of polystyrene latexes prepared with an iono-

genic monomer. Clean, monodisperse polystyrene latexes with varying amounts of the ionogenic monomer 2-acrylamido-2-methyl-propane sulfonic acid (AMPS) were prepared. The system was free of any added emulsifier, and all other remnants of the polymerization were removed by ion exchange. A highly accurate conductometric titration method was used to quantitatively characterize the different functional groups found on the polymer particle surface.

The electrostatic stability was investigated with an infrared light scattering technique used to determine coagulation kinetics. Parameters describing the resistance to coagulation were determined from existing theories of light scattering, coagulation kinetics, and electrostatic stability.

The molecular weight averages and molecular weight distribution were determined by gel permeation chromatography. Of particular interest was the presence of low molecular weight material, presumed to be polyelectrolyte, and if it was removed by ion exchange.

C H A P T E R II

THEORETICAL AND EXPERIMENTAL DETAILS

Materials

Styrene monomer (Fischer Scientific Company) was washed with 10% aqueous sodium hydroxide, dried over anhydrous sodium sulfate (100 g/l), and then distilled under a highly purified nitrogen atmosphere at 50 mm Hg to remove inhibitors and impurities. All water used in this work was deionized after being doubly-distilled. For polymerizations, the water was boiled and then cooled in an ice bath while being purged with nitrogen to remove oxygen from the water. Grade 5 ultrapure nitrogen (AIRCO) was used in all cases.

The ionogenic monomer 2-acrylamido-2-methylpropane sulfonic acid (AMPS) was of special process grade, and used as received from the Lubrizol Corporation. The structure of AMPS is

$$CH_2 = CH - \overset{O}{\overset{\|}{C}} - \overset{H}{\overset{|}{N}} - \overset{CH_3}{\overset{|}{\underset{CH_3}{\overset{|}{C}}}} - CH_2 - SO_3^-H^+$$

The recipes used for preparing polystyrene latexes with functional monomer by emulsifier-free polymerization is given in Table I. One set of polymerizations used the AMPS in the hydrogen

TABLE I

Latex Recipes

All recipes contain:	styrene	40 g
	water	140 g
	methanol	20 g
	sodium bicarbonate	0.4 g
	potassium persulfate	0.4 g

Latex Code	[AMPS,Na^+] mol/l_{aq}	Latex Code	[AMPS,H^+] mol/l_{aq}
SA-27	0.001	SA-10	0.0
SA-28	0.010	SA-2	0.0121
SA-29	0.025	SA-1	0.0422
SA-30	0.050	SA-13	0.0724
SA-31	0.075	SA-14	0.151
SA-32	0.100		

form (AMPS (H^+)) while the other used the sodium form (AMPS(Na^+)). A 0.32 M solution of AMPS (Na^+) was prepared by titrating an AMPS (H^+) solution with sodium hydroxide until a pH of 7 was reached. Methanol was used to increase the solubility of styrene in the aqueous phase in order to increase the probability of copolymerization with ionogenic monomer thus improving its incorporation.

The ion exchange resins, Dowex 50W-X4 (H^+) and Dowex 1-X4(OH^-) were supplied by the Dow Chemical Company. A rigorous purification procedure to clean the resins of impurities and polyelectrolyte was carried out. The procedure, developed by Vanderhoff[2], includes multiple washings of each resin separately with 3N NaOH, hot water, methanol, cold water, 3N HCl, hot water, methanol and cold water. This cycle is carried out repeatedly until the wash water has a conductivity as low as that of deionized, distilled water. The cationic and anionic resins are mixed in equal weights, washed with water and are then ready for use.

Tetrahydrofuran (THF) (reagent grade-Fischer Scientific) was used as the mobile phase for molecular weight determination by gel permeation chromatography (GPC). The solvent was filtered through a 0.2 μ fluropore filter (Millipore Corporation) to remove any particulate matter. Polystyrene standards (Water's Associates) of molecular weights 2350, 3600, 17500, 35000, 110000, 200000, 470000, 650000, 1440000, 2700000 and 3800000 were prepared as 0.1 wt% solu-

tions in THF to determine the calibration curve for GPC.

Latex Preparation

Two series of emulsifier-free latexes were prepared by emulsion polymerization in bottles. Twelve-ounce narrow mouth bottles with metallic caps were used. Two holes (0.2 cm in diameter) were drilled through the caps for purging of oxygen from the bottles and to inject the initiator solution. A rubber gasket was used inside the cap to seal the bottles. The gasket consisted of a hard PVC-SBR rubber disc and a smaller swellable butyl rubber (B. F. Goodrich) disc glued together with the soft rubber under the cap covering the two holes.

The ingredients of the polymerization recipe were charged in the following sequence.

1. The buffer, weighed separately, was added to the dry, preweighed bottle with cap.
2. The water (all but 10 ml) and methanol were added to the bottle next.
3. The proper amount of AMPS was added in solution or as a powder as required by the recipe.
4. The styrene monomer was added and the bottle was capped.
5. The sample was sparged with ultrapure nitrogen. Two needles were inserted through the cap; a nitrogen inlet needle and outlet vent needle.
6. The initiator solution was made up with the remaining water.

7. After the nitrogen purge is completed, the needles are removed and a drop of toluene is placed in the cap holes to swell the butyl rubber. The bottle is placed inside a canvas bag and then placed into a steel cage in the bottle polymerizer. The bottle is preheated to reaction temperature for 30 minutes.
8. The bottles are removed after preheating and the initiator solution is injected.
9. The bottles are replaced into the polymerizer for the required reaction time.
10. After the reaction is completed, the bottles are removed from the polymerization bath and placed in an oven for two hours at 90°C.

The bottle polymerizer operates at 70°C and can hold six bottles simultaneously. It tumbles the bottles end over end at approximately 35 RPM.

The bottles are preheated so that the reactants are all at the same temperature. After the polymerization is completed, the bottles were heated to 90°C to decompose any remaining initiator. Finally, the contents are filtered through glass wool to remove any coagulum. The coagulum is dried at 40°C and then weighed to determine the amount based on initial monomer content. The conversion is determined gravimetrically.

Particle Size

Particle size was determined by electron microscopy using a Philips 300 transmission electron microscope (TEM). One drop of highly diluted latex was placed on a copper grid and dried at room temperature. The grid was then shadowed with platinum at an angle of 45^{o}. Particle size was measured directly from the electron micrograph negatives using a calibrated magnifying eyepiece. Approximately 200 particles were counted for each latex.

The number average diameter was calculated from

$$\bar{D}_n = \frac{\Sigma\, n_i\, D_i}{n_i} \qquad (1)$$

The weight average diameter was calculated from

$$\bar{D}_w = \left[\frac{\Sigma\, n_i\, D_i^6}{\Sigma\, n_i\, D_i^3}\right]^{1/3} \qquad (2)$$

The latex dispersity is given by the uniformity ratio

$$U = \frac{\bar{D}_w}{\bar{D}_n} \qquad (3)$$

If the uniformity ratio is less than 1.05, the latex is considered to monodisperse.

Surface Characterization by Conductometric Titration

A quantitative and qualitative analysis of the latex particle surface was performed by conductometric titration. The type and amount of each surface group is determined by titration with base of a latex which has been cleaned by ion exchange so that all functional groups have hydrogen counterions. The titration method is sensitive to strong acid groups (sulfate and sulfonate) and weak acid groups (carboxyl). The equivalence points are determined by following the conductivity of the latex as it is titrated.

The latexes are cleaned by repetitive batch ion exchanges with purified, mixed bed (Dowex 1 and Dowex roW) ion exchange resins. The ion exchange cycles are repeated with fresh resin until consistent titration curves are obtained.

The conductivity of each latex (diluted to 2 wt.% solids) was monitored continuously while a 0.019N NaOH solution was added at a constant flow rate of 0.8 ml/min. The amount and type of each surface functional group was determined from the equivalent points on the titration curve. The number concentration of acid groups, n_i (gm-equiv/gm polymer) is given by

$$n_i = \frac{(V_i - V_{i-1})\,N}{S(1000)}$$

where $V_i - V_{i-1}$ = volume of NaOH added from last equivalence point

N = normality of titrant

S = weight of polymer solids titrated, gms.

The surface charge density σ_s (μcoul/cm^2) is given by

$$\sigma_s = \frac{n_i N_A \rho_p D}{\sigma} \tag{5}$$

where n_i = # of acid groups

N_A = Avogadro's number

ρ_p = polymer density

D = particle diameter, cm.

Finally, the area per charge A_c is determined from

$$A_c = \frac{\sigma}{n_i N_A D \rho_p} \tag{6}$$

Ultracentrifugation

An IEC preparative ultracentrifuge was used to separate the latex serum for microscopy studies to determine if polyelectrolyte formed during polymerization. Approximately 10 ml of latex was placed in a polycarbonate tube and then inserted into a swinging bucket rotor. The sample was spun at 35,000 RPM for thirty minutes. The serum was drawn off by syringe and saved for further

centrifugations. The polymer particles were redispersed in water and centrifuged again to encourage desorption of any polyelectrolyte still adsorbed on the particle surface. The serum collected from each run was combined and centrifuged to remove any remaining latex particles. One drop of the serum was then diluted and placed on a carbon grid and dried for observation by the TEM.

Coagulation Rate Studies

The stability of a latex can be measured by its resistance to coagulation by an electrolyte. The rate at which a latex coagulates can be related to parameters which describe the electrostatic stability in terms of repulsive and attractive forces. These stability parameters were obtained through an initial rate of coagulation technique. The coagulation kinetics were measured by following the change in optical density as a function of time. As the concentration of the electrolyte that is added to the latex is increased, the initial slope of the optical density-time curve increases until an electrolyte concentration is reached, beyond which the initial slope remains constant. The concentration at which the slope becomes constant is the critical coagulation concentration (c.c.c.). Electrolyte concentrations less than the c.c.c. correspond to slow coagulation, while greater concentrations belong to the rapid coagulation regime, where every collision leads to irreversible contact.

The stability of a latex is determined by the potential of

interaction between two particles. The potential of interaction V is given by the summation of attractive Van der Waals potential and the electrostatic repulsive double layer potential. This is represented schematically in Figure 1 by showing the potential of interaction as a function of particle separation distance s. The height of the primary maximum determines the stability of the latex. For irreversible coagulation to occur, a particle must have sufficient energy to overcome this repulsive barrier and fall into the primary minimum. If the secondary minimum is large enough, it is possible for agglomerates to form in this trough. This type of coagulation is reversible if the depth of the secondary minimum is less than about 5kT.

The stability factor W is the fraction of irreversible collisions that occur during slow coagulation. Expressed in terms of rate constants

$$W = \frac{k_r}{k_s} \qquad (7)$$

where k_r and k_s are the rate constants for rapid and slow coagulation respectively. W also represents the area under the primary maximum.[3] The greater the potential barrier and area under this curve, the greater W will be, indicating greater stability.

Silebi[4] derived a relationship between the rate of change of turbidity as a function of the coagulation rate constant, particle

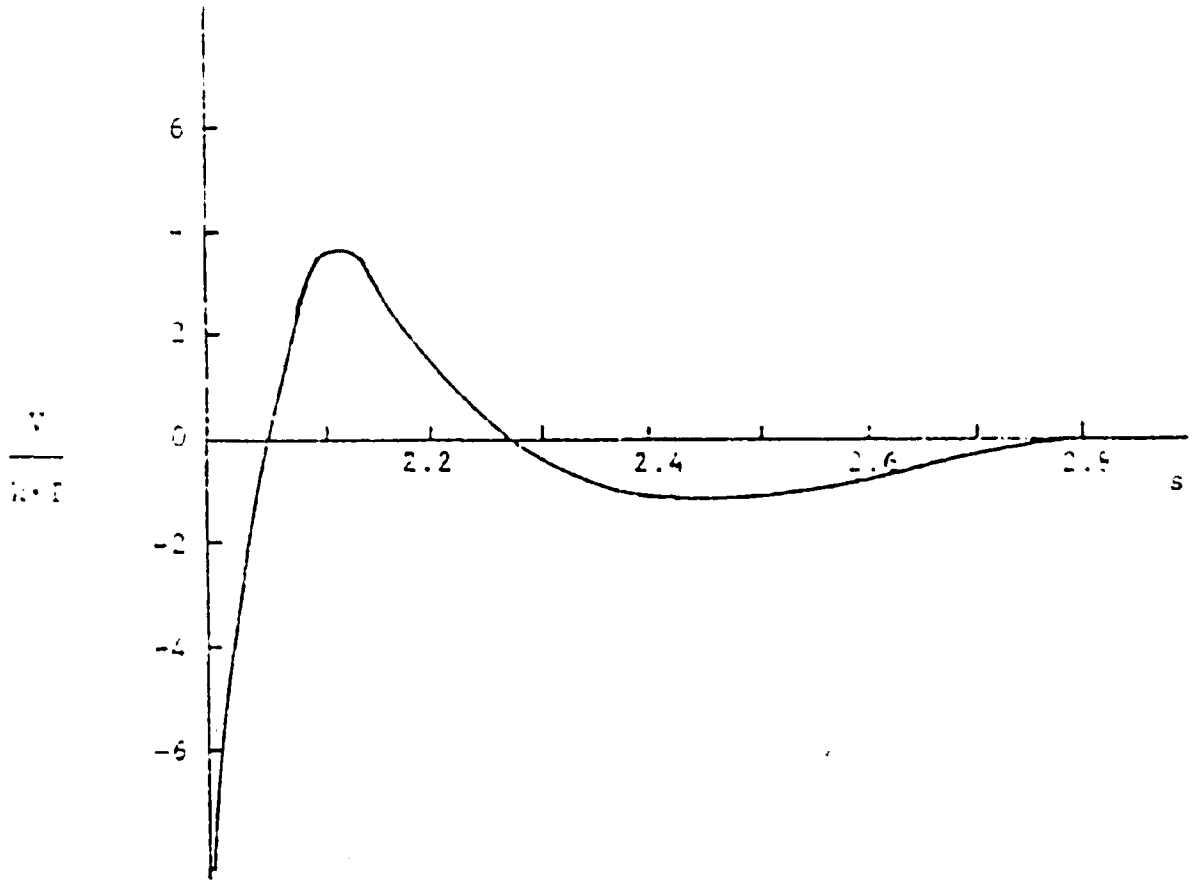

Figure 1. Schematic diagram of potential of interaction curve for two particles as a function of their separation distance s.

concentration and the scattering cross-section of the particles determined from the Mie theory of light scattering. Equation 8 accounts for the hydrodynamic interaction and potential of interaction and differs from a similar equation derived by Wu[5] by a factor of two:

$$\left.\frac{d\tau}{dt}\right|_{t=o} = Np\ kr\ L\ R_1 \left[\frac{R_2}{R_1} - 2\right] \qquad (8)$$

Where Np = particle concentration

L - cell path length

R_1, R_2 = scattering cross section of singlet and coublet particle agglomerates

$O.D. = \log \frac{I_o}{I}$ = optical density

$\tau = \ln \frac{I_o}{I} = 2.303 \log \frac{I_o}{I}$ = turbidity

I_o, I = light intensity in reference and sample cells, respectively.

The fast coagulation rate constant can be determined experimentally from Eqn. 8 by measuring the initial slope of the optical density-time curve.

As discussed earlier, the initial slope is a function of the electrolyte concentration. The initial slope increases from slow to rapid coagulation as the rate of coagulation increases with greater electrolyte concentration. For rapid coagulation, the rate of coagulation and initial slope are constant. The stability

factor W can then be determined from the slopes obtained experimentally by

$$W = \frac{k_r}{k_s} = \frac{\left.\frac{d\tau}{dt}\right|_{t=o,\ C_E\ =\ c.c.c.}}{\left.\frac{d\tau}{dt}\right|_{t=o,\ C_E}} = \frac{\left.\frac{d(O.D.)}{dt}\right|_{t=o,\ C_E=c.c.c.}}{\left.\frac{d(O.D.)}{dt}\right|_{t=o}} \qquad (9)$$

The limiting slope, $\left.\frac{d(O.D.)}{dt}\right|_{t=o,\ C_E=\ c.c.c.}$ where C_E = electrolyte Concentration, is determined from the average of several fast coagulation runs. For rapid coagulation W is defined as 1.[6]

The optical density-time curve is determined by measuring the light intensity ratio of an infrared source as it passes through the latex in the reference and sample cells. A Cary 14 spectrophotometer was used to measure the change in optical density. A schematic of the Cary 14 is shown in figure 2. All runs were carried out at a wavelength of 1370 nm. The quartz sample cells had a 1 cm path length and a 5 ml capacity. Three milliliters of dilute latex was added to each cell. The concentrations of the latex in the cell ranged from 0.015 to 0.025 wt% after addition of electrolyte. Since the stability curves are independent of solids content, an optimum concentration was chosen to get the best signal.[7] One milliliter of water was added to the reference cell so that the concentration of latex would be the same in both cells after the electrolyte was added. The sample cells were then

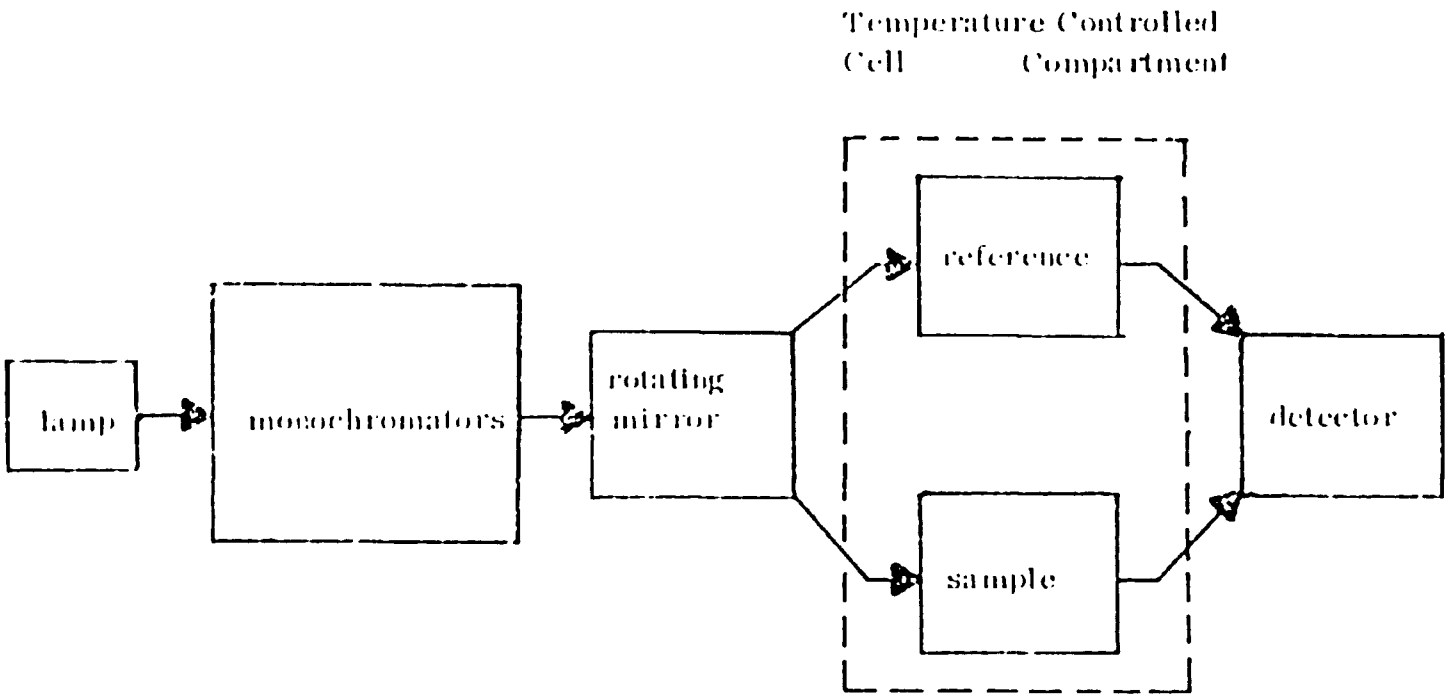

Figure 2. Schematic diagram of Cary 14 spectrophometer.

placed into the Cary 14 spectrophotometer cell compartment where they were allowed to come to thermal equilibrium. The cell compartment was maintained at 25.0 ± 0.1°C by a constant temperature bath. One milliliter of $BaCl_2$ electrolyte solution of the appropriate concentration was injected into the sample cell by a syringe. A quick injection was considered sufficient to thoroughly mix the electrolyte solution and latex. No other stirring mechanism was used. Negligible differences were found in parallel experiments conducted with and without stirring.[7] Coagulation was detected within 1 or 2 seconds for fast coagulation runs and within 5 seconds for very low electrolyte concentrations. Optical density was recorded as a function of time immediately after injection.

The stability ration W was determined by calculating the limiting slope from all rapid coagulations runs. (For rapid coagulation, W = 1.) Using the initial slopes of the slow coagulation runs, W is calculated from Eqn. 9. Stability curves were then drawn as suggested by Reerink and Overbeek.[6] They showed that the DLVO theory predicts a log-linear relationship between W and the electrolyte concentration C_E:

$$\log W = -k_1 \log C_E + k_2 \qquad (10)$$

The slope of the stability curve k_1, can then be related to the

particle radius, surface potential and electrolyte valence by

$$k_1 = -\frac{d \log W}{d \log C_E} = \frac{2.15 \times 10^7 a}{\nu^2} \tanh^2 \frac{\nu e \Psi_\delta}{4kT} \qquad (11)$$

Where a = particle radius

ν = electrolyte valence

e = electronic change

Ψ_δ = Stern or surface potential

k = Boltzman constant

T = temperature

The critical coagulation concentration is determined experimentally from the electrolyte concentration that borders slow and fast coagulation. The DLVO theory defines the c.c.c. by the following expression:[8]

$$c.c.c. = \frac{8.0 \times 10^{-22}}{A^2 \nu^6} \tanh^4 \left(\frac{\nu e \Psi_\delta}{4kT} \right) \qquad (12)$$

where A is the Hamaker constant. By combining Eqns. 11 and 12, the Hamaker constant can be determined experimentally from the slope of the stability curve and the c.c.c.:

$$A = \left[\frac{1.73 \times 10^{-36} \left(\frac{d \log W}{d \log C_E} \right)^2}{a^2 \nu^2 \quad c.c.c.} \right]^{1/2} \qquad (13)$$

Eqns. 11, 12, and 13 apply when water is the medium, the temperature is 25°C, and $\kappa a \gg 1$ (κ is the reciprocal double layer thickness), which implies that the particles are large compared to the double layer thickness (high electrolyte concentration) and large enough so that the flat plate model approximates that of a spherical model.

Eqn. 12 is also known as the Schulze-Hardy rule and predicts an inverse sixth power dependence between the electrolyte valence and the c.c.c. If $\nu\Psi_\delta \leq 25$ mv, the hyperbolic tangent of Eqn. 12 can be approximated by its argument and the c.c.c. is then given by[4]

$$\text{c.c.c.} = \frac{6.98 \times 10^{-30} \Psi_\delta^4}{A^2 \nu^2} \tag{14}$$

This result shows an inverse second power relationship between the c.c.c. and electrolyte valence. The surface potential is dependent on electrolyte concentration, but can be related to the surface charge density which is constant if the former dependence occurs. The surface charge density and surface potential are then related by the expression:[8]

$$\sigma = \frac{2 \pi k T C_E}{\varepsilon} \quad \text{Sinh} \quad \frac{\nu \Psi_\delta e}{2 kT} \tag{15}$$

If the surface charge density is constant and $\psi_s \leq 25$ mv Eqns. 14 and 15 can be combined, with the hyperbolic sine being approximated by its argument, resulting in the following expression:

$$c.c.c. = \frac{3.2 \times 10^{-12} \sigma^{4/3}}{A^{2/3} \nu^2} \qquad (16)$$

The degree of dissociation of the strong acid groups on the particle surface can be obtained from experimentally determined values of the c.c.c. and σ (conductometric titration). The value of the c.c.c. is substituted into Eqn. 16 and a calculated value of the surface charge density is obtained, which when compared to the experimental value of conductometric titration gives the degree of dissociation.

Molecular Weight Determination

The molecular weight and distribution of each latex was determined by gel permeation chromatography (GPC). GPC allows the determination of a number, weight or z-average molecular weight for the polymer and a molecular weight distribution over the entire range of polymer molecular weights. Therefore, it can be used to detect the presence of low molecular weight material, such as oligomers or polyelectrolyte, and is also then, a good measure of the degree to which the latex has been cleaned by ion exchange.

A Water's Associates model 201A GPC equipped with a differen-

tial refractometer detection was used. Four μ-Styragel columns were used with pore sizes 10^3, 10^4, 10^5, and 10^6 allowing analysis of a molecular weight range of approximately 1,000 to 5,000,000. Tetrahydrofuran (THF) was used as the mobile phase. Narrow distribution polystyrene polymers were used as calibration standards, ranging from a molecular-weight of 2350 to 3,900,000. Calibration samples were prepared at a concentration of 0.1 wt.%, filtered, and injected in quantities of 50-300 μl.

All latex samples were dried at 60°C for several days, before dissolving in THF at concentrations of 0.2 to 0.4 wt%. All samples were filtered through a 0.5 μ fluropore filter before injection. Care was taken to keep filtration rates slow to prevent shear degradation of the polymer. Samples were injected in 200-400 μl quantities.

A Fortran IV program was used to analyze the results obtained from the chromatograms. Average molecular weights and molecular weight distributions were determined from the height of the chromatogram at any elution volume, which is directly related to the molecular weight. The number average molecular weight is given by

$$\overline{M}_N = \frac{\Sigma N_i M_i}{\Sigma N_i} = \frac{\Sigma \text{ heights}}{\Sigma N_i} \qquad (17)$$

The weight average molecular weight is

$$\bar{M}_w = \frac{\Sigma N_i M_i^2}{\Sigma N_i M_i} \qquad (18)$$

and the z-average molecular weight is given by:

$$\bar{M}_z = \frac{\Sigma N_i M_i^3}{\Sigma N_i M_i^2} \qquad (19)$$

The weight average is the molecular weight most often reported. The dispersity of polymer is given by the ratio of weight average and number average molecular weights:

$$D = \frac{\bar{M}_w}{\bar{M}_N} \qquad (20)$$

The area under the chromatogram is proportional to the amount of material injected. All chromatograms are normalized to a constant area or injection size. The normalized chromatogram is then used to calculate a cummulative molecular weight distribution.

C H A P T E R III

RESULTS AND DISCUSSION

Coagulum

The coagulum from each polymerization was collected and dried. Figure 3 shows the percent coagulum based on the monomer phase versus the AMPS (Na^+) concentration. The coagulum level decreased to 4 wt%, and then gradually increased to 7.5 wt% as the functional monomer concentration increased. The decreasing coagulation level indicates that more of the primary particles formed in the early part of the polymerization are more stable due to incorporation of the AMPS and therefore are more resistent to flocculation because of their greater electrostatic stability. At increased levels of functional monomer, the functional monomer far exceeds the concentration of styrene in the aqueous phase. The probability of homopolymerization to form polyelectrolyte is therefore greater. However, the addition of methanol increases the solubility of styrene in the water phase, therefore increasing the AMPS-styrene ratio and improving the chances of copolymerization of the AMPS into the polymer particle.

The polyelectrolyte also adsorbs on the particle surface at several sites and causes flocculation of particles by bridging. The more AMPS present, the greater the amount of polyelectrolyte that is formed.

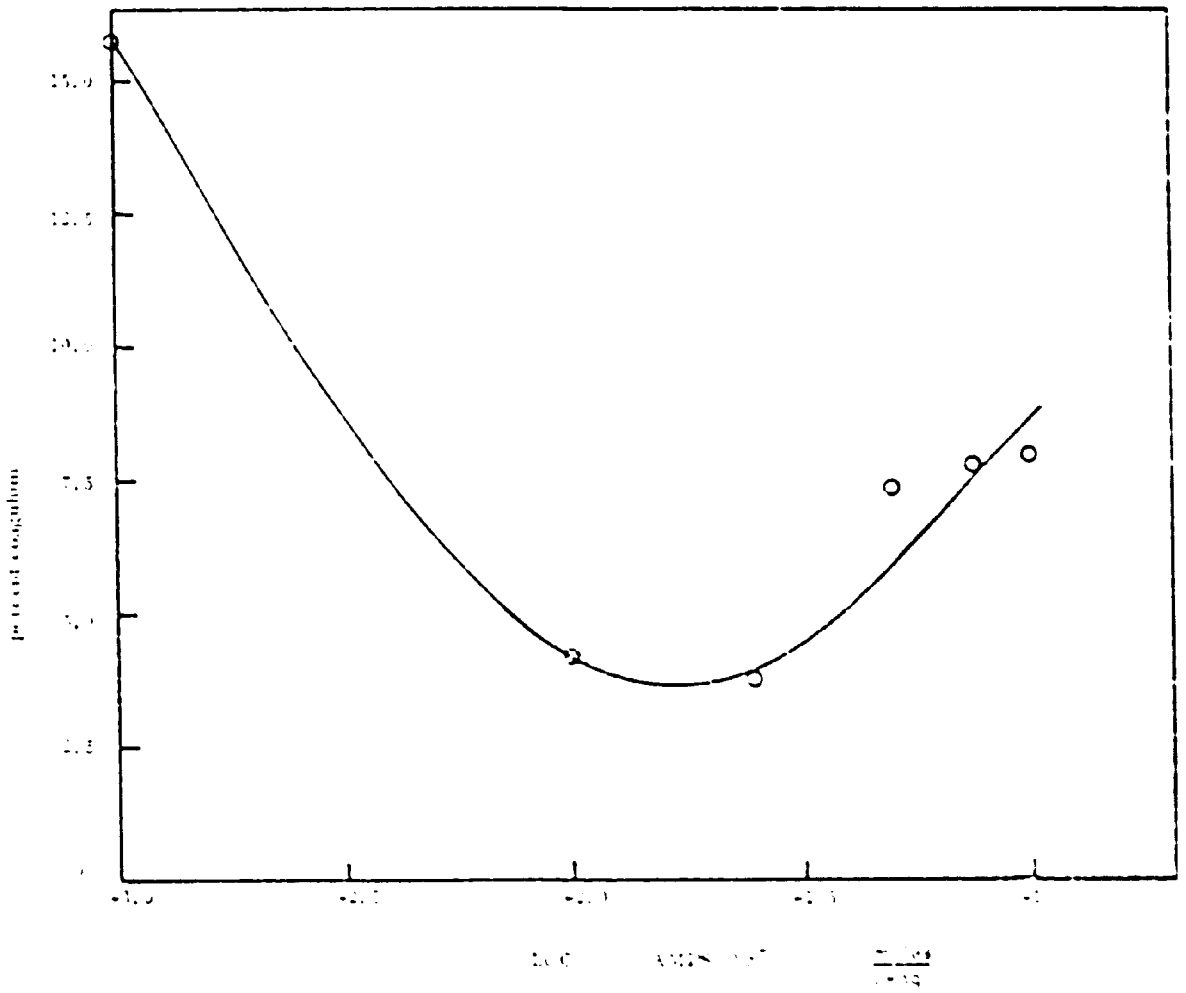

Figure 3. The effect of AMPS concentration on the level of coagulum formed during polymerization.

Particle Size

The particle size of the latexes were determined by transmission electron microscopy. A plot of the number average particle diameter, calculated from the electron micrographs versus the charged concentration of AMPS is shown in Figure 4. A trend similar to that found in the coagulation levels was observed; the particle size decreased to a minimum and then increased again.

The following mechanism is proposed to explain this trend. As described earlier, as more AMPS is present in the system, it will be incorporated into more of the primary particles. With the additional stabilizing charge from the functional monomer and already present initiator fragments, the primary particles will be less likely to flocculate. With a greater number of stable particles present, the monomer will be distributed over a greater number of polymerization sites resulting in a smaller final particle size. However, as the AMPS concentration increases, more polyelectrolyte is formed which causes flocculation of particles. This will decrease the number of polymerization sites, and therefore, the final particle size will be greater.

The technique used to prepare the latexes resulted in monodisperse particle size distributions. The bottles were preheated with all constituents except the initiator so that the system had a homogeneous temperature distribution. The rate of polymerization would then be constant throughout, so all particles formed would grow at the same rate early in the polymerization. This also

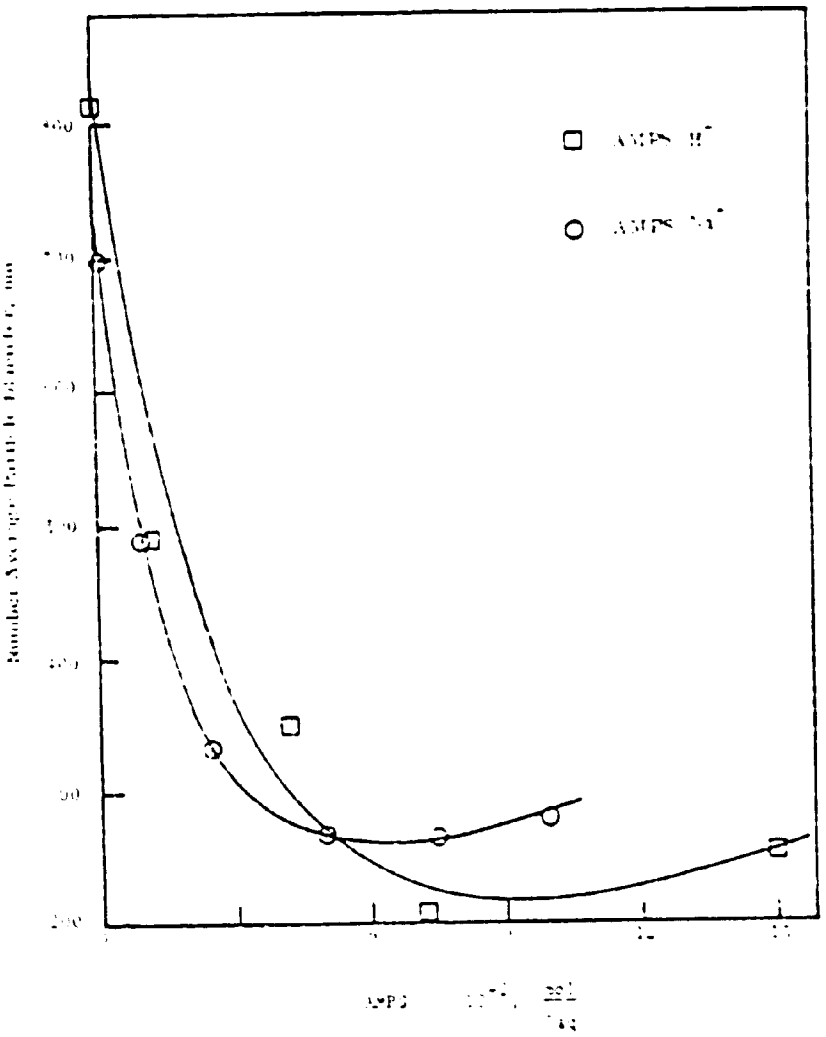

Figure 4. The effect of AMPS concentration on the particle size of the latexes.

minimizes the particle nucleation stage and lengthens the growth stage which a]so encourages the formation of a monodisperse latex.[5] The uniformity ratio varied from 1.001 to 1.048 for all latexes prepared. A uniformity ratio of less than 1.05 indicates a monodisperse system. Table II give the uniformity ratio, number average and weight average particle diameters for all latexes prepared. Figure 5 shows an electron micrograph of latex SA-28 which had a uniformity ratio of 1.001.

Surface Characterization

The nature of the surface groups was determined by conductometric titration. The latexes were first cleaned with mixed bed ion exchange resins until the results of the titrations were consistent. From two to six cycles with fresh resins were required to accomplish this. Each latex was titrated with a 0.019N sodium hydroxide solution. Tables III and IV show the titration results for the AMPS(Na^+) and AMPS(H^+) latexes respectively. The titration curves for AMPS(H^+) and AMPS(Na^+) latexes are given in Appendix I.

The AMPS(Na^+) latexes were found to have strong acid groups only, while strong and weak acid groups were found on the AMPS(H^+) latexes. Figure 6 shows only one strong acid equivalence point and no weak acid end points. The strong acid charge represents that due to sulfate groups from persulfate initiator and sulfonate groups from the AMPS comonomer. The persulfate initiator generates both sulfate and hydroxyl radicals which can both initiate polymer-

TABLE II

Latex	D_n (nm)	D_w (nm)	U
SA-27	697	710	1.018
SA-28	487	488	1.001
SA-29	333	334	1.002
SA-30	266	278	1.046
SA-31	265	265	1.004
SA-32	280	280	1.001
SA-10	816	856	1.048
SA-2	489	490	1.002
SA-1	351	351	1.001
SA-13	209	211	1.012
SA-14	254	257	1.010

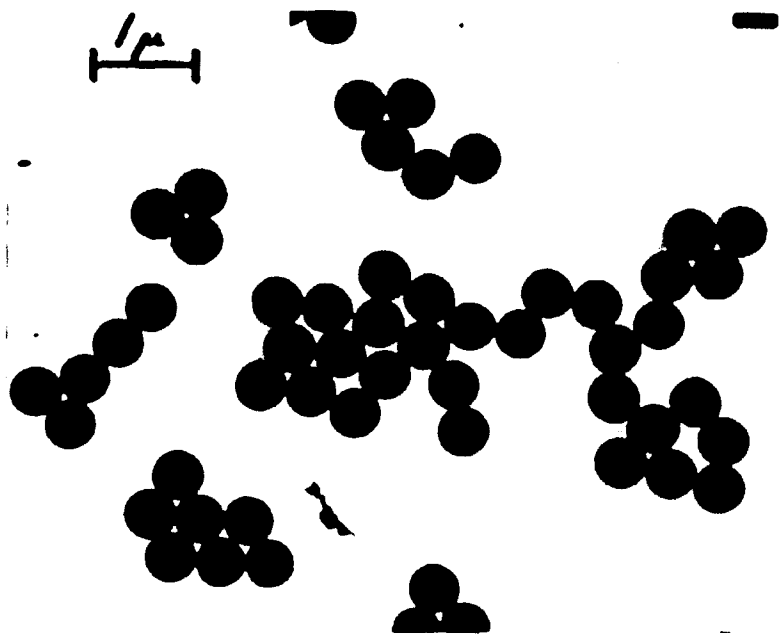

Figure 5. Electron micrograph of latex SA-28: Diameter = 487 nm, Uniformity ratio = 1.001.

TABLE III

Titration Results for AMPS (H^+) Series

Latex	[AMPS, H^+]	pH	Strong Acid Charges N_i	σ_s	A_c	Weak Acid Charges N_i	σ_w	A_c
	moles/liter		$\frac{\mu eqv}{gm}$	$\frac{\mu coul}{cm^2}$	$(nm^2)/10^2$	$\frac{\mu eqv}{gm}$	$\frac{\mu coul}{cm^2}$	$(nm^2)/10^2$
SA-10	0.0	7.5	8.0	22.1	72.5	9.4	26.0	61.6
SA-2	0.0121	6.5	13.0	21.5	74.5	5.1	8.4	190.7
SA-1	0.0422	2.2	14.3	17.0	94.2	6.4	7.6	210.8
SA-13	0.0724	2.1	22.9	16.2	98.9	9.0	6.4	232.2
SA-14	0.151	6.8	45.0	38.7	41.4	19.9	17.1	93.7

TABLE IV

Titration Results for AMPS (Na^+) Series

Latex	[AMPS,Na^+] $\frac{\text{moles}}{\text{liter}}$	strong acid charges N_i $\frac{\mu\text{eqv.}}{\text{gm}}$	σ_s $\frac{\mu\text{coul}}{\text{cm}^2}$	A_c $(\text{nm}^2)/10^2$	pH after polymerization
SA-27	0.001	10.4	12.2	131	7.9
SA-28	0.010	15.7	12.9	124	7.7
SA-29	0.025	21.6	12.2	132	7.7
SA-30	0.050	32.3	15.0	111	8.2
SA-31	0.075	34.2	15.3	105	7.7
SA-32	0.100	40.7	19.3	83	7.5

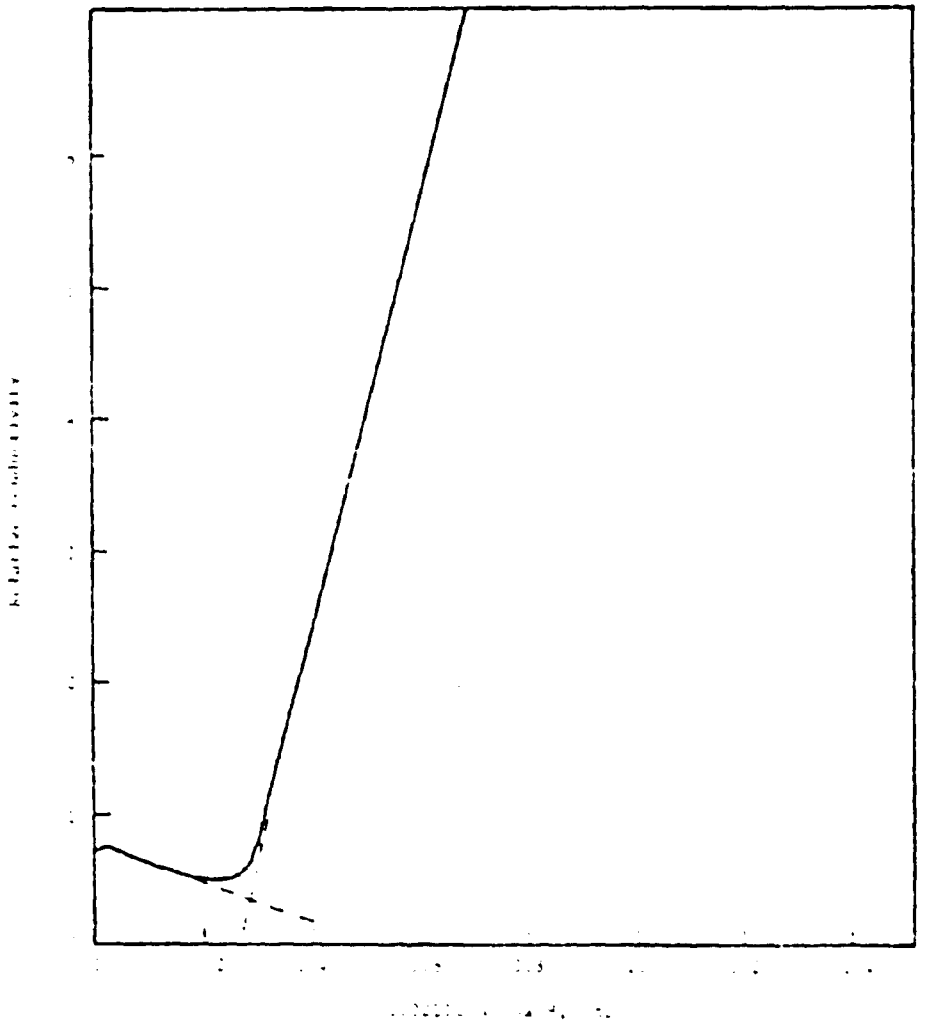

Figure 6. Conductometric titration of SA-27 after 5 ion exchange cycles showing strong acid surface functional groups.

ization. However, the hydroxyl groups do not contribute electrostatically to stability. The weak acid groups found on the AMPS(H^+) latexes are formed by the oxidation of these surfaces hydroxyl groups to carboxyl groups.[2] They could also be formed by hydroylsis of the AMPS sulfonate groups at acidic pH's.

Figure 7 shows a conductometric titration of a AMPS(H^+) latex with strong and weak acid end points. This is encouraged by the acidic medium of the AMPS(H^+) recipes. The decrease in pH of the system increases the formation of a greater proportion of hydroxyl radicals which can be oxidized to carboxyl groups.[5] Although both recipes had sodium bicarbonate as a buffering agent, the acidic nature of the AMPS(H^+) was not neutralized. Table III shows that as the concentration of AMPS(H^+) increases, so does the total amount (n_i) of carboxyl groups found. All these latexes (of the AMPS(H^+) series) had acidic pH's. The pH of AMPS(Na^+) series was fairly neutral and ranged from 7.5 to 8.2.

For all latexes prepared, the total amount of strong acid charge increased as the AMPS concentration increased. The increase in total amount of charge implies that more of the AMPS has been incorporated into the particle surface. But by examining the surface charge density, the concentration of strong acid groups on the surface barely increases by a factor of 1.5 while the charged concentration of AMPS increased 100-fold. It is evident that the relative amount of AMPS that ends up on the particle surface decreases as the charged AMPS concentration in-

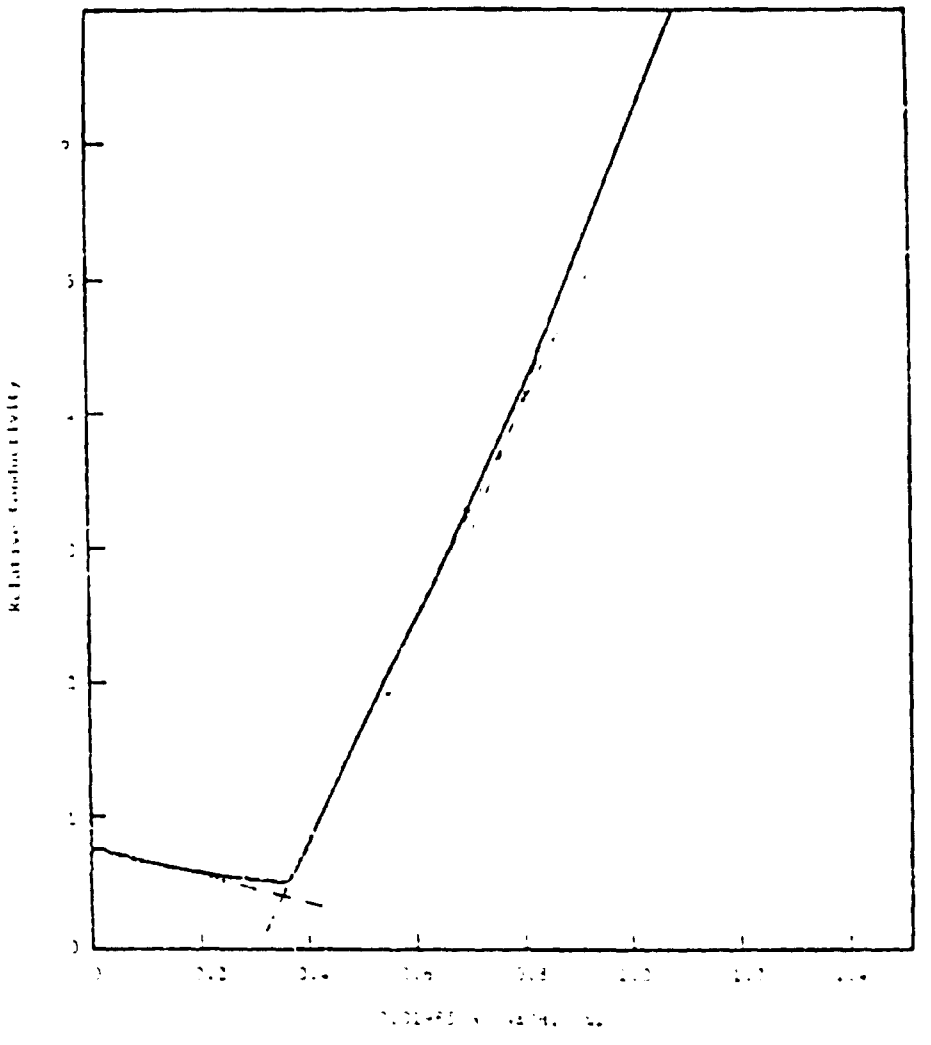

Figure 7. Conductometric titration of SA-10 after 2 ion exchange cycles showing strong and weak acid surface functional groups.

creases. Table V shows the amount of total charge that would be found on the particles surface if total incorporation had occurred.

Ultracentrifugation

The preparative ultracentrifuge was used to isolate the serum phase to detect the presence of polyelectrolyte. Figures 8-10 shows an electromicrograph of the serum phase of SA-13. A continuous film is shown which contains some latex particles. This film is probable evidence of polyelectrolyte formed by homopolymerization of AMPS present in the aqueous phase. This polyelectrolyte can cause particle flocculation by bridging thereby controlling particle size and contributing to coagulum formation.

Latex Stability

The stability of a latex was determined by measuring the initial rates of coagulation as a function of electrolyte concentration. The c.c.c. and slope of the stability curve were determined from these runs. Figure 11 shows a typical optical density versus time curve for a series of coagulation runs at different electrolyte concentrations. Optical density-time curves for the remaining AMPS latexes are given in Appendix II. The initial slope was measured from each of these runs from which W values can be calculated. The initial slopes of the optical density versus time curves were found to increase in magnitude until at a concentration approximately equivalent to

TABLE V

Expected and Experimental Amounts of Strong Acid Surface Charge

Latex	[AMPS,Na^+] charged (mol/laq)	N_i (SO_4^- & SO_3^-) experimentally determined (μeqv./gm)	N_i (SO_3^-) theoretical (μeqv./gm)
SA-27	0.001	10.4	4.0
SA-28	0.010	15.7	40.0
SA-29	0.025	21.6	100.0
SA-30	0.050	32.3	200.0
SA-31	0.075	34.2	300.0
SA-32	0.100	40.7	400.0

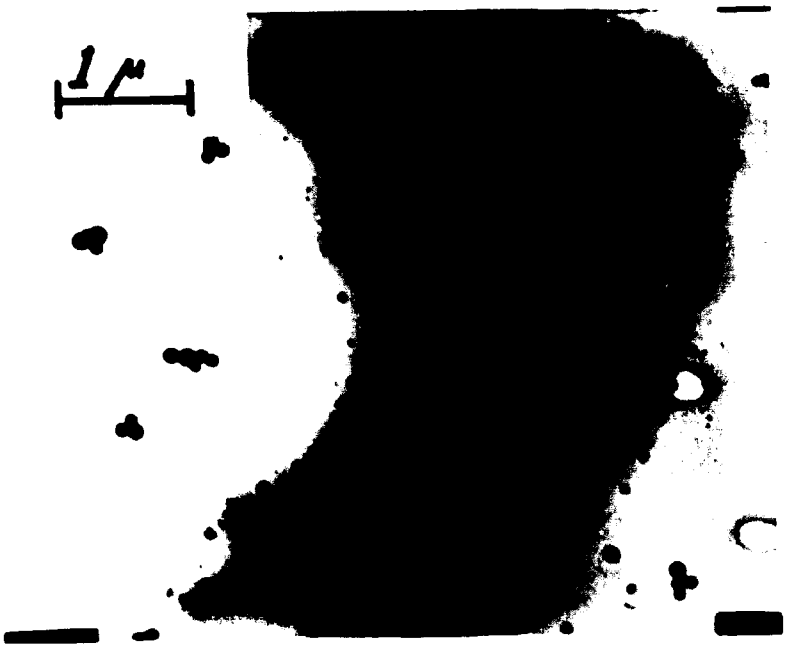

Figure 8. Electron micrograph of a polyelectrolyte film with some flocculated latex particles.

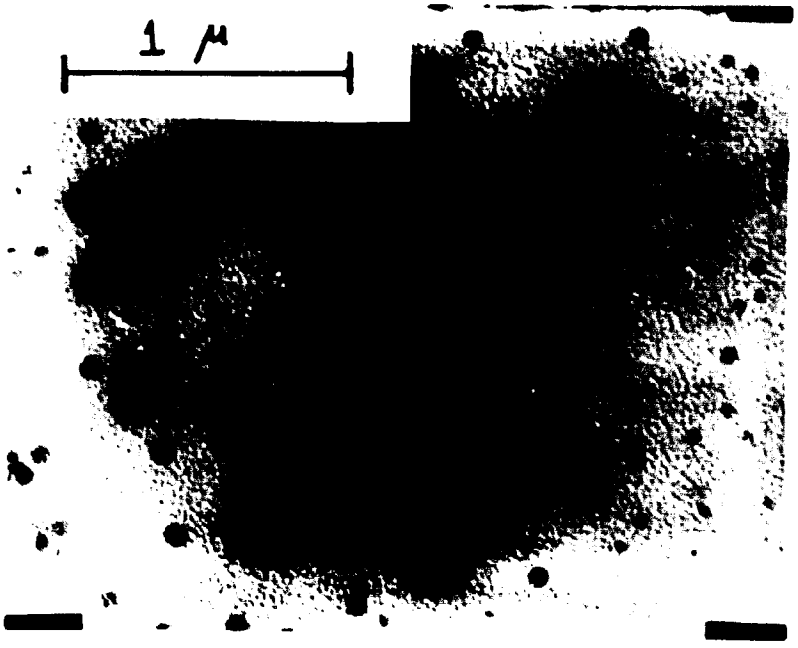

Figure 9. Electron micrograph of latex particles flocculated by polyelectrolyte.

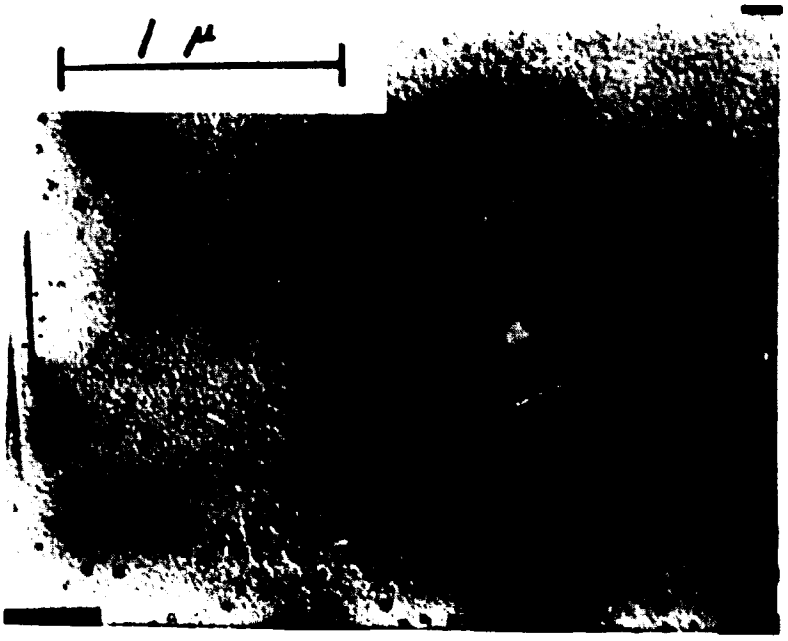

Figure 10. Electron micrograph of latex particles flocculated by polyelectrolyte.

the c.c.c. where they decreased again. This could be due to the different densities of the flocs formed during coagulation. At the higher concentration of electrolyte, tightly packed flocs are formed which scatter less light than a loosely packed floc. The loosely packed flocs are formed due to coagulation in the secondary minimum which could occur at c.c.c. electrolyte levels. At electrolyte concentrations less than the c.c.c., the rate of coagulation decreases and the initial slope of the optical density versus time curve decreases correspondingly.

A typical stability curve is given in Figure 12 which shows the stability ratio versus electrolyte concentration (see Appendix II for the remaining stability curves). The increasing log W values of the slow coagulation regime are linear with respect to the log of the electrolyte concentration. Values of fast coagulation are horizontally linear and are by definition fit at W=1. The intersection of the fast and slow coagulation curves gives the c.c.c. The slopes and c.c.c.'s determined from the stability curves are given in Table VI. The stability curve slope for the AMPS(Na^+) series increased to a maximum and decreased, while the c.c.c.'s followed a more or less random pattern ranging from 13.1 to 18.3 mmoles/liter. The slopes of the AMPS(H^+) series increased, while the c.c.c. reached a maximum and decreased.

Eqns. 11 and 12 predict that as particle size and surface charge density increase, the c.c.c. and slope of the stability curve and therefore overall electrostatic stability should in-

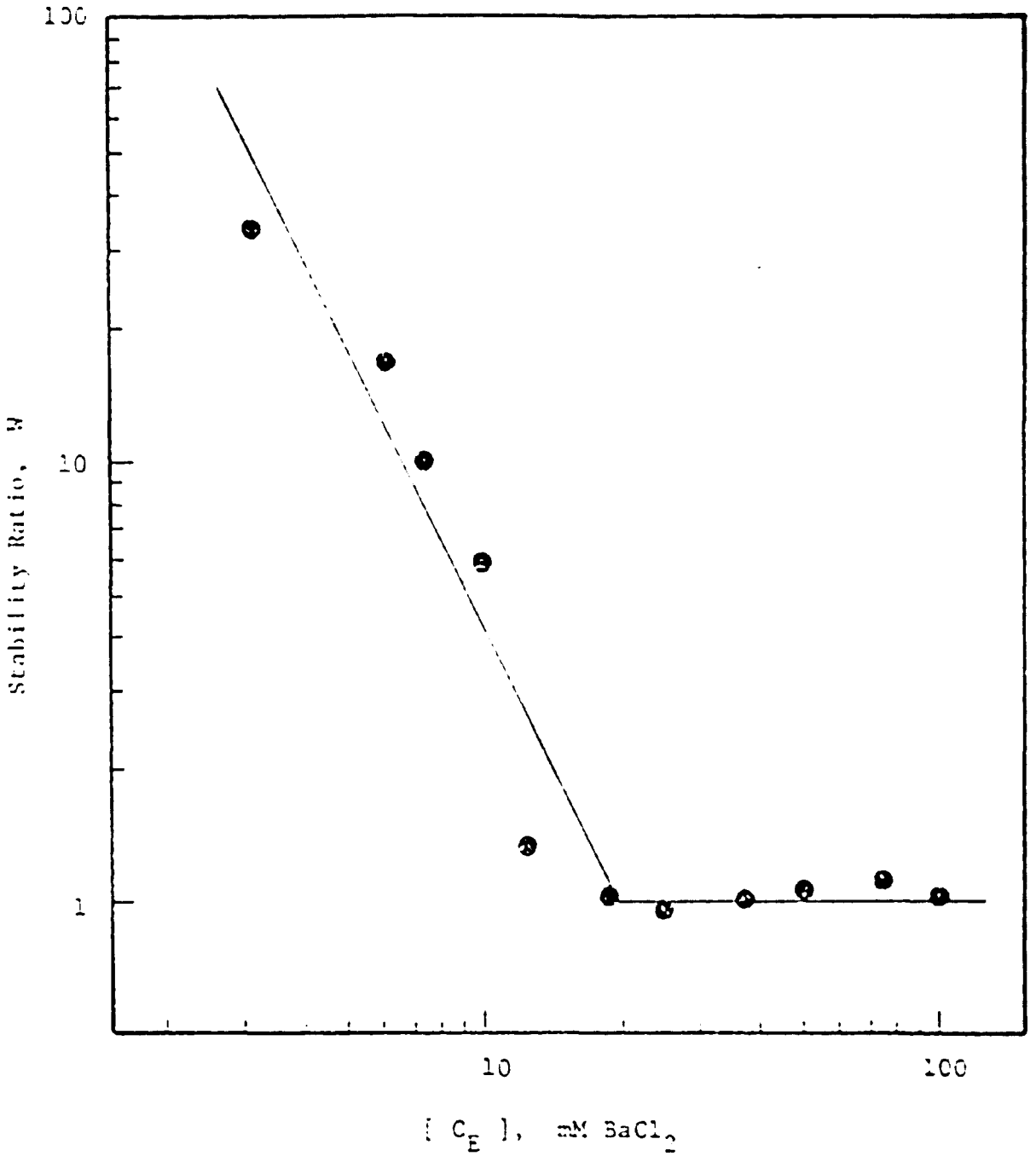

Figure 12. Stability curve for latex SA-2.

TABLE VI

Results of Stability Analysis

Latex	$\bar{D}_N$ (nm)	σ_s $\frac{ueqv}{gm}$	σ_w $\frac{ueqv}{gm}$	$-\frac{d \log W}{d \log C_E}$	c.c.c. (mmole/l)
SA-27	697	10.4	--	1.15	16.8
SA-28	487	15.7	--	1.08	17.4
SA-29	333	21.6	--	2.57	18.0
SA-30	266	32.3	--	3.57	13.1
SA-31	265	34.2	--	2.88	14.5
SA-32	280	40.7	--	2.81	18.3
SA-10	816	22.1	26.0	1.19	12.5
SA-2	489	21.5	8.4	2.10	19.7
SA-1	351	17	7.6	1.76	30.8
SA-13	209	16.2	6.4	2.76	34.3
SA-14	254	38.7	17.1	3.42	17.7

crease. Therefore, one might expect little increase in stability of the AMPS latexes since the particle size decreases and surface charge increase. However, this assumes coagulation occurs in the primary minimum. Wiese and Healy[10] showed that, if coagulation occurred in the secondary minimum, the stability of the latex would decrease as particle size increased. Furthermore, secondary minimum coagulation would most likely occur in particles greater than 100 nm. Then for the AMPS latexes, the stability should increase because of the decreasing particle size and increasing surface charge density. Figures 13 and 14 show composites of all the stability curves for AMPS(H^+) and AMPS(Na^+) latexes which show the general trend of increasing stability with AMPS concentration.

However, the random trends found in the c.c.c.'s seem to infer that there is no dominant mechanism of stabilization. The steric influences of the functional groups extending from the surface group could influence stability either positively or negatively, which could account for this. A schematic representation of the different functional groups on the surface is shown in Figure 15. Strong-acid pendant chains could give highly concentrated regions of electrostatic and steric repulsion giving improved stability.[11] Polyelectrolyte, so strongly absorded that it cannot be removed by ion exchange, or in some way polymerized in-situ to the surface, could cause flocculation by bridging. This would lead to decreased stability in latexes prepared with higher con-

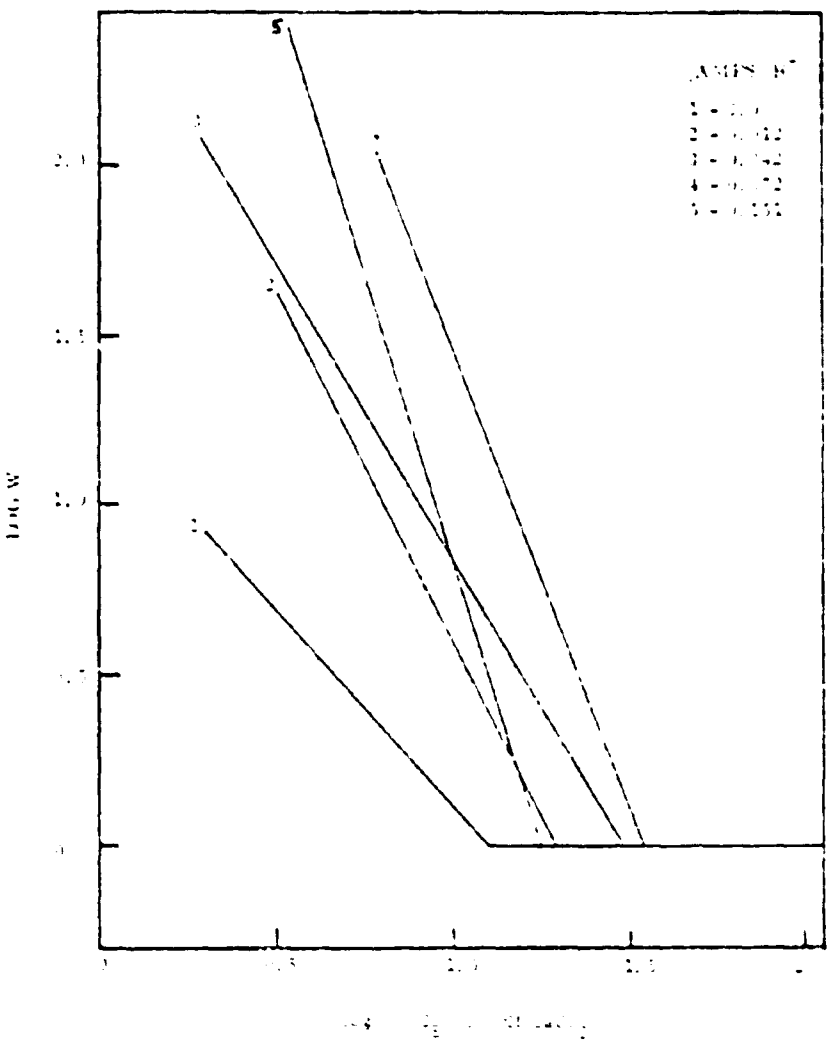

Figure 13. Stability curves for latexes of the AMPS(H^+) series.

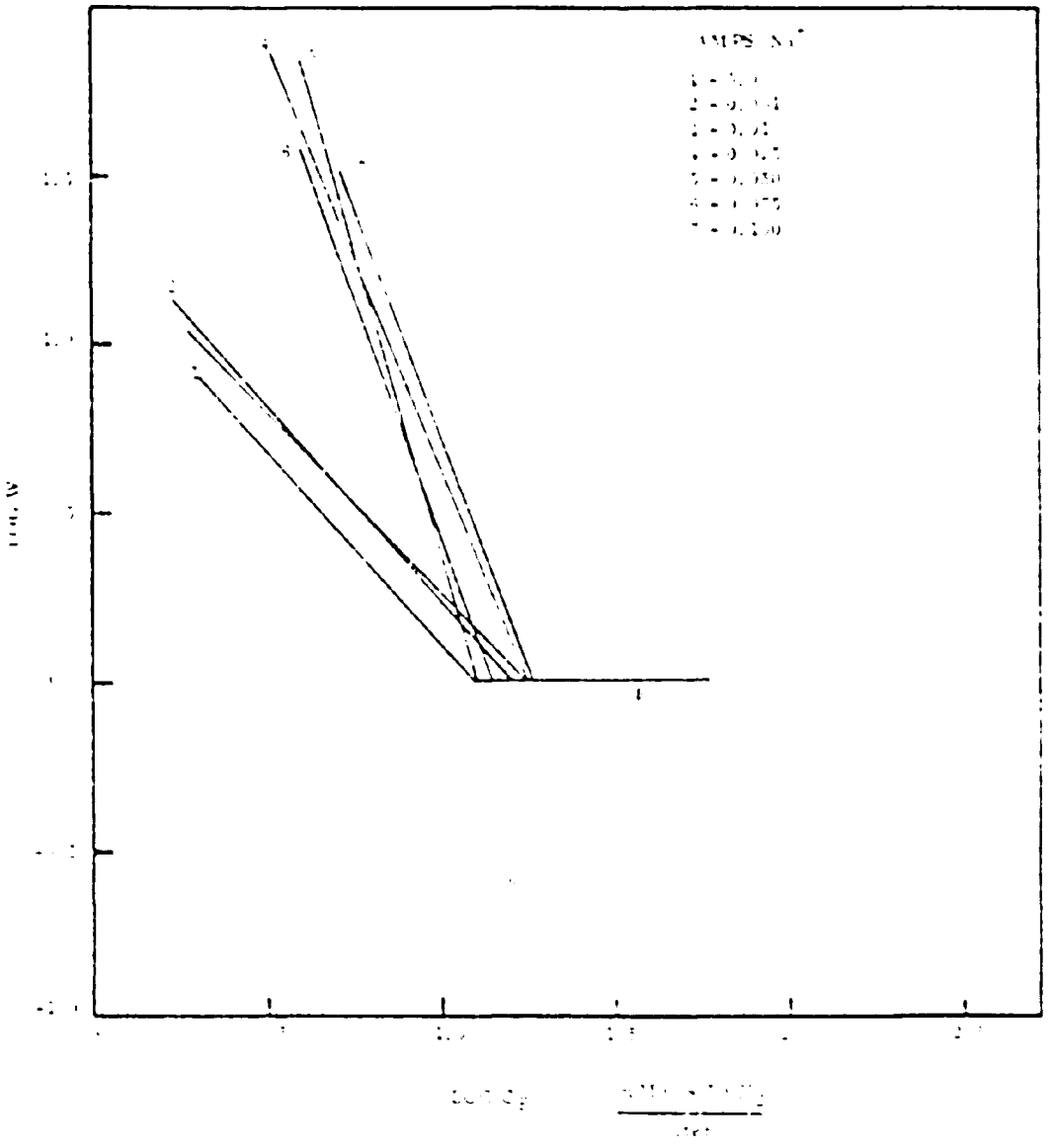

Figure 14. Stability curves for latexes of the AMPS(Na^+) series.

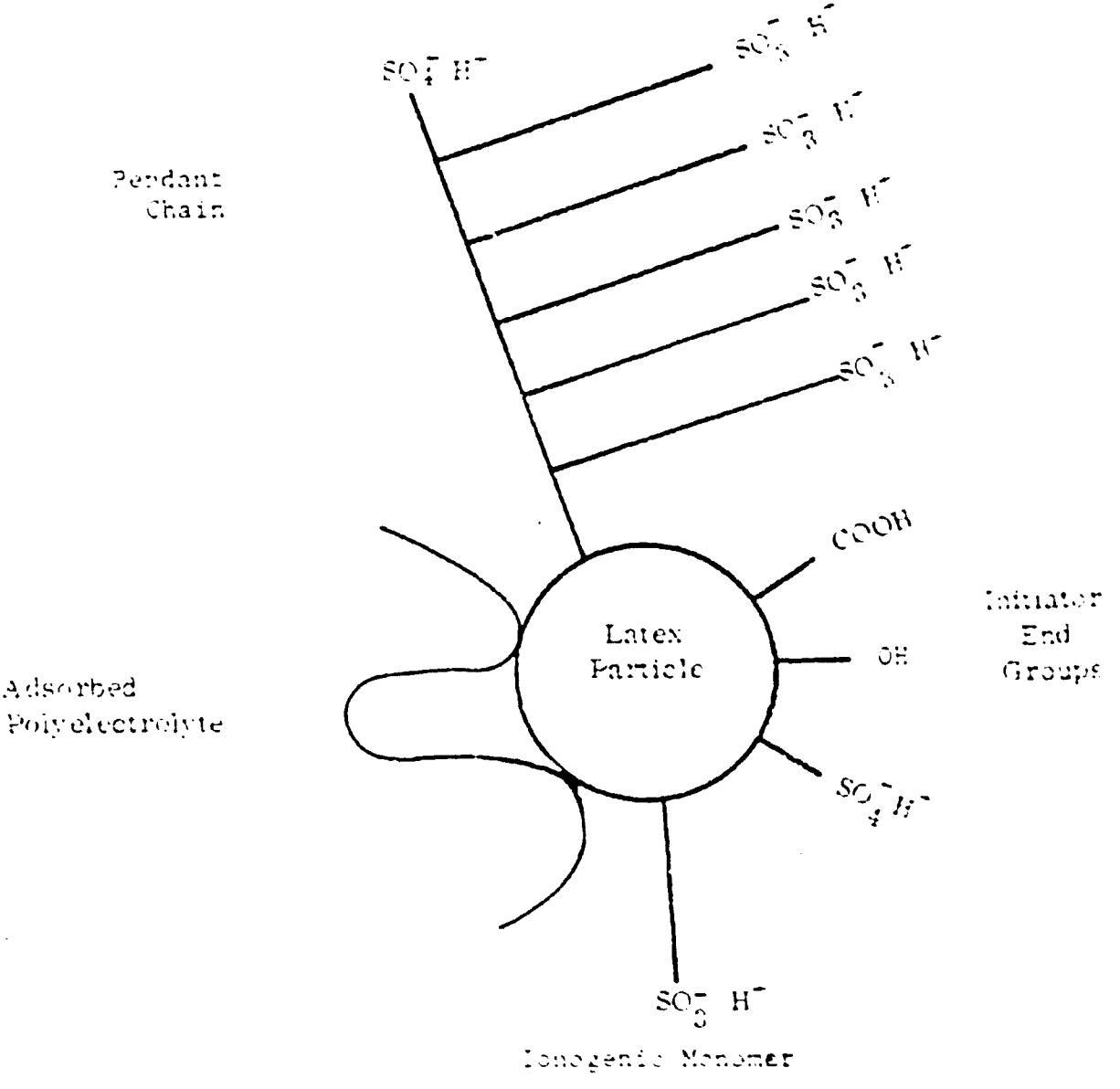

Figure 15. Schematic diagram of the different functional groups on the latex particle surface.

centrations of ionogenic monomer where polyelectrolyte is more prevalent. Steric stabilization could also occur by the formation of vincinal water about the hydroxyl groups on the surface.[12,13]

The Hamaker constant and Stern potential calculated from Eqns. 13 and 11 respectively, are given in Table VII. The Stern potential increases with charged AMPS concentrations for both series. If it is assumed that surface charge density is constant, then the Stern potential must vary with electrolyte concentration. However, since the c.c.c.'s of all the latexes are similar and the Stern potential is determined at the c.c.c., the increased surface potential implies increasing latex stability. The Hamaker constant was found to be of the same order of magnitude as that calculated by Fowkes[14] for polystyrene (5.0×10^{-14} ergs) and experimentally determined by others.[12,13] The increasing value of the Hamaker constant is due to the changing nature of the particle surface which has several different functional groups. The calculation of the Hamaker constant is also based on an approximate model employing several assumptions which could also contribute to the variations.

Table VIII shows the degree of dissociation α calculated from the surface charge density and from Eqn. 16. When the c.c.c. and Hamaker constant determined experimentally were used, the values of α were slightly lower than when the theoretical value of 5.0×10^{-14} ergs was used in Eqn. 16. The degree of dissociation ranged from

TABLE VII

Hamaker Constant & Stern Potential

Latex	A (ergs/10^{-14})	Ψ_δ (mvolts)
SA-27	0.53	4.0
SA-28	0.70	4.7
SA-29	2.39	8.8
SA-30	4.88	11.7
SA-31	3.75	10.5
SA-32	3.09	10.1
SA-10	0.54	3.8
SA-2	1.27	6.5
SA-1	1.19	7.1
SA-13	2.97	11.6
SA-14	4.21	11.7

TABLE VIII

Degree of Dissociation

Latex	c.c.c. mmols / ℓ	σ^1 Statcoul. / cm^2	σ^2 Statcoul. / cm^2	σ^3_{exp} Statcoul. / cm^2	α %	α %
SA-27	16.8	2031.9	657.8	31180	6.5	2.1
SA-28	17.4	2086.1	776.7	47070	4.4	1.7
SA-29	18.0	2139.8	1476.7	64760	3.3	2.3
SA-30	13.1	1686.0	1665.6	96830	1.7	1.7
SA-31	14.5	1819.5	1574.6	102530	1.8	1.5
SA-32	18.3	2166.5	1701.1	122020	1.8	1.4
SA-10	12.5	1627.8	531.9	66250	2.5	.8
SA-2	19.7	2289.6	1150.0	64460	3.6	1.8
SA-1	30.8	3201.3	1586.2	50970	6.3	3.1
SA-13	34.3	3470.5	2671.2	48570	7.1	5.5
SA-14	17.7	2112.9	1938.1	116020	1.8	1.7

1. $A = 5.0 \times 10^{-14}$ ergs.
2. A determined from eqn. 13.
3. Determined by conductometric titration.

0.8 to 7.1%. These low values were attributed to the high concentrations of surface charge. However, even if an acid group is partially dissociated it will contribute to latex stability.

The complexity of the particle surface with its many different functional groups does not lend itself well to comparison of the predictions of the DLVO theory. Combined electrostatic and steric effects contribute to the overall stability and each stabilizing mechanism cannot be distinguished by the experimental techniques used.

The rate constant for fast coagulation was calculated for Eqn. 8 and the limiting slopes of the optical density - time curves. Scattering cross-sections calculated from the Raleigh-Debye theory for singlets and doublets and from the Mie theory for singlets are given in Table IX. The Raleigh-Debye scattering cross-sections varied from 7 to 20% of the Mie theory value. Table X gives the rate constants determined for fast coagulation and half life of coagulation determined by $\theta = 1/N_p k_r$, where N_p is the particle concentration. The average value of k_r was determined to be $(2.923 \pm 1.086) \times 10^{-12}$ cm^3/particle-sec. Silebi[4] calculated a value of $(2.71 \pm 0.06) \times 10^{-12}$ cm^3/ (sec-particle) including hydrodynamic and potential of interaction effects. Wu[5] calculated a value of 11.0×10^{-12} cm^3/particle-second based on the Raleigh theory of light scattering (valid for particle diameters less than one-tenth the incident wavelength). The Smoluchowski value for k_r is 6.2×10^{-12} cm^3/particle-second.[13] Excellent

TABLE IX

Scattering Cross Sections

Latex	Cross Section of a Singlet $(cm^2)/10^{-14}$ Raleigh-Debye	Mie	Scattering Cross Section of a Doublet $(cm^2)/10^{-14}$ Raleigh-Debye
SA-27	79794.	96448	219540.
SA-28	16148.	18915	45837
SA-29	2425.4	2804.6	7888.6
SA-30	721.5	795.8	2508.5
SA-31	706.6	762.5	2459.3
SA-32	956.1	1062.2	3279.6
SA-10	158710	200320.	440510
SA-2	16461	19277.	46667
SA-1	3194.6	3713.9	10202
SA-13	186.6	205.2	682.3
SA-14	558.9	612.5	1765.1

Table X
Fast Coagulation Rate Constant

Latex	N_p $\frac{\text{Particles}}{cm^3}$ / 10^9	Limiting Slope $\frac{\text{abs units}}{\text{sec}}$ / 10^{-3}	k_r $\frac{cm^3}{\text{particle-sec}}$ / 10^{-12}	θ (sec)
SA-27	1.074	0.376	2.351	912
SA-28	3.150	1.285	4.267	171
SA-29	9.848	2.225	3.402	69
SA-30	19.32	1.430	1.358	88
SA-31	19.54	2.784	2.625	45
SA-32	16.57	2.450	2.568	54
SA-10	3.500	1.444	2.083	2202
SA-2	10.52	4.550	3.805	173
SA-1	49.80	4.809	5.016	436
SA-13	27.75	4.793	2.000	23
SA-14	0.502	0.135	2.676	31

agreement with Silebi's treatment was obtained, while the rate constant only varied by a factor of 2 to 4 from other predictions.

The half-life for coagulation ranged from 23 to 2202 seconds. Therefore the technique used to measure the rate of coagulation was valid since the initial slope could be measured after 1 to 5 seconds after injection of electrolyte.

Molecular Weight Analysis

Molecular weight and molecular weight distribution were determined by gel permeation chromatography. In GPC, separation is based on the hydrodynamic volume of a polymer in solvent. The hydrodynamic size, which is proportional to molecular weight, determines the residence time in the chromatograph columns. The larger the polymer molecular weight, the shorter its residence time will be since it will be unable to penetrate into the many smaller pores in the packing. A calibration curve, molecular weight versus elution volume, can be determined by running narrow distribution polymers. Figure 16 shows the calibration curve for polystyrene in THF at 25^{o}C and at a flow rate of 2 ml/min. Narrow distribution polystyrene standards were used.

Latexes SA-10 and SA-27 to SA-32 were prepared for GPC in THF. Polymer latex cleaned by ion exchange and not cleaned at all were analyzed. Figures 17 and 18 show the normalized chromatogram and cumulative molecular weight distribution of the uncleaned and cleaned latexes of SA-27 superimposed. Two peaks were observed: a high molecular peak of approximately 200,000 and a low molecu-

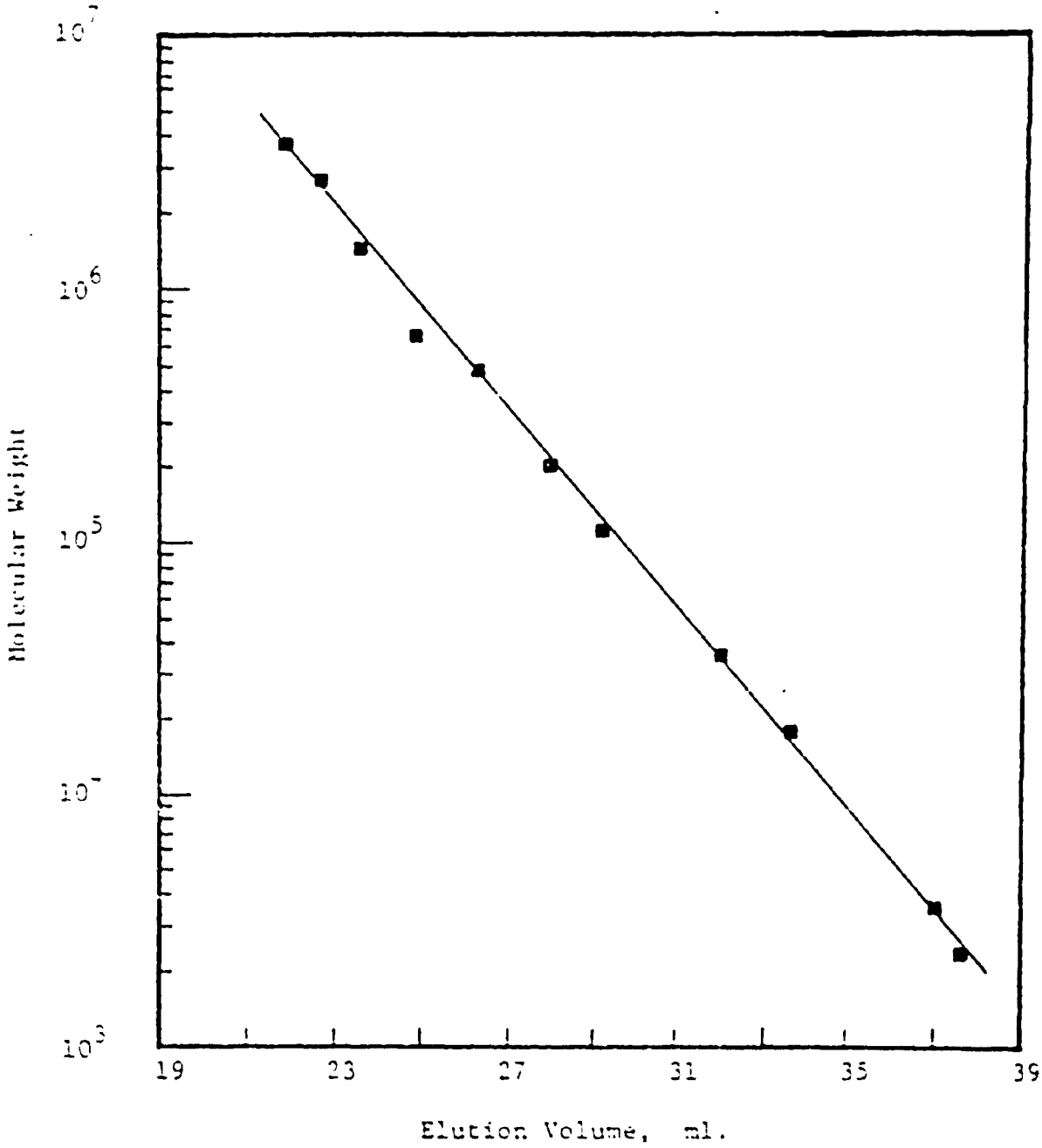

Figure 16. Gel permeation chromatography calibration curve obtained for polystyrene in THF at 25°C and a flow rate of 2 ml/min.

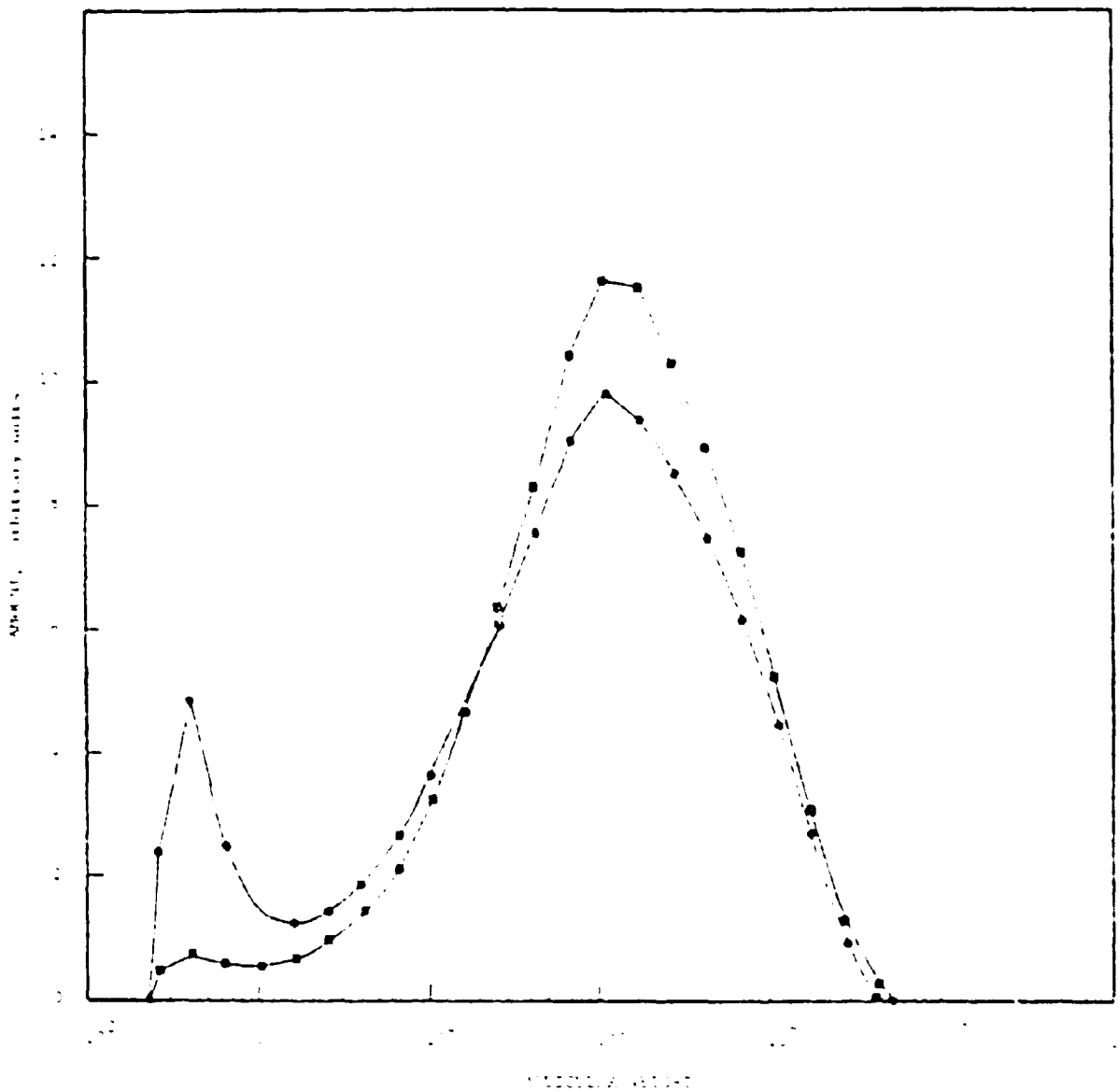

Figure 17. Normalized chromatogram of SA-27 before (●) and after (■) ion exchange.

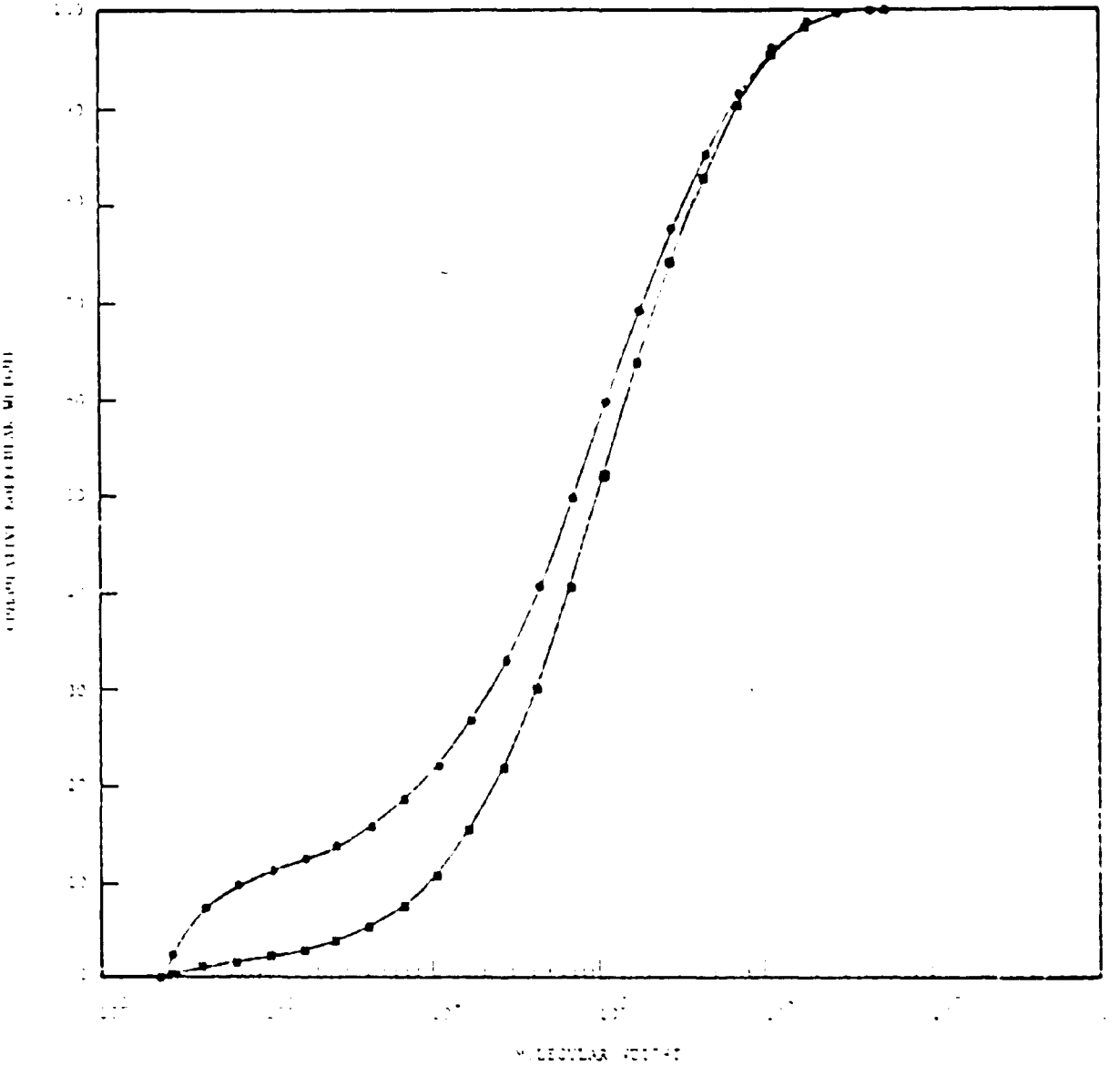

Figure 13. Cumulative molecular weight distribution of SA-27 before (●) and after (■) ion exchange.

lar peak at about 500. The high molecular peak consists of the expected long-chain polystyrene. The peak shape and size is consistent for all the uncleaned and cleaned latexes. The low molecular peak is thought to consist of polyelectrolyte AMPS, styrene oligomers, or short-chain surface-active styrene-AMPS copolymer. It is important to note that the ion exchange process removes most of the low molecular weight material. The small remaining amount of oligomer sized material, evidenced by a small, low molecular weight peak in the clean latex chromatogram, is due to oligomeric material which has been buried inside the polymer particle. By dissolving the polymer, this material is released. Similar chromatograms and distributions were obtained for all other latexes as shown in Appendix III. Figure 19 shows the chromatogram for SA-10. The uncleaned latex has little low molecular weight material as would be expected since there is no AMPS present. The material removed by ion exchange can be attributed to surface active oligomeric styrene.

Because of the column set up, it is difficult to quantitatively determine the molecular weight of this low material or to separate it into different fractions. The lower exclusion limit of a 10^3 μ-styragel column is approximately 1,000 MW. But this material is of a greater molecular weight than THF or water, which also gives another peak of even greater elution volume, implying lower molecular weight. (These peaks are not shown.) Below the lower exclusion limit, the calibration curve also becomes nonlinear.

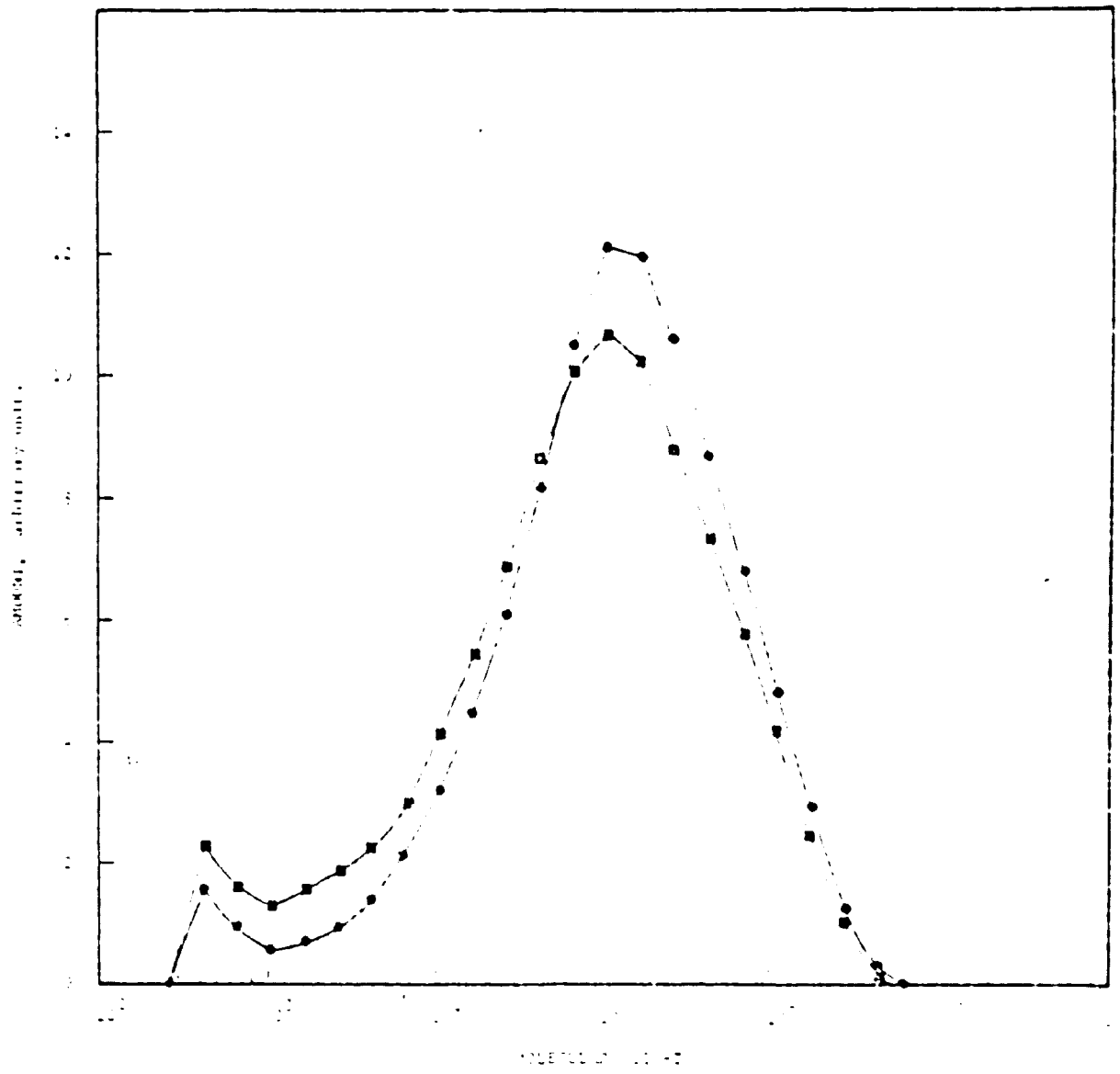

Figure 19. Normalized chromatogram of SA-10 before (●) and after (■) ion exchange.

Therefore the determination of low molecular weight material is qualitative, but still important since it shows the presence of oligomeric material and the ability of ion exchange to remove it completely, assuming that any of the remaining material was buried within the particle and therefore not adsorbed polyelectrolyte.

The cumulative molecular weight distribution shows the removal of low molecular weight material, while the amount of high molecular weight material has not changed.

Table XI shows the molecular weight averages and polydisperity ratio of the clean latexes. For emulsion polymerization of styrene, the bimolecular termination reactions are dominant over transfer reactions in controlling molecular weight development.[17] In this case, the molecular weight development depends on particle size, particle size distribution and termination rate of the radicals inside the particles. Hamielec and Friis[17] showed that for the special case of a monodisperse latex, Smith-Ewart Case II kinetics, and instantaneous termination of a growing radical when a second radical enters the particle ($\bar{n} = 0.5$), the polydispersity ratio of the polymer would equal 2. The polydispersity ratio of the styrene-AMPS latexes varied from 25 to 40. The large discrepancy of polydispersity ratios illustrates the deviations from Smith-Ewart Case II behavior since the particle size distribution is uniform and therefore should not effect the molecular weight distribution. For large particle sizes, $\bar{n}$ (the average number of radicals/particle)

Table XI

Molecular Weight Averages

Latex	$\bar{M}_n/10^4$	$\bar{M}_w/10^5$	$\bar{M}_z/10^6$	D
SA-10-C	1.173	3.078	1.142	26
SA-27-C	1.264	3.170	1.137	25
SA-28-C	0.840	2.571	.981	31
SA-29-C	1.777	3.976	1.218	22
SA-30-C	1.789	4.117	1.334	23
SA-31-C	1.422	5.671	2.000	40
SA-32-C	1.925	6.191	2.073	32

will deviate significantly from 0.5 since it is more likely for more than one radical to grow simultaneously without encountering another living polymer chain. Therefore the assumption of instantaneous termination and Case II kinetics are not valid in particles greater than 200 nm.[17] As the polymer particle grows, and instantaneous termination no longer occurs as frequently, the polymer chains grow at different rates, terminating more randomly thereby broadening the distribution.

The effect of AMPS on the kinetics could also be significant. If termination occurs through chain transfer to some of the AMPS radicals, this could limit the growth of some of the chains early in the polymerization when it is present in greater quantities. After the AMPS has been consumed, polymerization would follow Case II kinetics until the particles were greater than 200 nm, when $\bar{n}$ would begin to increase significantly; all contributing to a broader distribution. The addition of functional monomer influences the molecular weight average, increasing with the concentration of AMPS as shown in Table XI.

The determination of molecular weight averages allows the calculation of the number of strong acid groups per molecule, thereby measuring the degree of incorporation of functional monomer. Table XII shows the degree of incorporation, determined by calculating the expected and actual amount of strong acid groups from functional monomer and initiator assuming two sulfate groups per molecule. Latex SA-27 shows total incorporation of the functional monomer,

TABLE XII

Incorporation of AMPS

Latex	ACTUAL strong acid groups / polymer molecule	EXPECTED strong acid groups / polymer molecule	Incorporation %
SA-27	3.3	3.3	100
SA-28	4.0	12.3	32.5
SA-29	8.6	41.8	20.6
SA-30	13.3	84.3	15.8
SA-31	19.4	172.1	11.3
SA-32	25.2	249.6	10.1

although error in the measurement of the total charge might reduce this somewhat. The degree of incorporation falls off very rapidly as the concentration is increased 100 fold to approximately 10%, even though 12 times more strong acid groups are present in SA-32 than in SA-27.

C H A P T E R IV

SUMMARY AND CONCLUSIONS

The results of the characterizations by conductometric titration, coagulation kinetics, and gel permeation chromatography show that, as the AMPS concentration increases, more of the AMPS is found on the particle surface as evidenced by increased surface charge. However, the relative amount of AMPS incorporated decreases and high amounts of AMPS do not necessarily provide greater stability. Therefore a balance between economics and improved properties for the most efficient use of ionogenic monomers must be found. Specifically, this thesis found:

1. The coagulum level and particle size were found to vary with AMPS concentration. As the AMPS concentration increased, a greater number of primary particles formed and were more stable. This reduces the coagulum and particle size. At high AMPS concentrations, the excess ionogenic monomer homopolymerizes to form polyelectrolyte which causes flocculation most probably by bridging. This is evident through increased coagulum and particle size levels with greater concentrations of AMPS.
2. Increased concentrations of AMPS leads to greater surface charge densities and strong acid groups per polymer molecule. But, the level of incorporation dropped from

100% at low AMPS concentrations to 10.1% at 0.1M AMPS.

3. Surface carboxyl groups which were formed from oxidation of hydroxyl groups, were found at acidic pH levels. When pH was controlled at approximately 7.5 in the AMPS(Na^+) series, no carboxyl groups were observed.
4. Ultracentrifugation studies of the latex serum showed that polyelectrolyte from the homopolymerization of AMPS was formed.
5. The stability of the latexes as determined by coagulation kinetics generally increased.
6. The Hamaker constant was found to be of the same order of magnitude as calculated by Fowkes and reported by other workers. It was also found to vary as a function of the amount of AMPS on the particle surface and in the range of 0.5-5.0 x 10^{-14} ergs for both AMPS series.
7. The low values of the surface potential showed that the latexes did not follow the inverse sixth power law of Schulze-Hardy.
8. The degree of dissociation of the surface groups was found to vary from 0.8 to 7.1%.
9. The fast coagulation rate constant was experimentally determining to be (2.923 ± 1.086) x 10^{-12} cm^3/particle-sec. based on Raleigh-Debye scattering and agreeing well with the theoretical value of Silebi[4] and others.[5,13]
10. The weight average molecular weight of the AMPS(Na^+)

latexes varied from 2.571×10^5 to 6.191×10^5. The molecular weight distribution was also fairly broad, indicating a variation from Smith-Ewart Case II kinetics.

11. The molecular weight distribution of the uncleaned latex showed the presence of low molecular weight material. The majority of this was removed by ion exchange and attributed to polyelectrolyte. Low molecular weight material remaining in the clean latex was attributed to oligomeric polystyrene.

12. The combined data from titration and stability analyses were found to correlate well with high values of surface charge giving high levels of stability. Increased surface charge led to increased latex stability as determined by stability curve slope, c.c.c., and the Stern potential. Deviations in the expected results were attributed to the particle surface being a poor model for studying the DLVO theory. Combined steric and electrostatic effects from the unique structure of the particle surface were evident by the existing experimental deviations from the trends as predicted by the DLVO theory.

REFERENCES

1. Functional Monomers, Vol. 1, Yocum, R. H. and E. B. Nyquist, Ed., Marcel Dekker, Inc., New York, 1973.

2. Vanderhoff, J. W., H. J. van den Hul, R. J. M. Tausk, and J. Th. G. Overbeek, in Clean Surfaces: Their Preparation and Characterization for Interfacial Studies, Goldfinger, G., Ed., Marcel Dekker, Inc., New York, 1970, p. 15.

3. Fuchs, N., Z. Physik, 89, 736 (1934).

4. Silebi, C., W. C. Wu, M. S. El-Aasser, and J. W. Vanderhoff, "Flocculation of Monodisperse Polystyrene Latexes: Correlation of Experiment with Theory." Presented at ACS Annual Meeting, Miami Beach, 1978.

5. Wu, W. C., Ph.D. Thesis, Lehigh University (1977).

6. Reerink, H. and J. Th. G. Overbeek, Disc. Farad. Soc. 66, 490 (1970).

7. Greene, B. W. and F. L. Saunders, J. Colloid and Interface Science, 33, 393 (1970).

8. Overbeek, J. Th. G. and E. J. W. Verwey, Theory of the Stability of Lyophobic Colloids, Elsevier, New York, 1948.

9. Troelstra, S. A., Ph.D. Thesis, Utrecht, 1941.

10. Wiese, G. R. and T. W. Healy, Trans. Farad. Soc., 66, 490 (1970).

11. White, W. W. in Advances in Emulsion Polymerization and Latex Technology: Short Course Notes, Poehlein, G. W., Ed., Lehigh University, 1977.

12. Drost-Hansen, W., J. Colloid and Interface Sci., 58, 251 (1977).

13. Johnson, G. A., et al., Disc, Farad. Soc., 42, 120 (1966).

14. Fowkes, F. M., Ind. Eng. Chem., 56, 40 (1964).

15. Watillon, A. and A. M. Joseph-Petit, Disc. Farad. Soc., 42, 143 (1966).

16. Ottewill, R. H. and J. N. Shaw, Disc. Farad. Soc. 42, 154 (1966).

17. Hamielec, A. E. and N. Friis, Polymer Reaction Engineering: An Intensive Short Course on Polymer Production Technology, Vol. 1, McMaster University, 1977.

APPENDICES

APPENDIX I

Results of Conductometric Titration

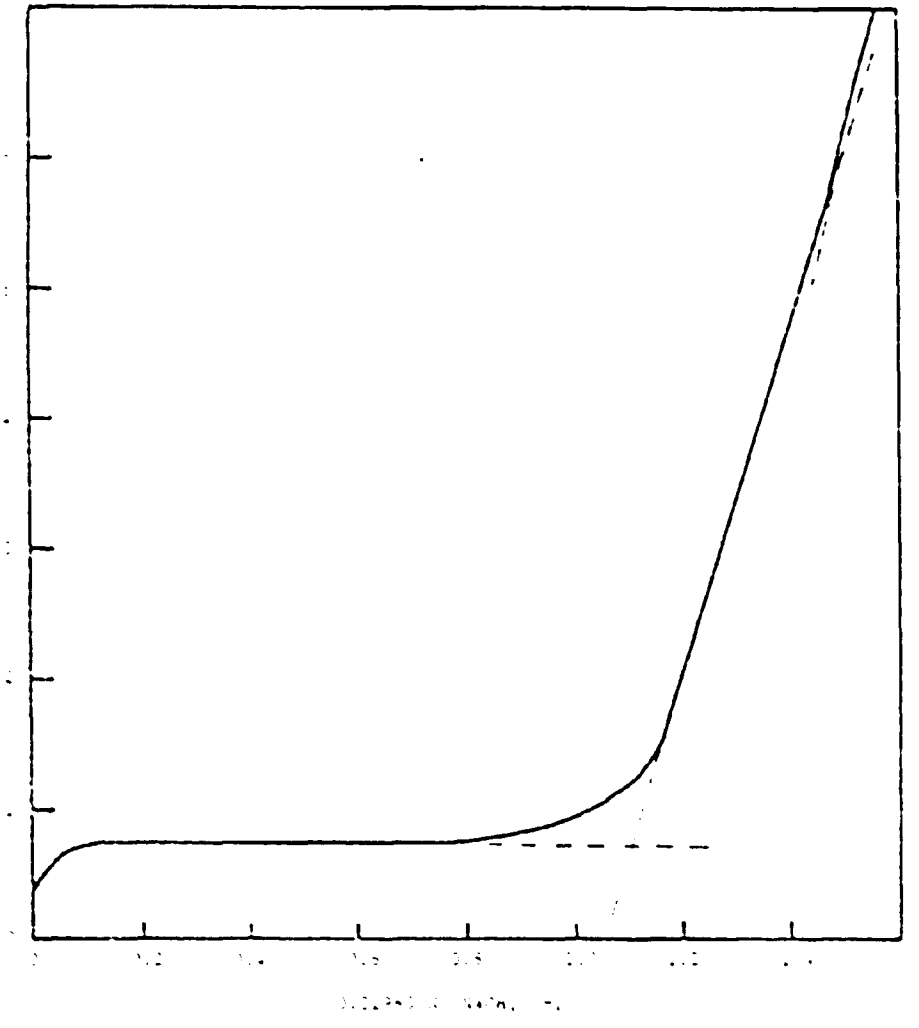

Figure I-A.1 Conductometric titration of SA-2 after 2 ion exchange cycles.

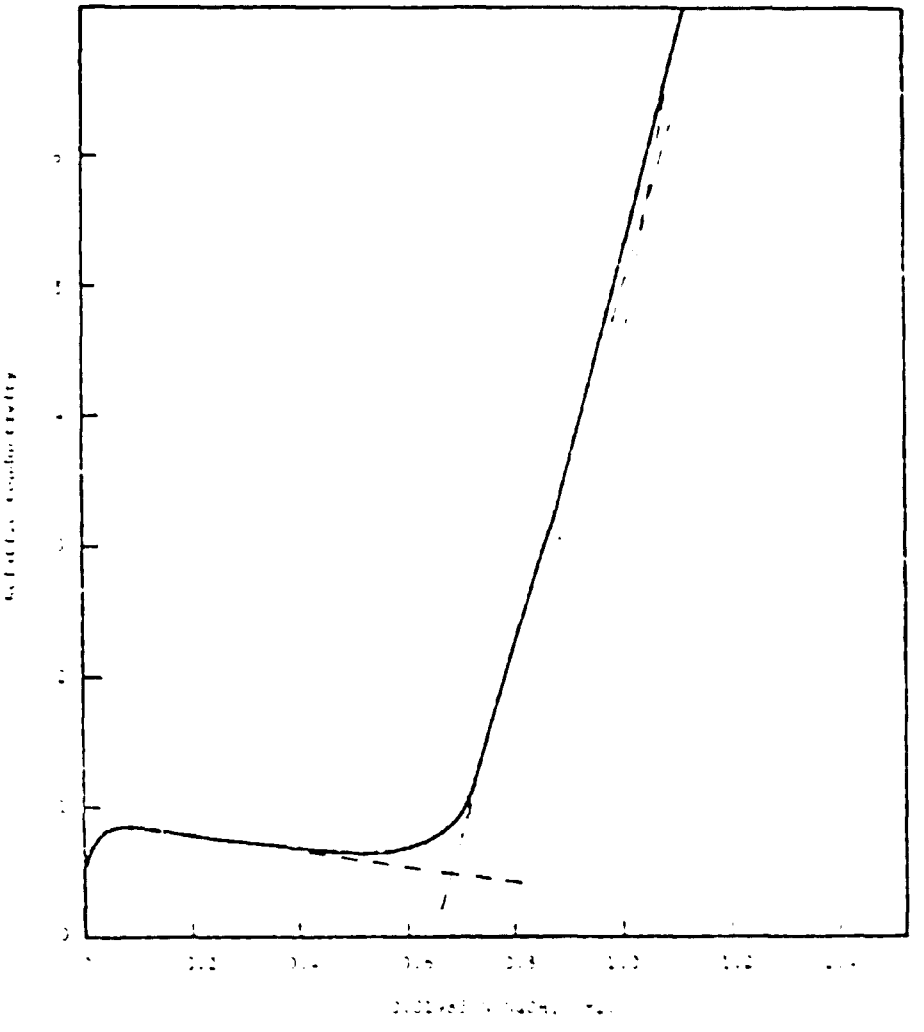

Figure I-A.2 Conductometric titration of SA-1 after 2 ion excnange cycles.

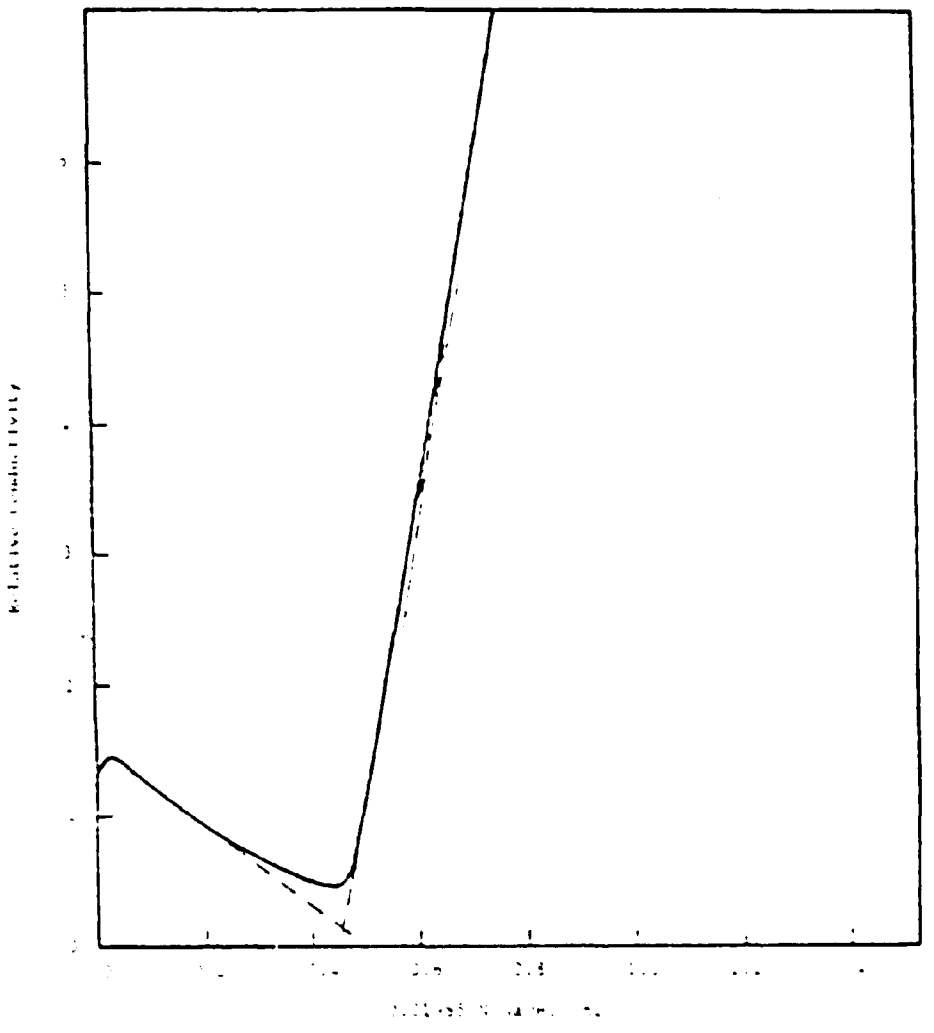

Figure I-A.3 Conductometric titration of SA-13 after 2 ion exchange cycles.

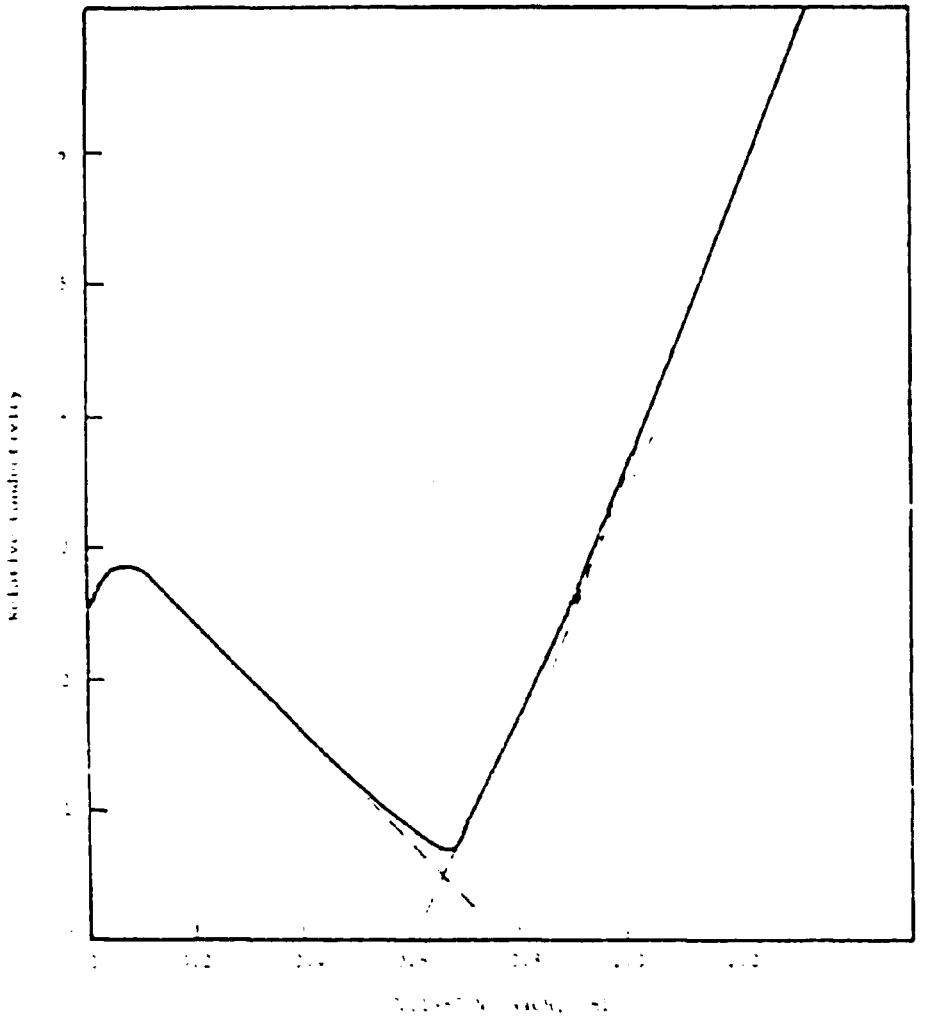

Figure I-A.4 Conductometric titration of SA-14 after 2 ion exchange cycles.

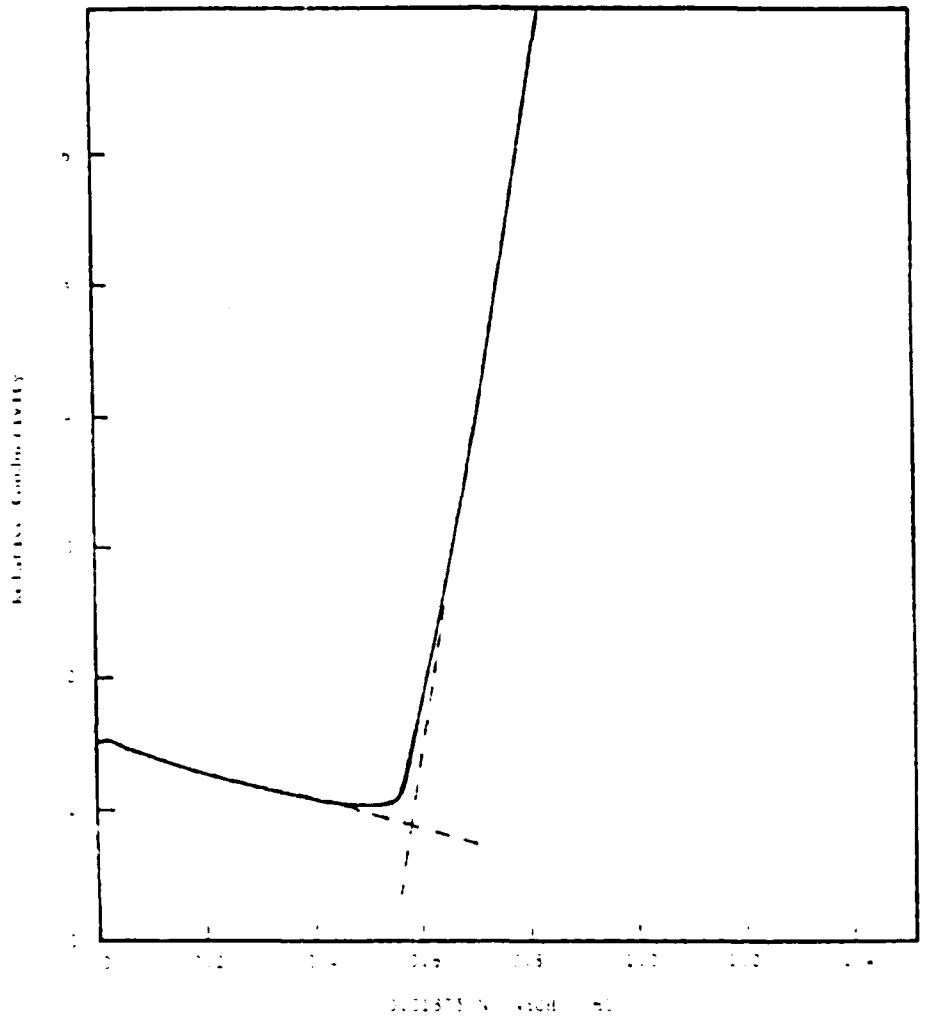

Figure I-A.5 Conductometric titration of SA-23 after 4 ion exchange cycles.

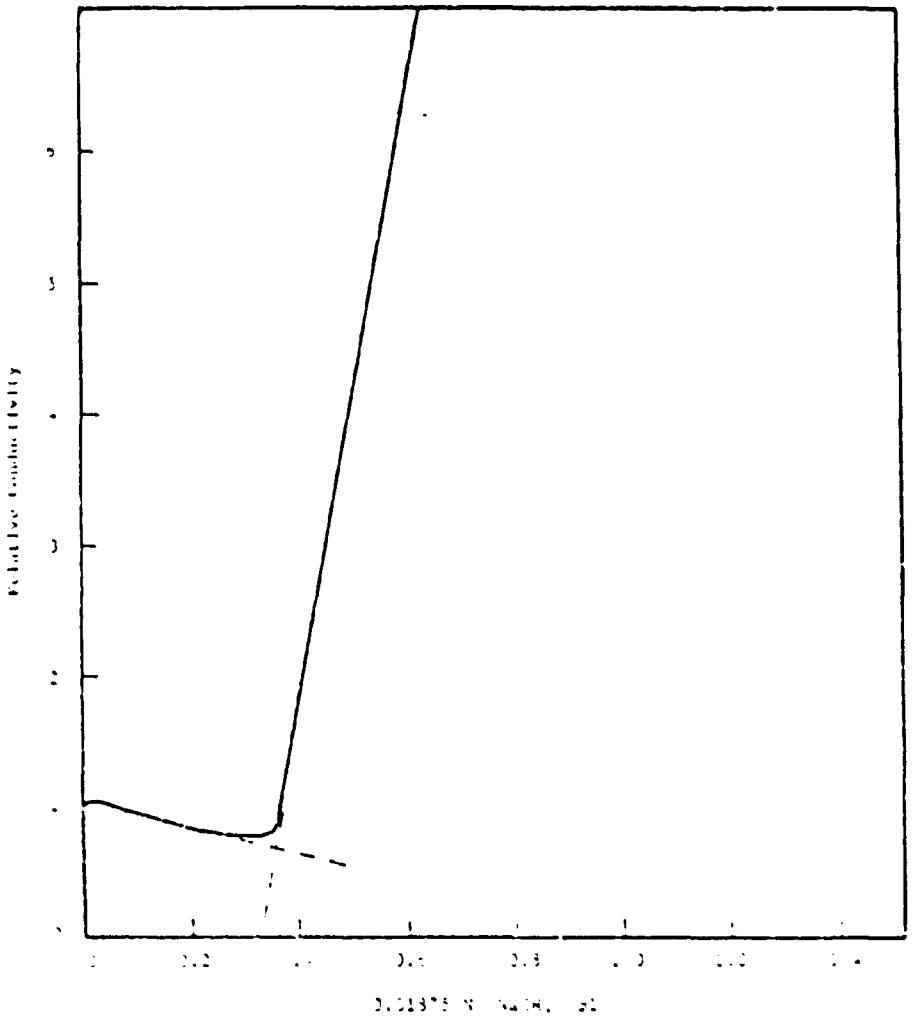

Figure I-A.6 Conductometric titration of SA-29 after 4 ion exchange cycles.

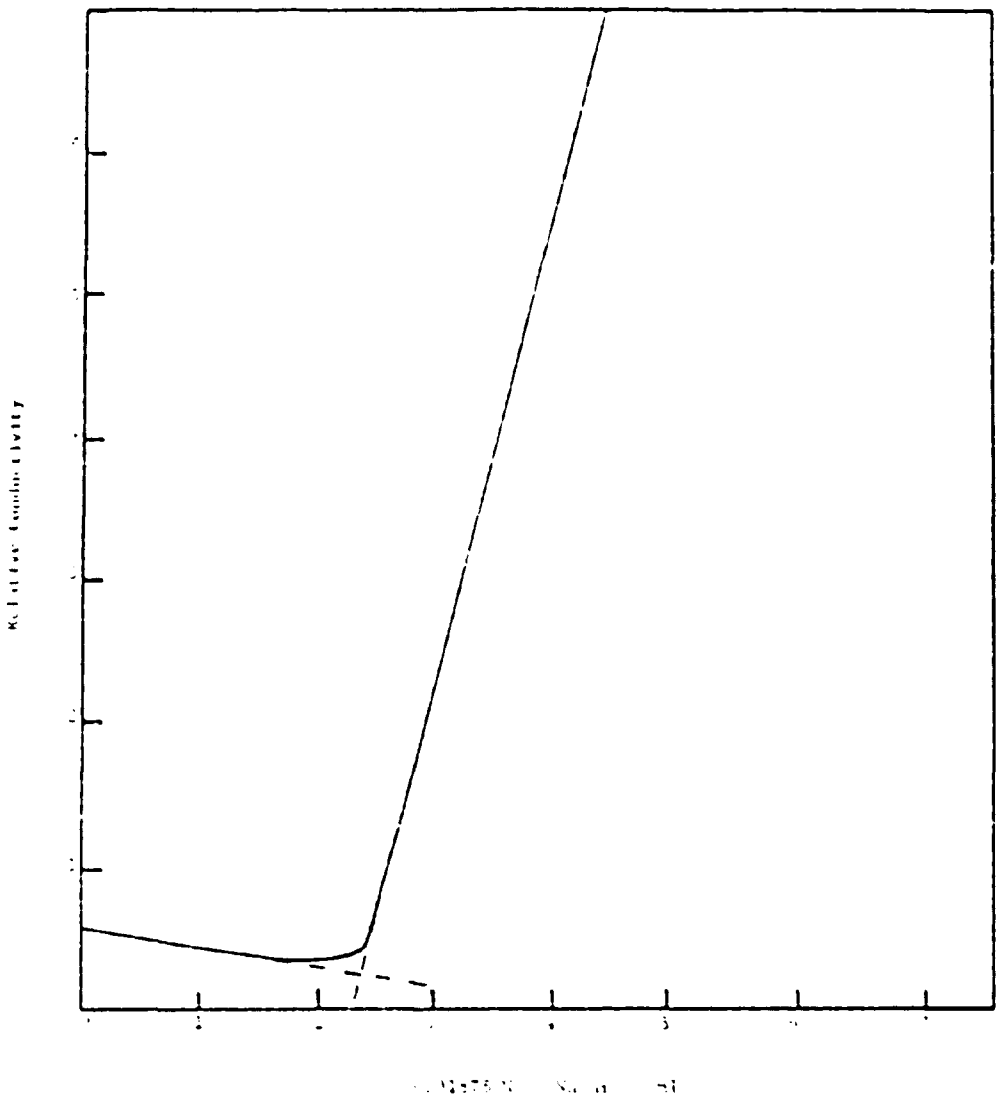

Figure I-A.7 Conductometric titration of SA-30 after 6 ion exchange cycles.

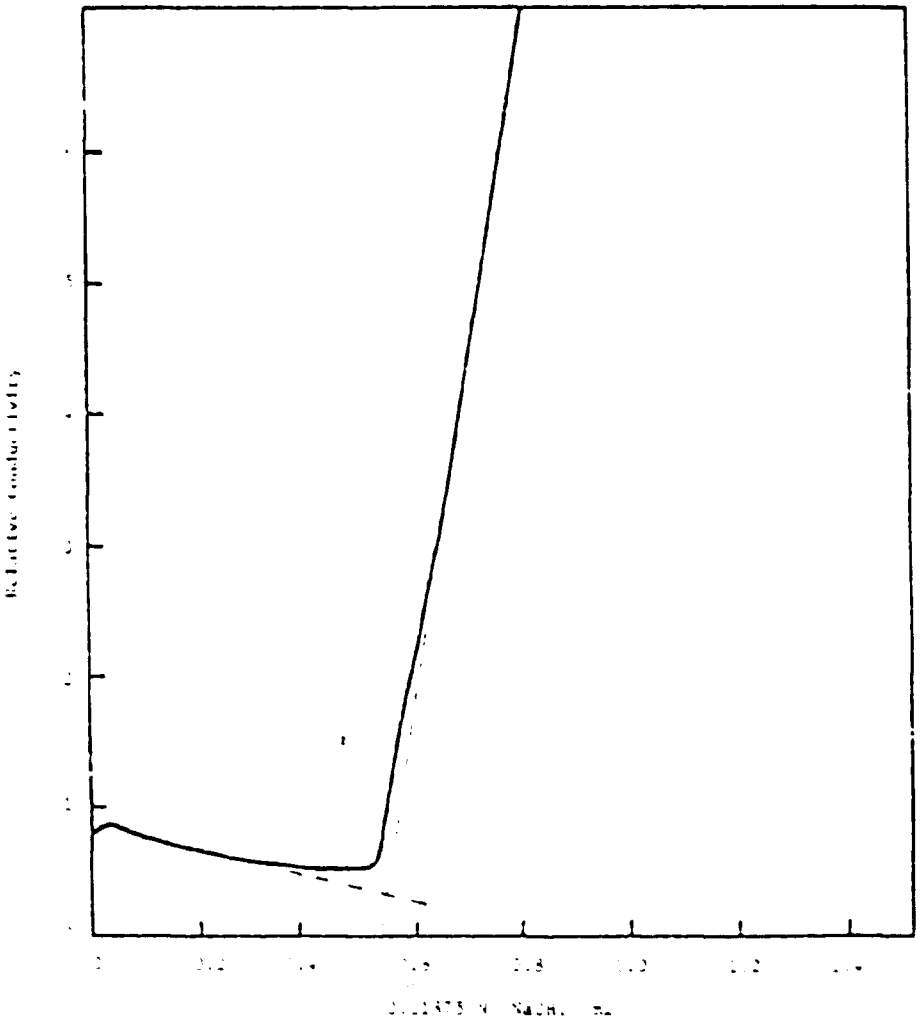

Figure I-A.8 Conductometric titration of SA-31 after 6 ion exchange cycles.

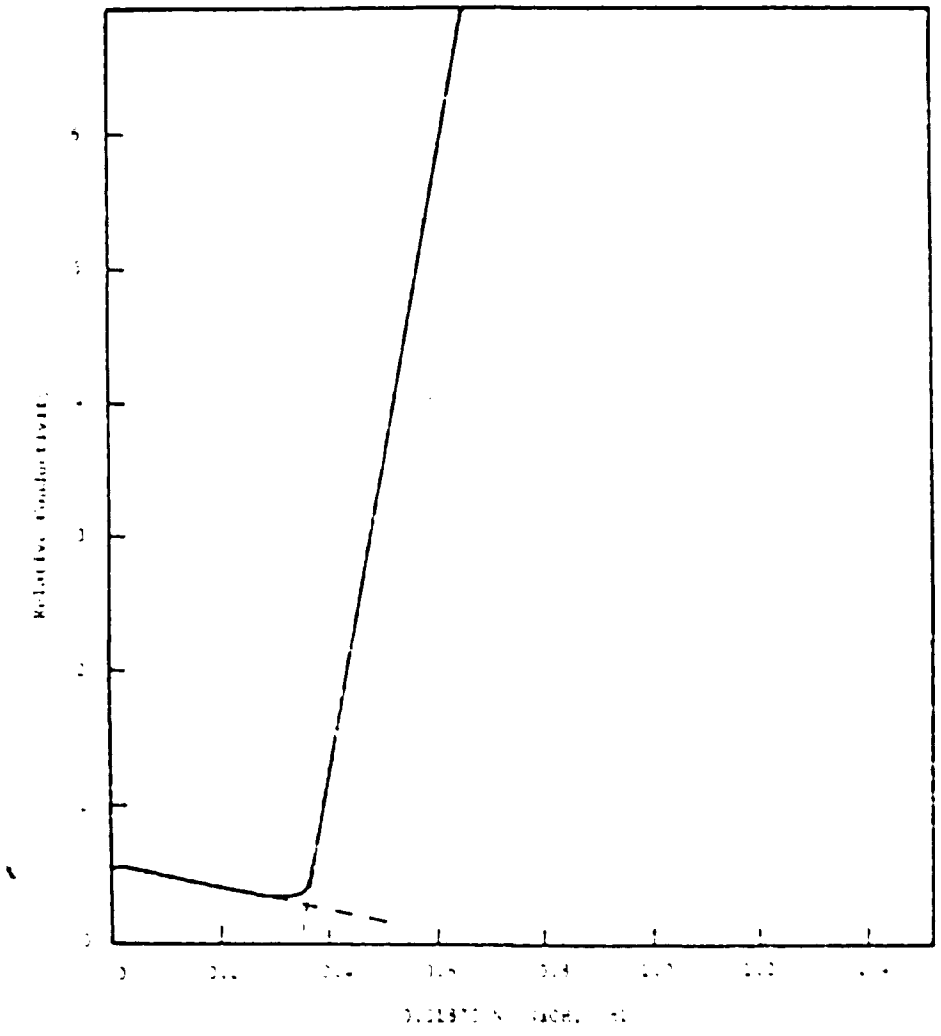

Figure I-A.9 Conductometric titration of SA-32 after 6 ion exchange cycles.

APPENDIX II

Results of Stability Analysis

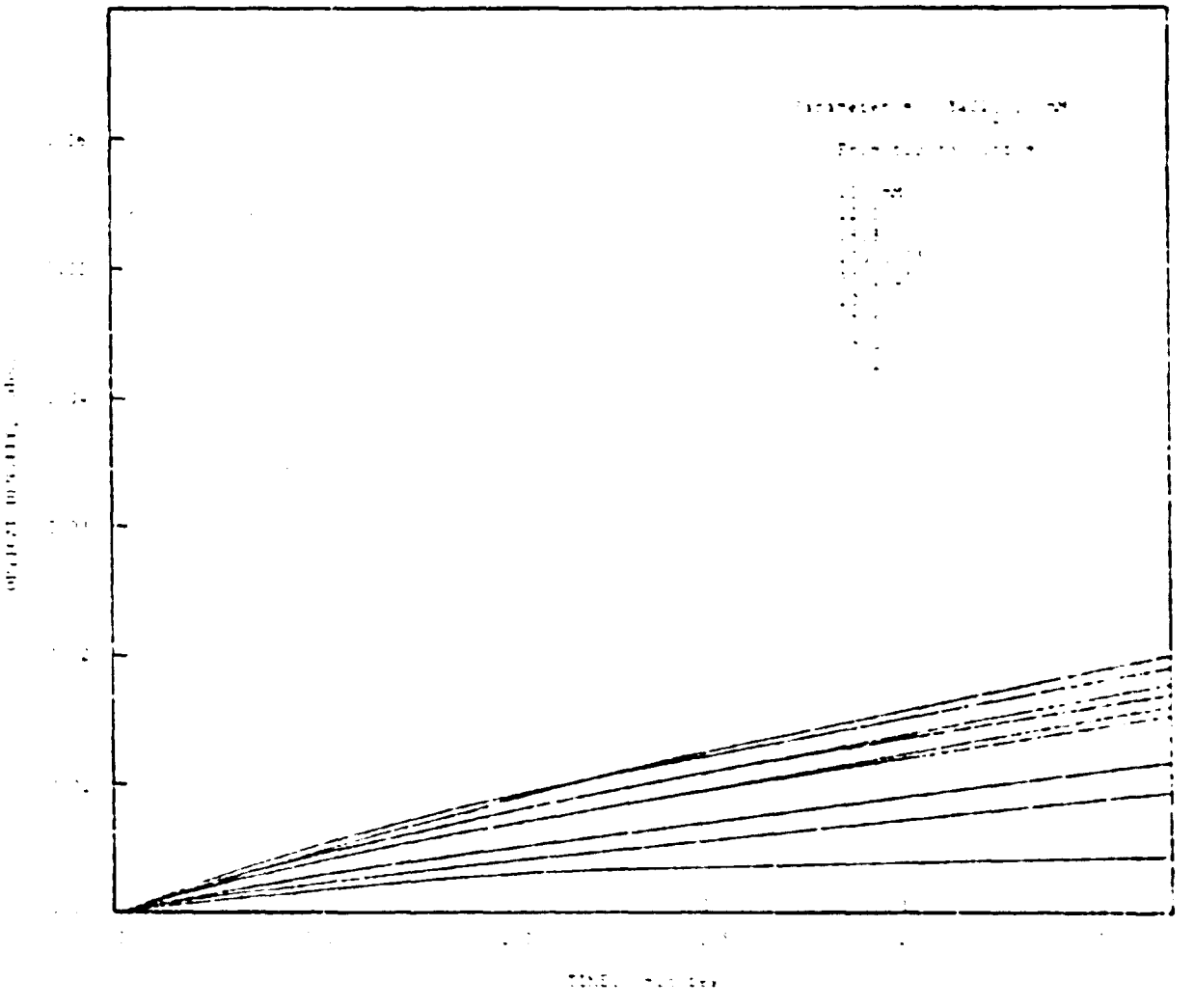

Figure II-A.1 Optical density-time curves for SA-10.

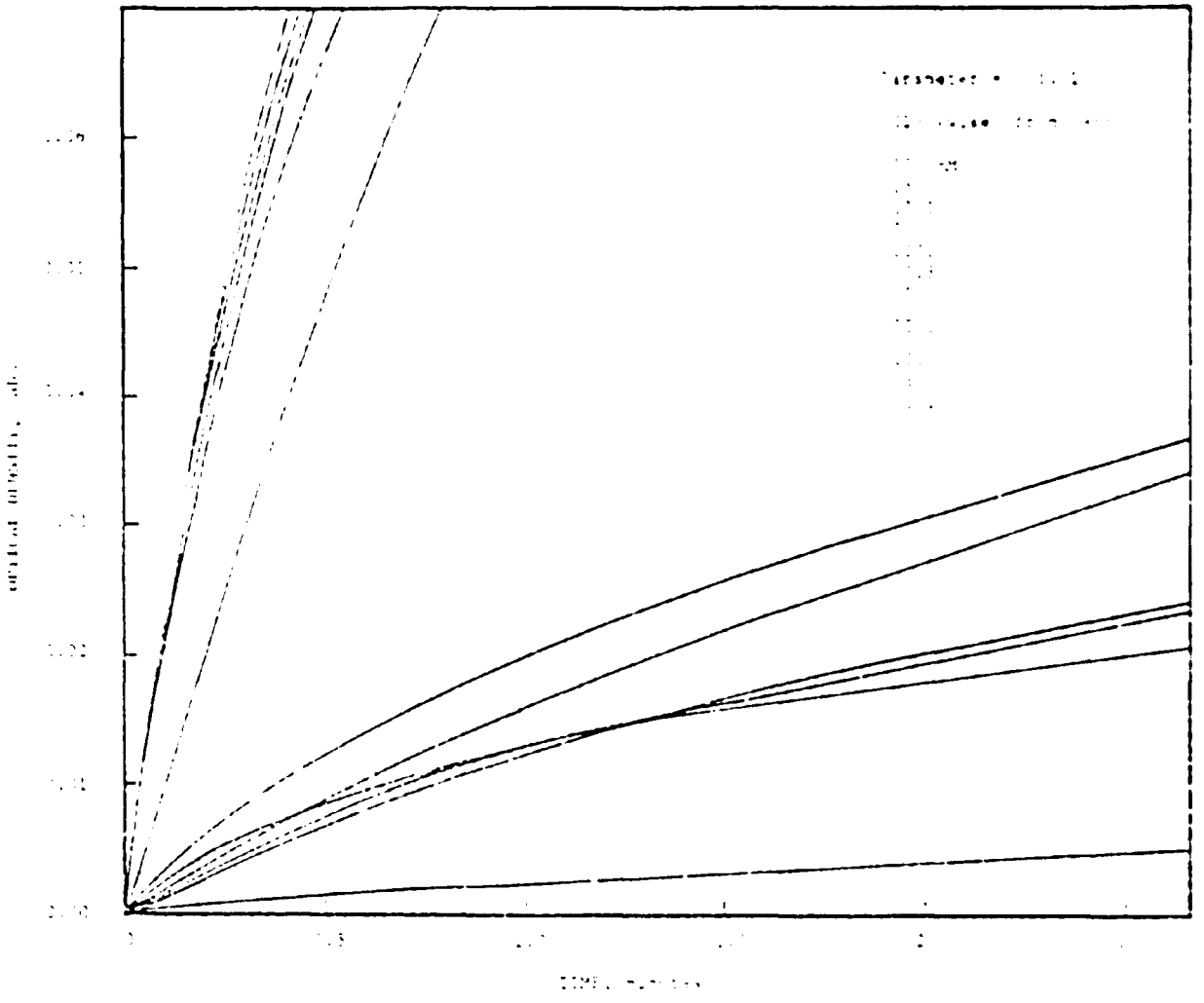

Figure II-A.2 Optical density-time curves for SA-1.

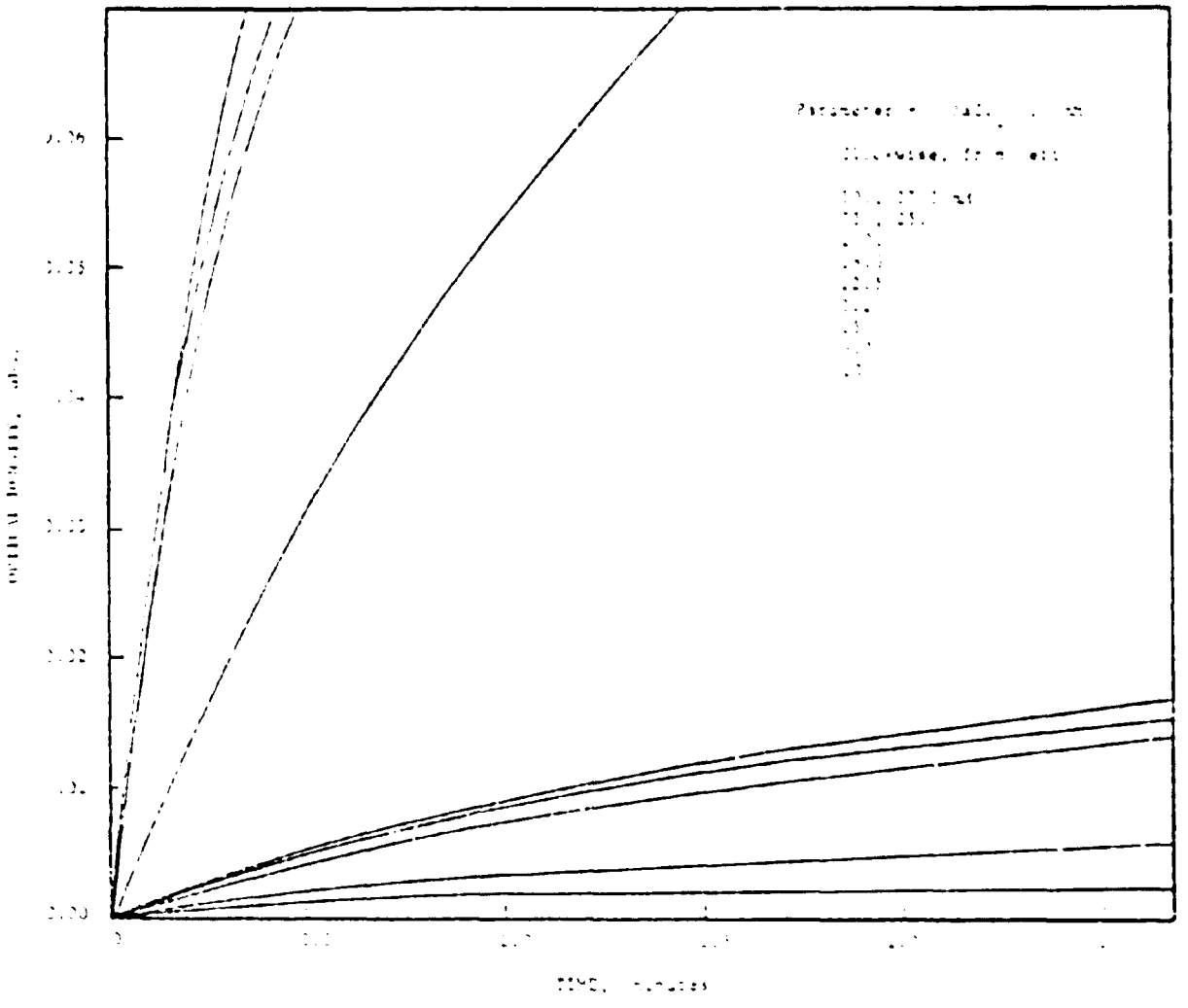

Figure II-A.3 Optical density-time curves for SA-13.

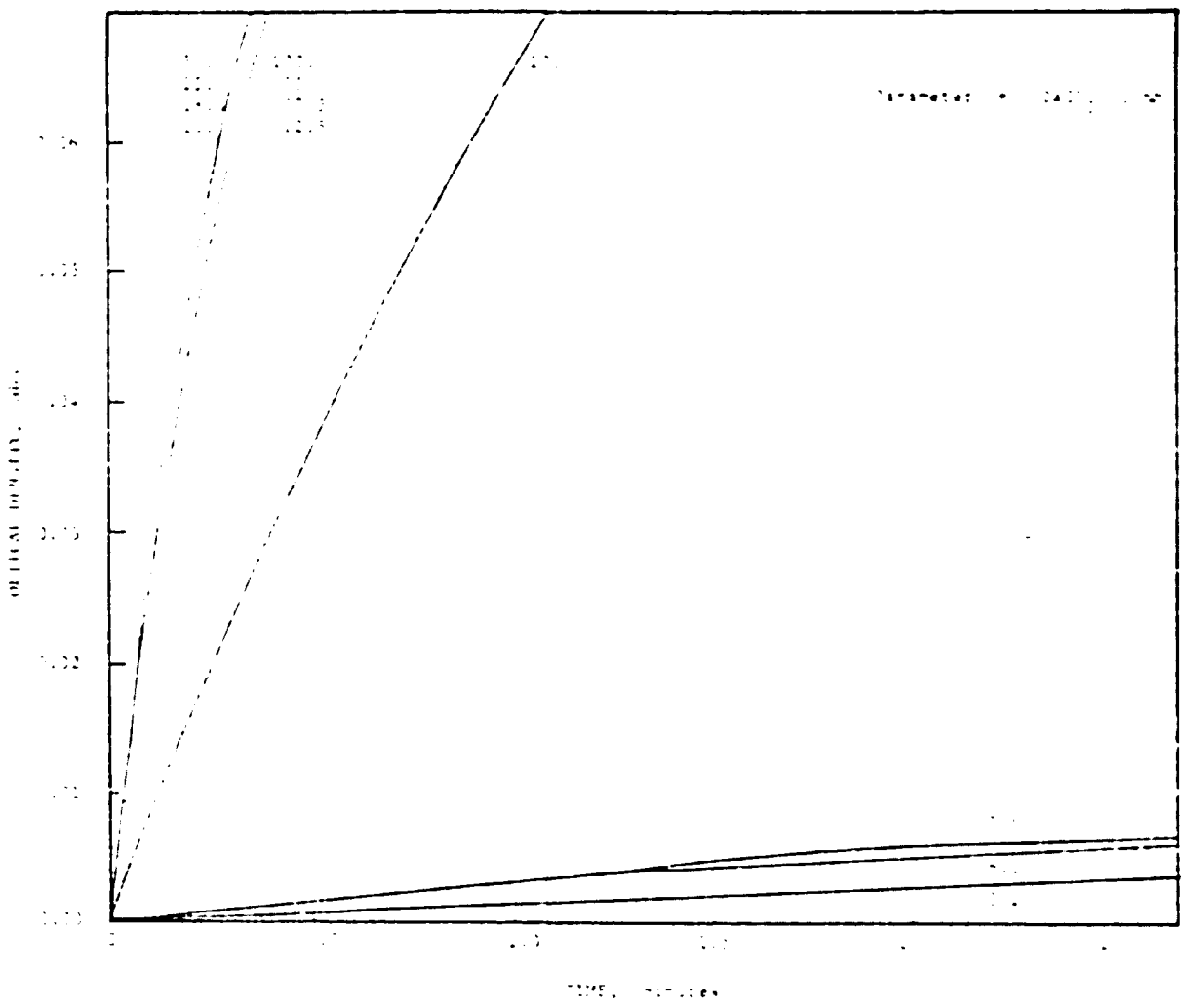

Figure II-A.4 Optical density-time curves for SA-14.

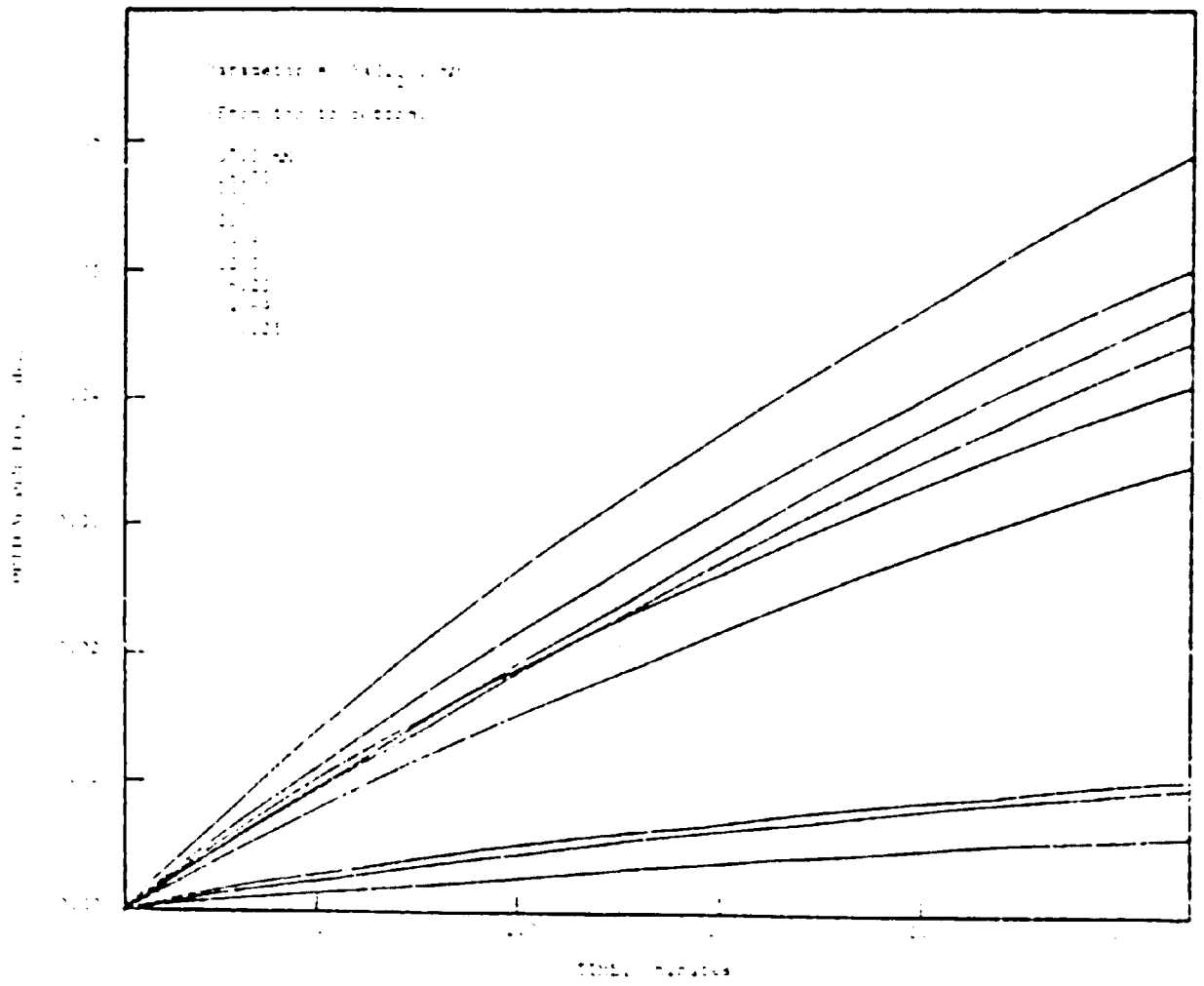

Figure II-A.5 Optical density-time curves for SA-27.

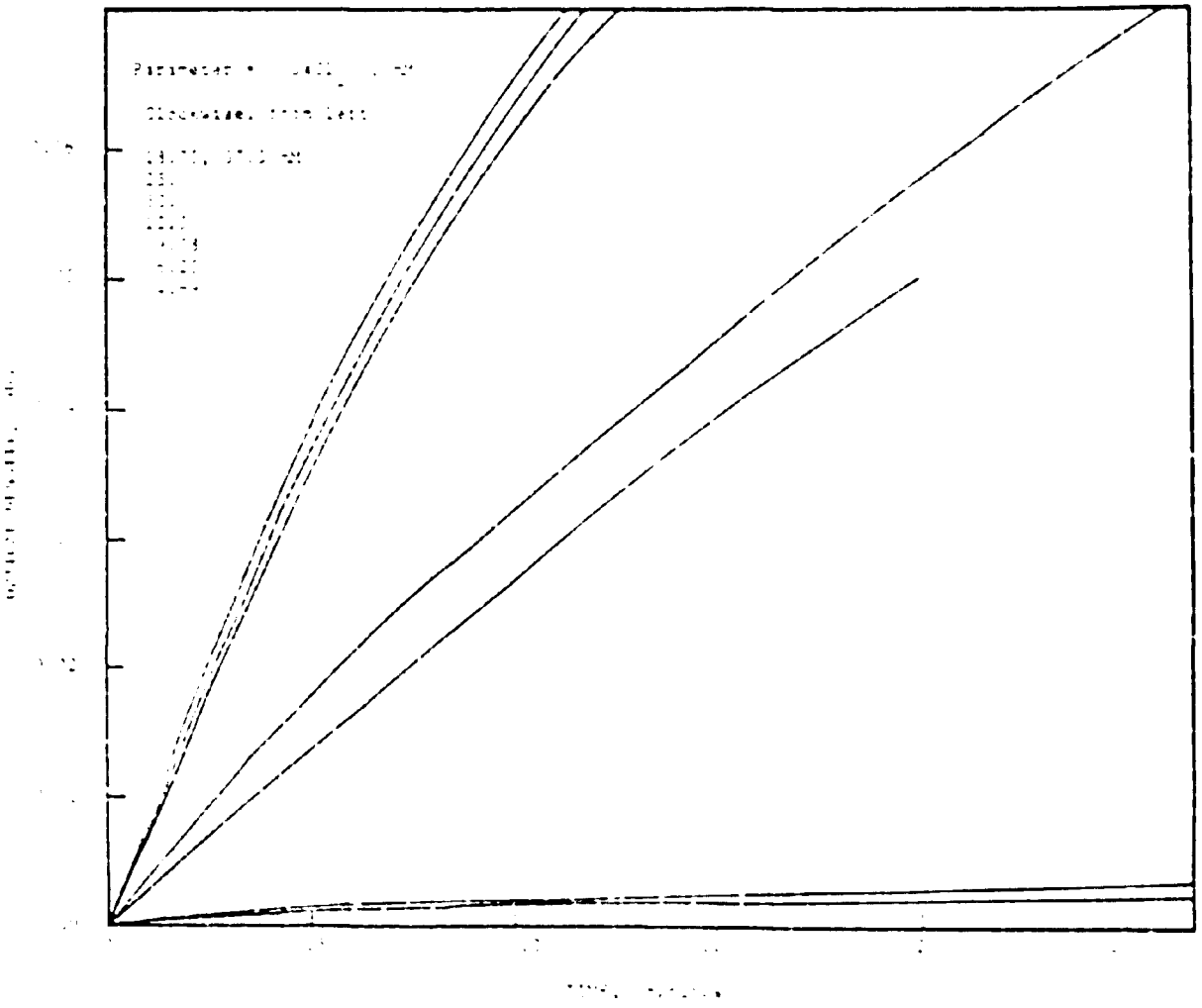

Figure II-A.6 Optical density-time curves for SA-28.

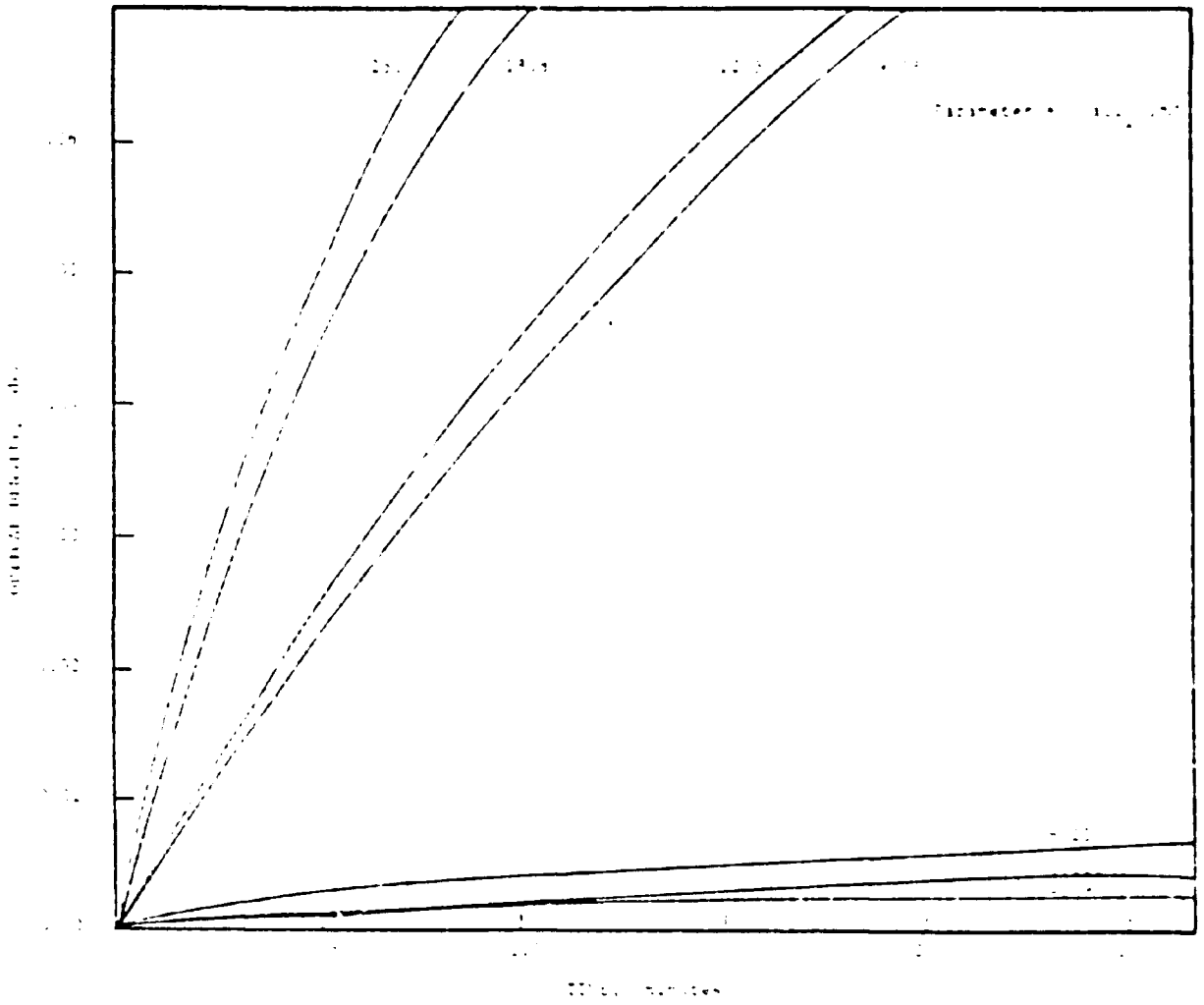

Figure II-A.7 Optical density-time curves for SA-29.

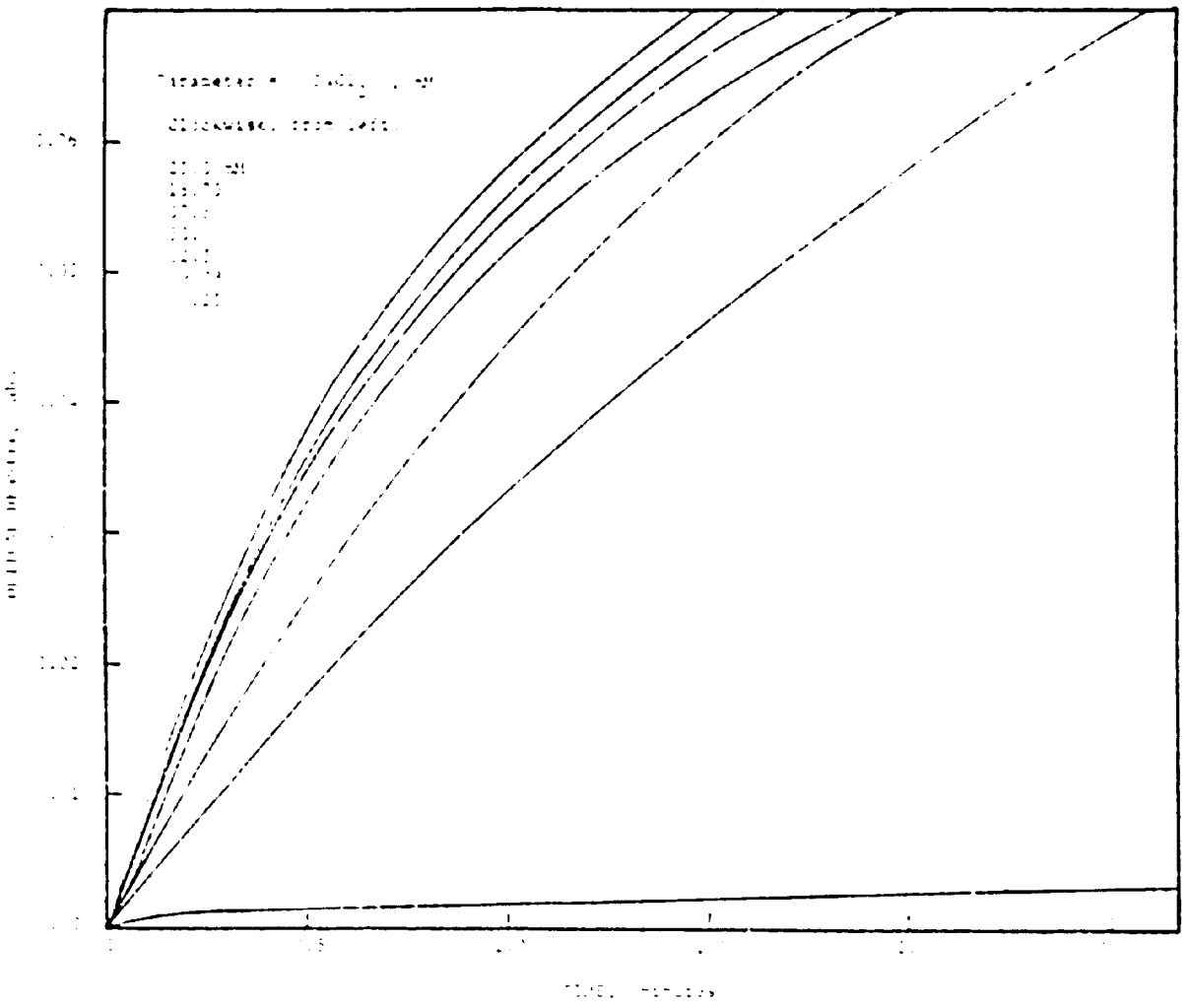

Figure II-A.8 Optical density-time curves for SA-30.

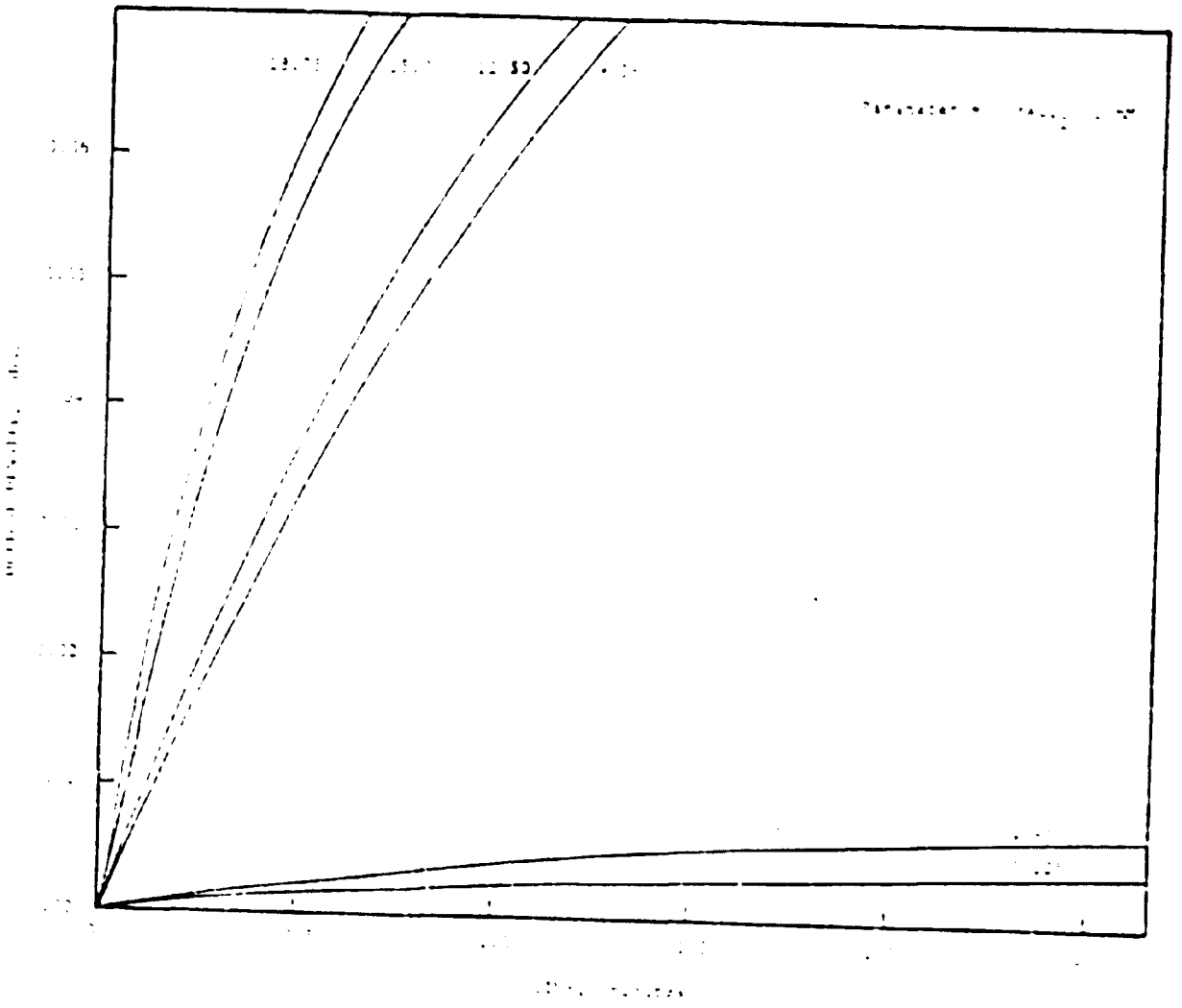

Figure II-A.9 Optical density-time curves for SA-31.

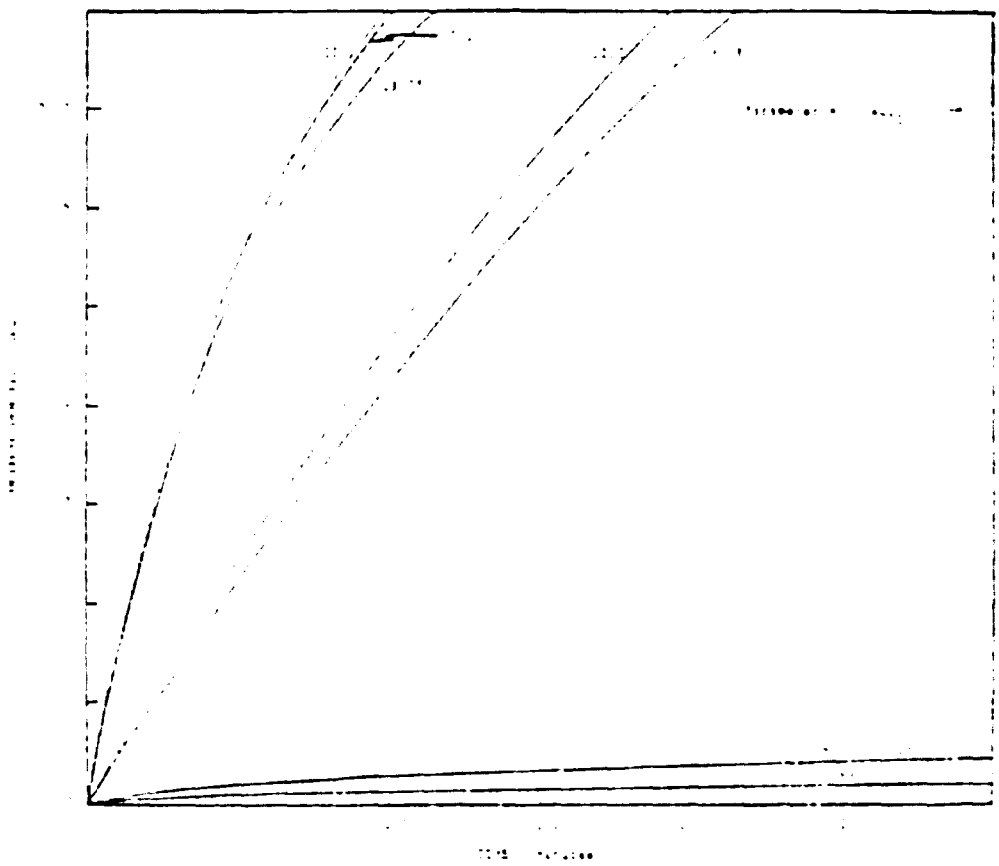

Figure II-A.10 Optical density-time curves for SA-32.

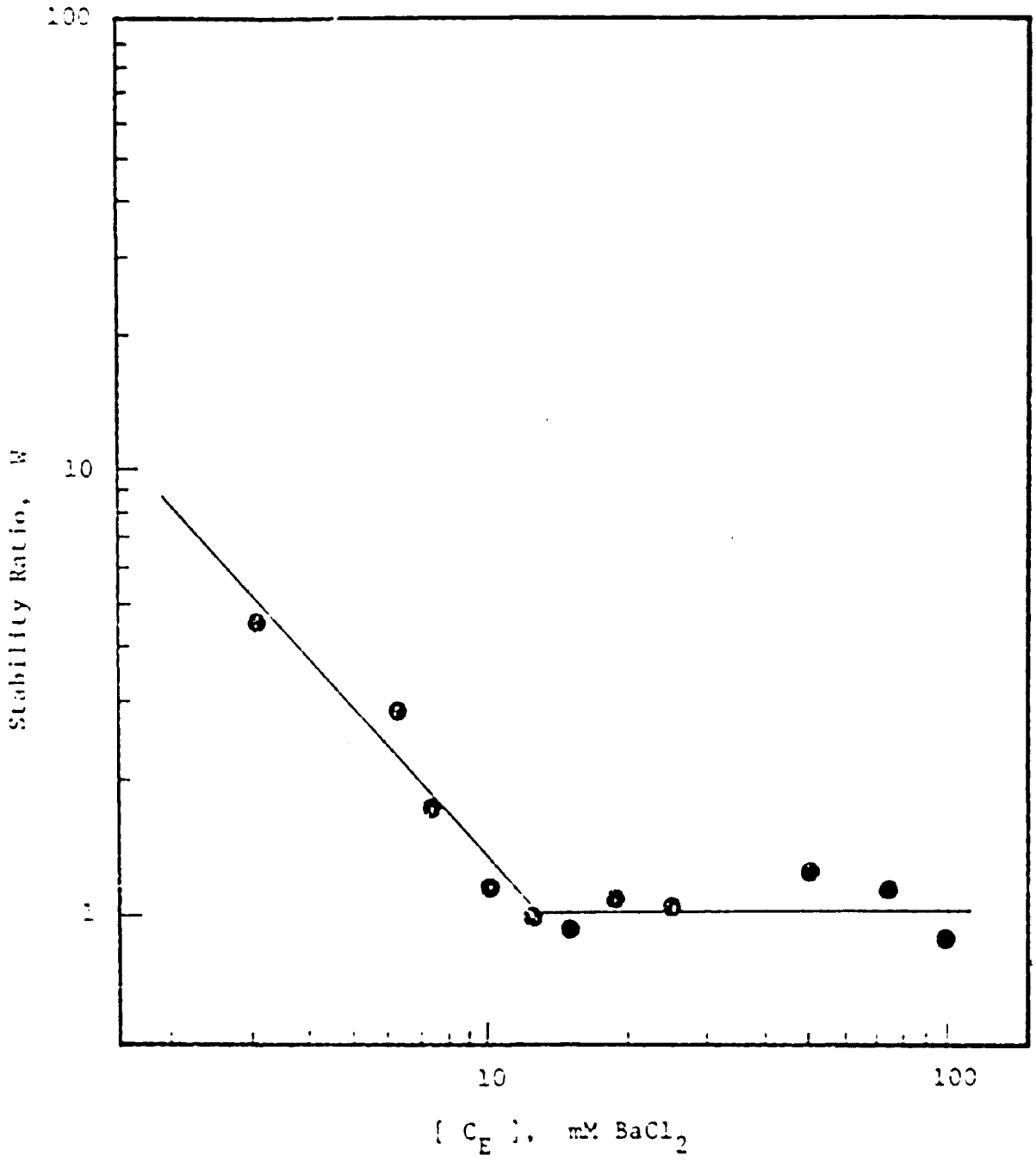

Figure II-A.11 Stability curve for latex SA-10.

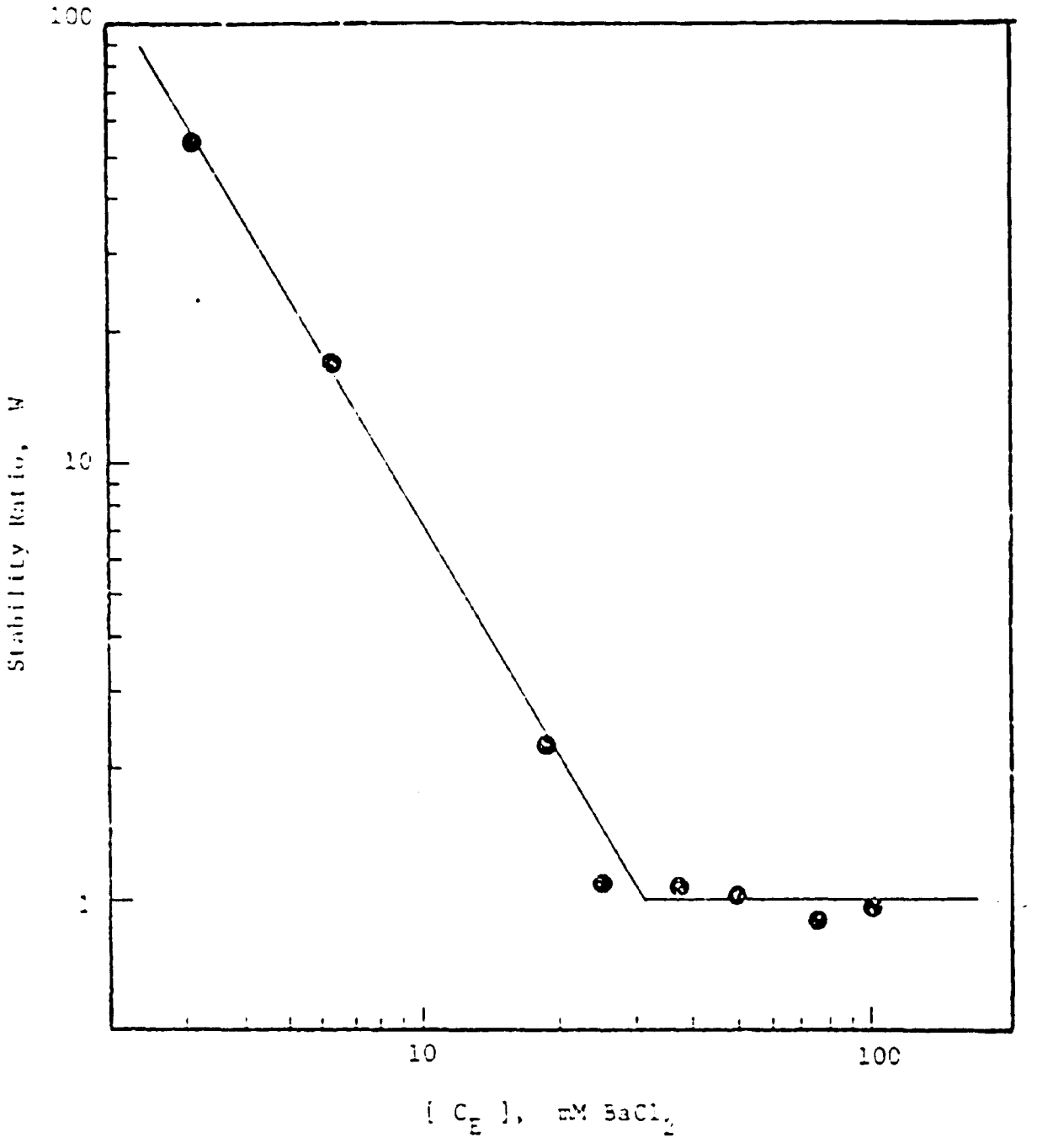

Figure II-A.12 Stability curve for latex SA-1.

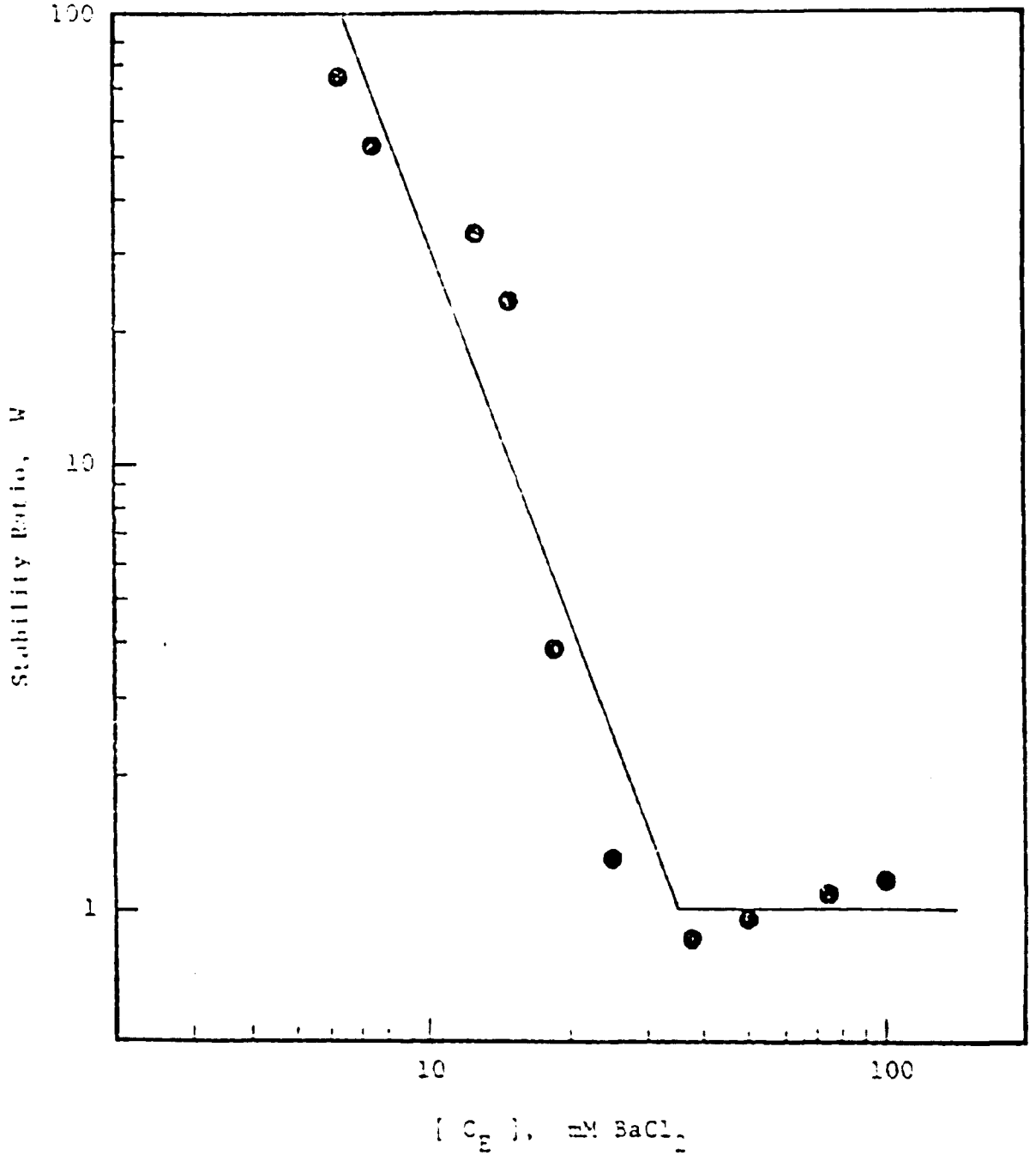

Figure II-A.13 Stability curve for latex SA-13.

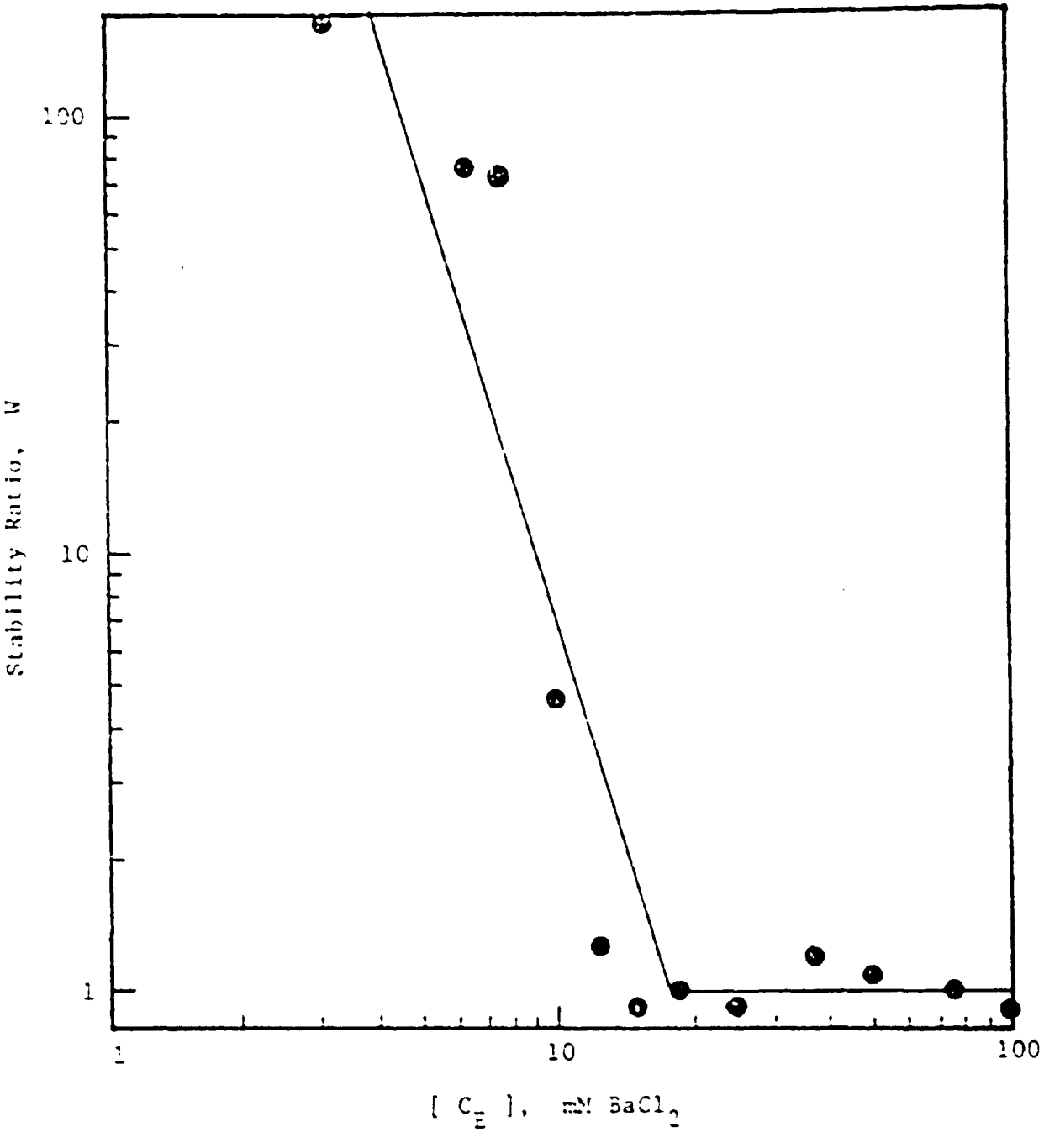

Figure II-A.14 Stability curve for latex SA-14.

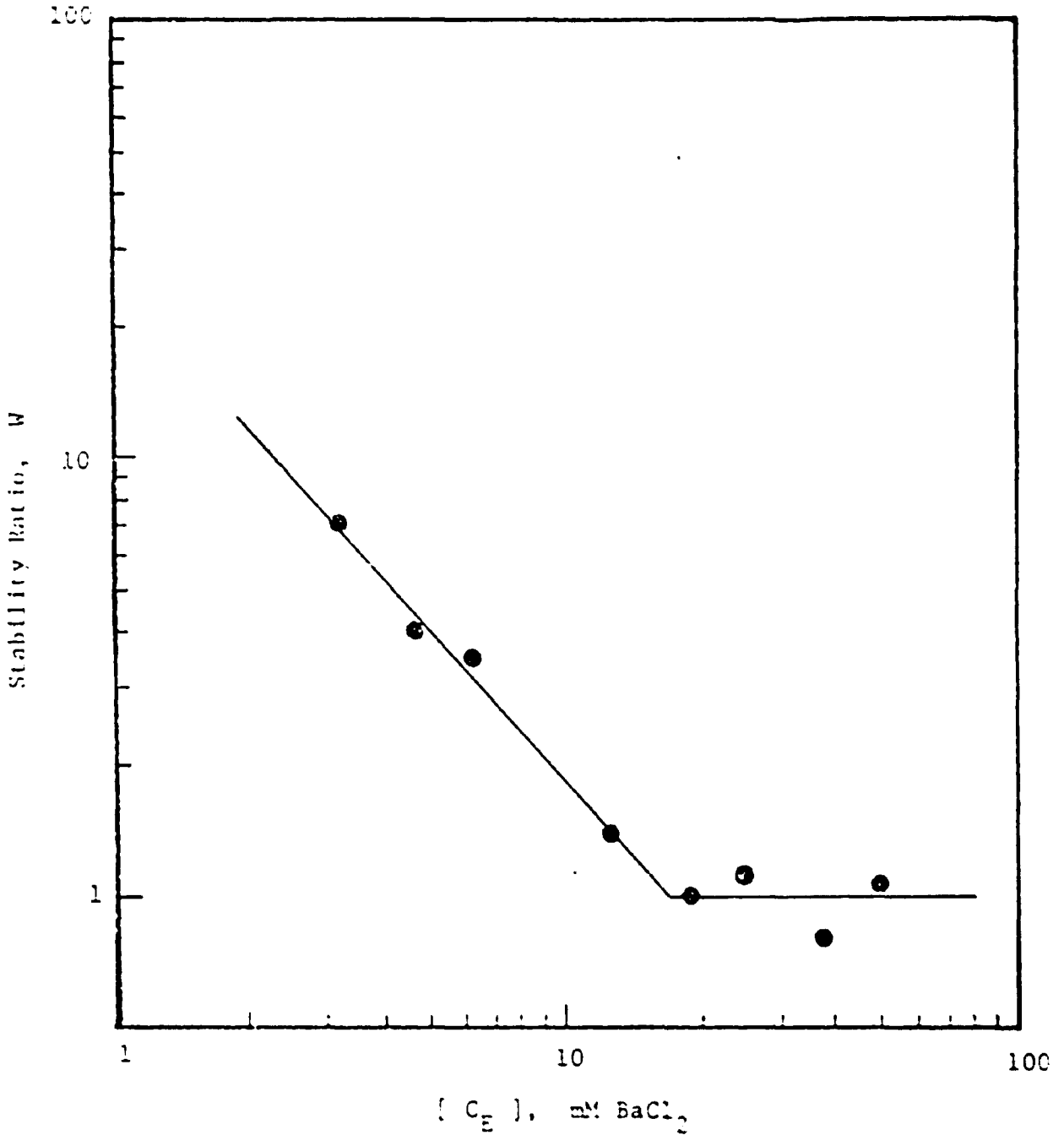

Figure II-A.15 Stability curve for latex SA-27.

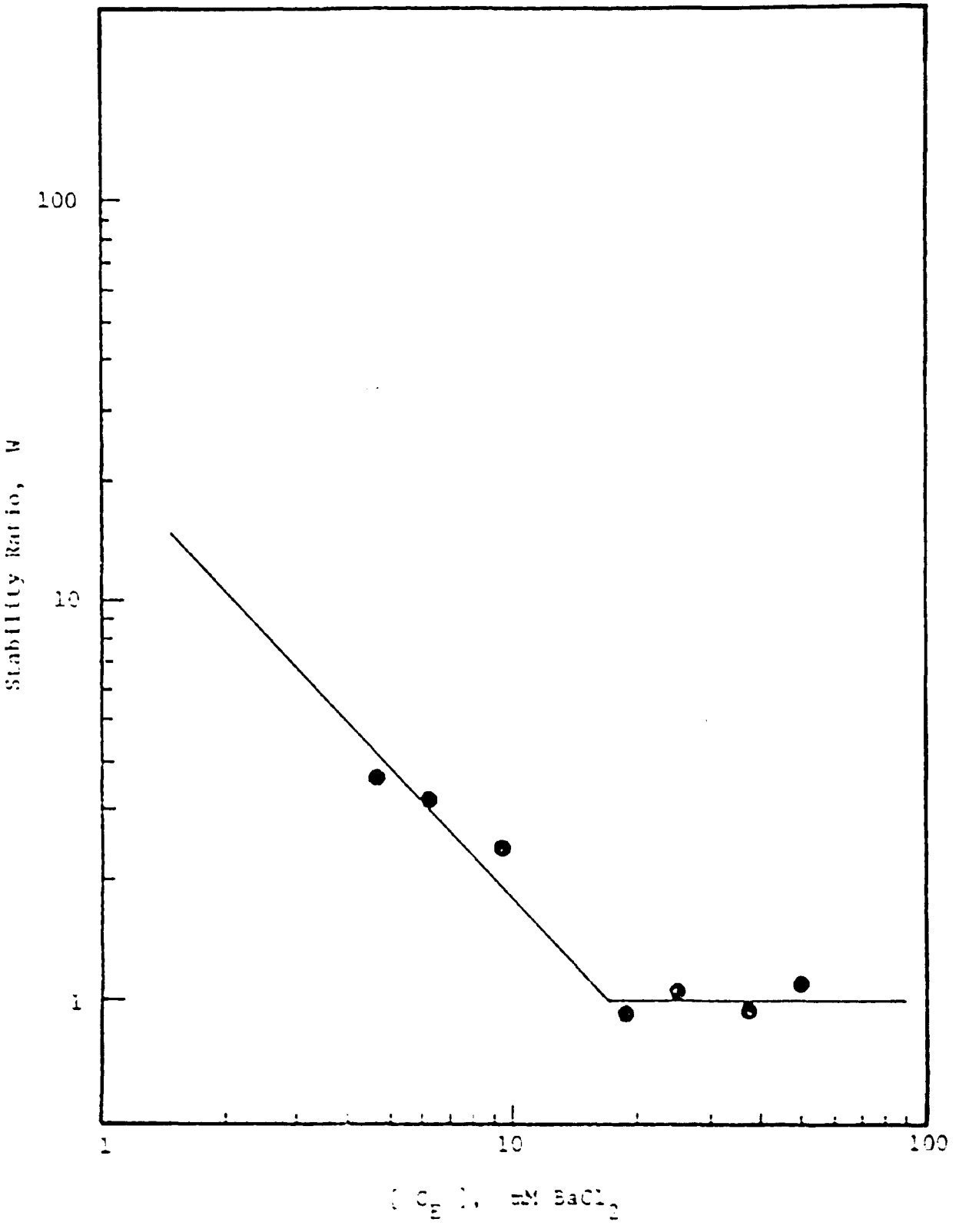

Figure II-A.16 Stability curve for latex SA-28.

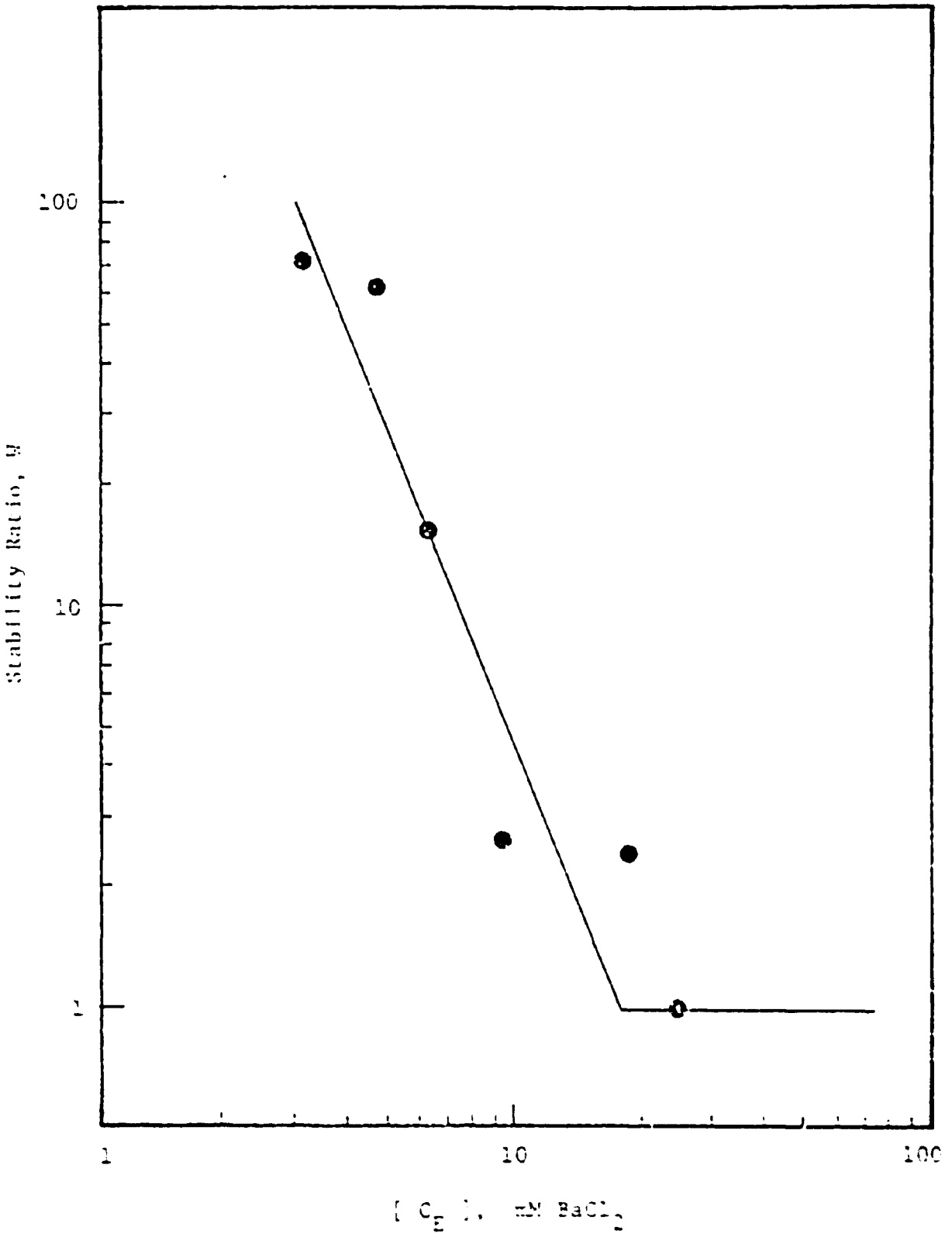

Figure II-A.17 Stability curve for latex SA-29.

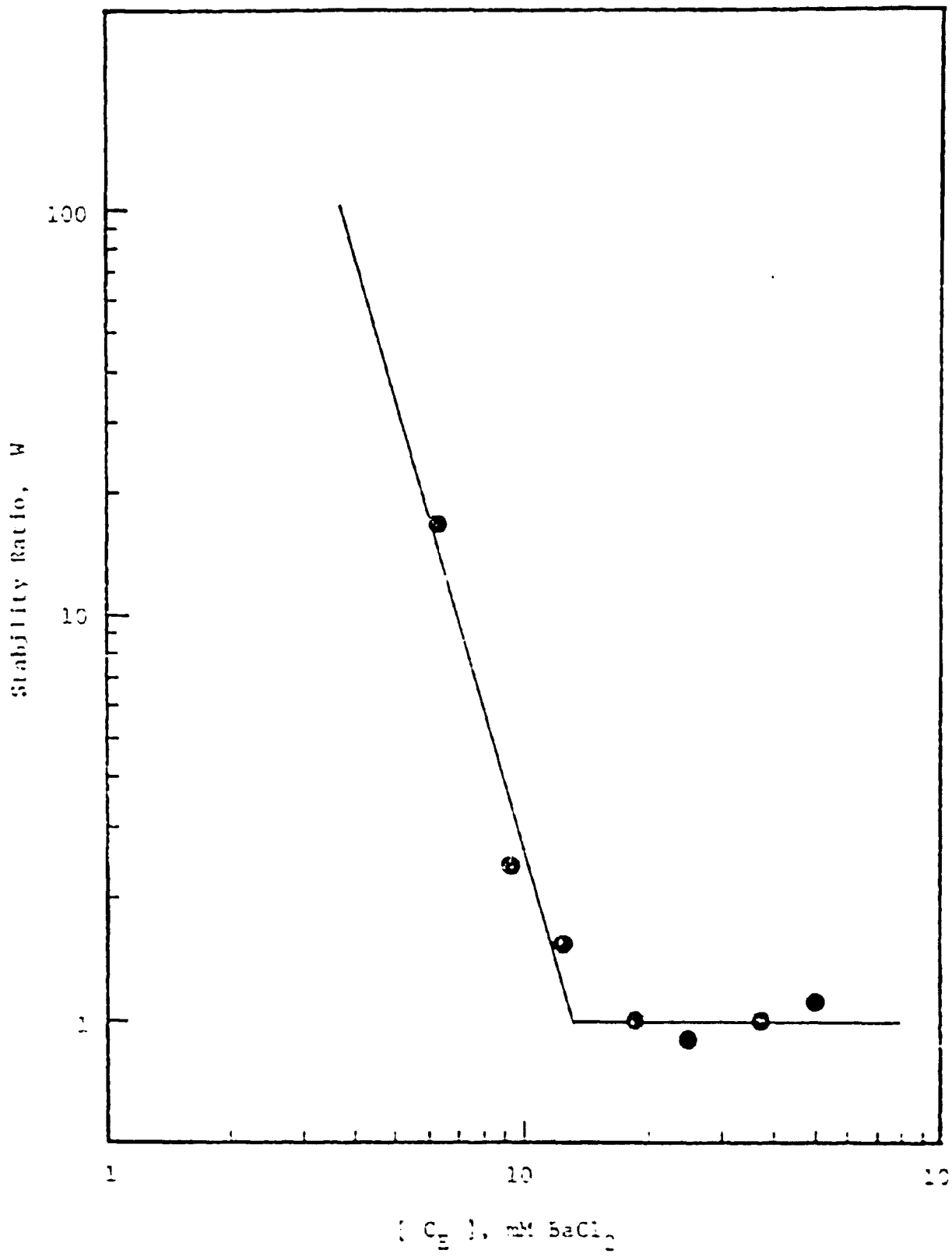

Figure II-A.18 Stability curve for latex SA-30.

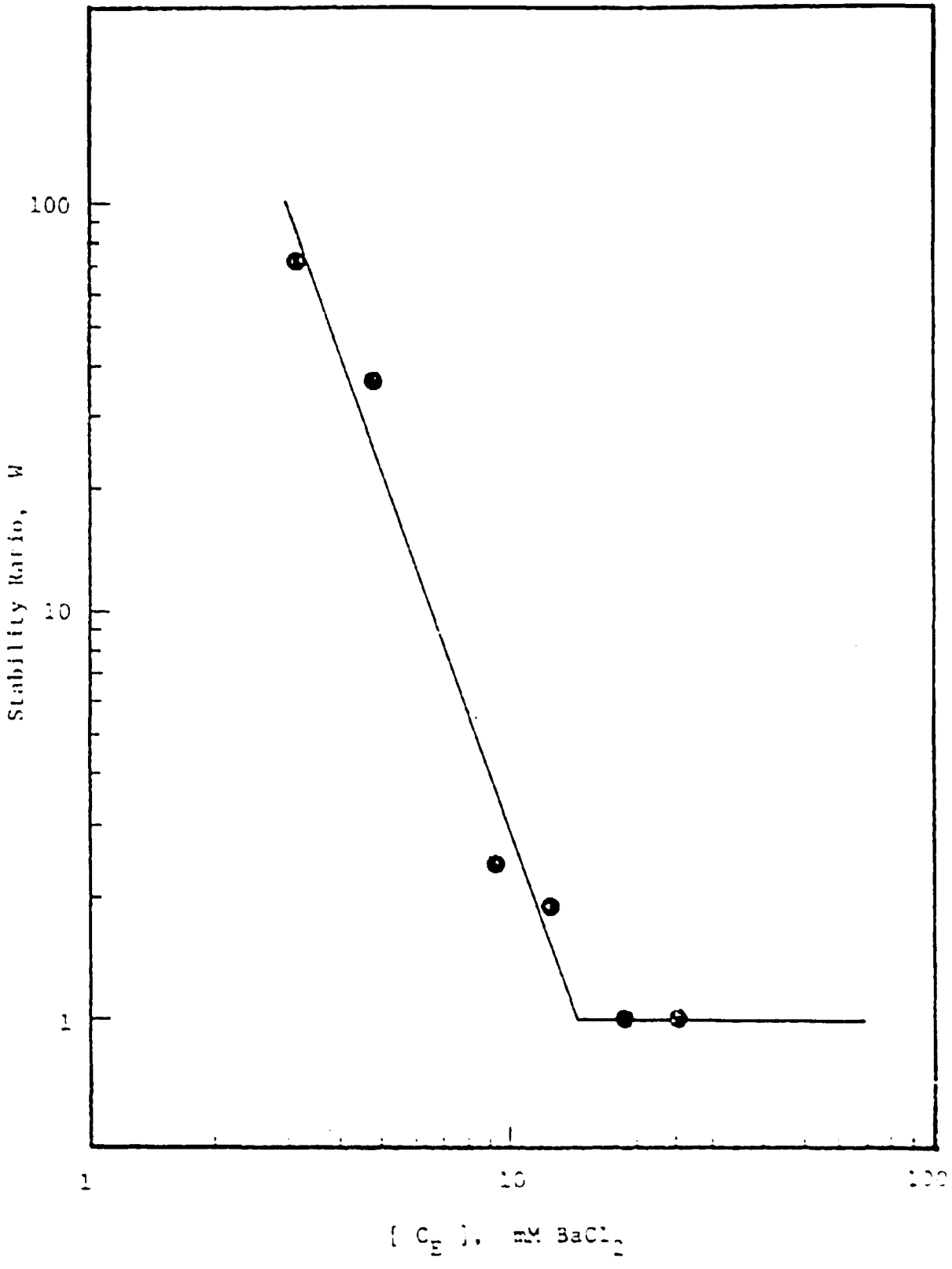

Figure II-A.19 Stability curve for latex SA-31.

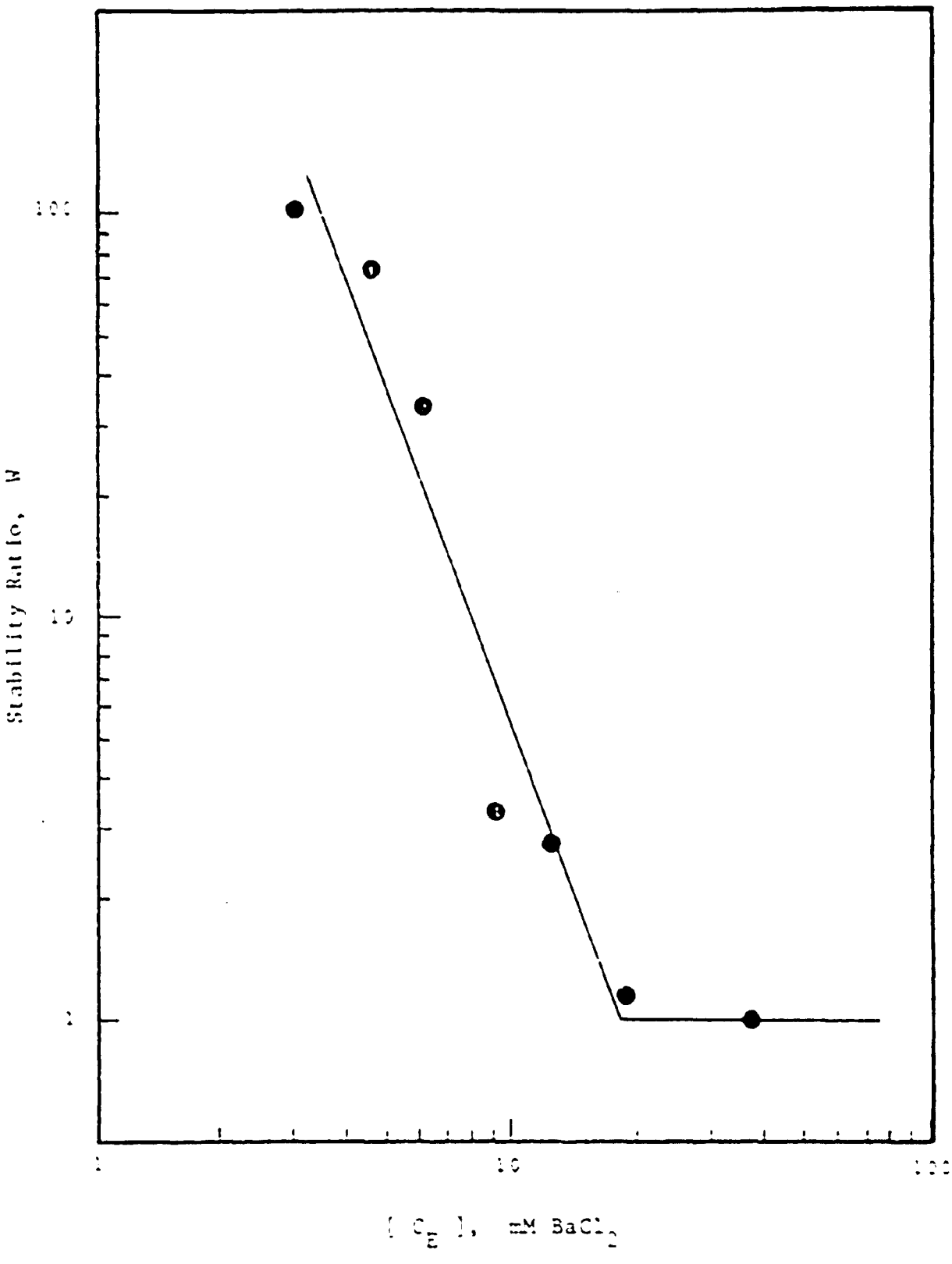

Figure II-A.20 Stability curve for latex SA-32.

APPENDIX III

Results of Molecular Weight Analysis

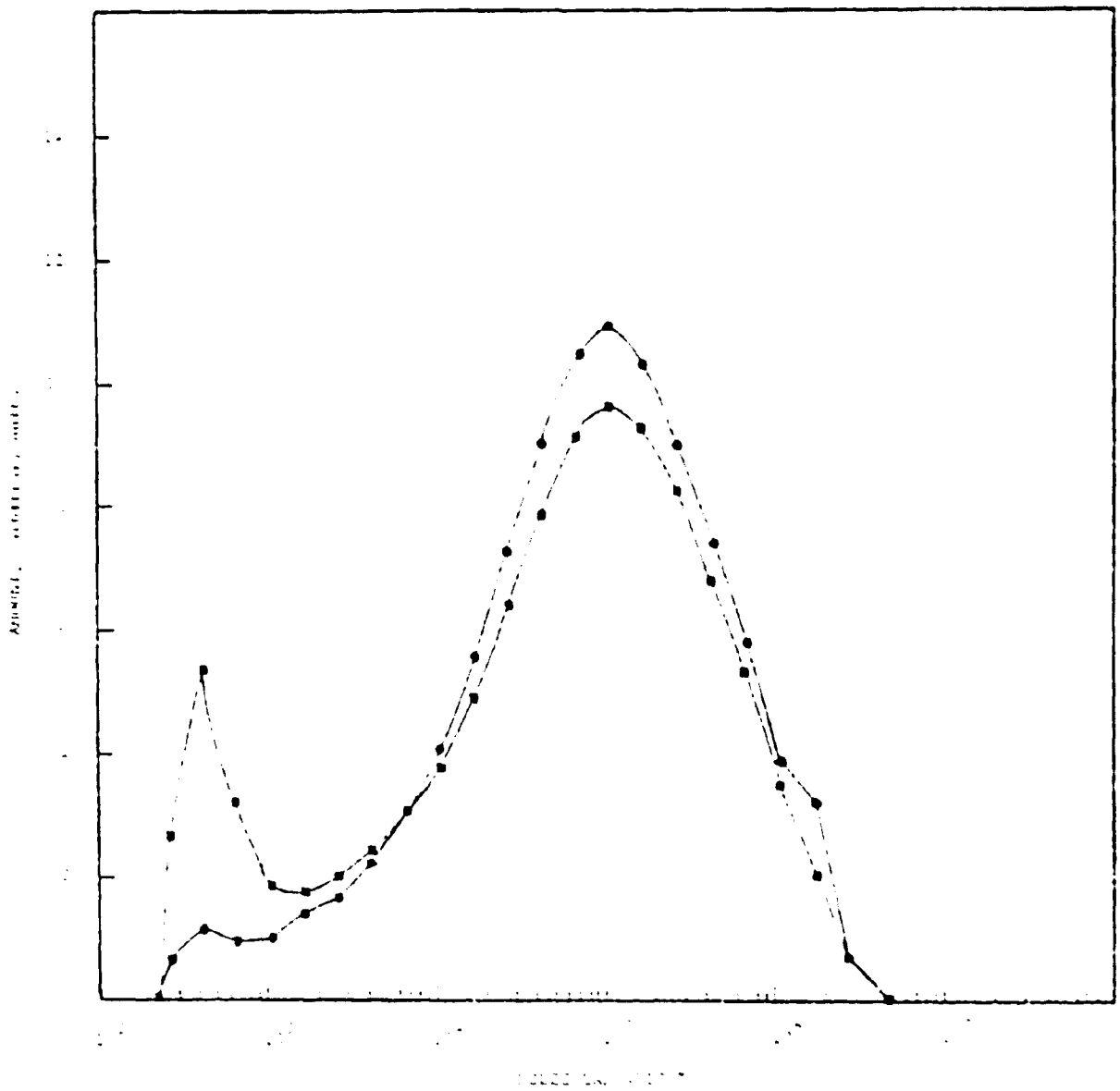

Figure III-A.1 Normalized chromatogram of SA-28 before (●) and after (■) ion exchange.

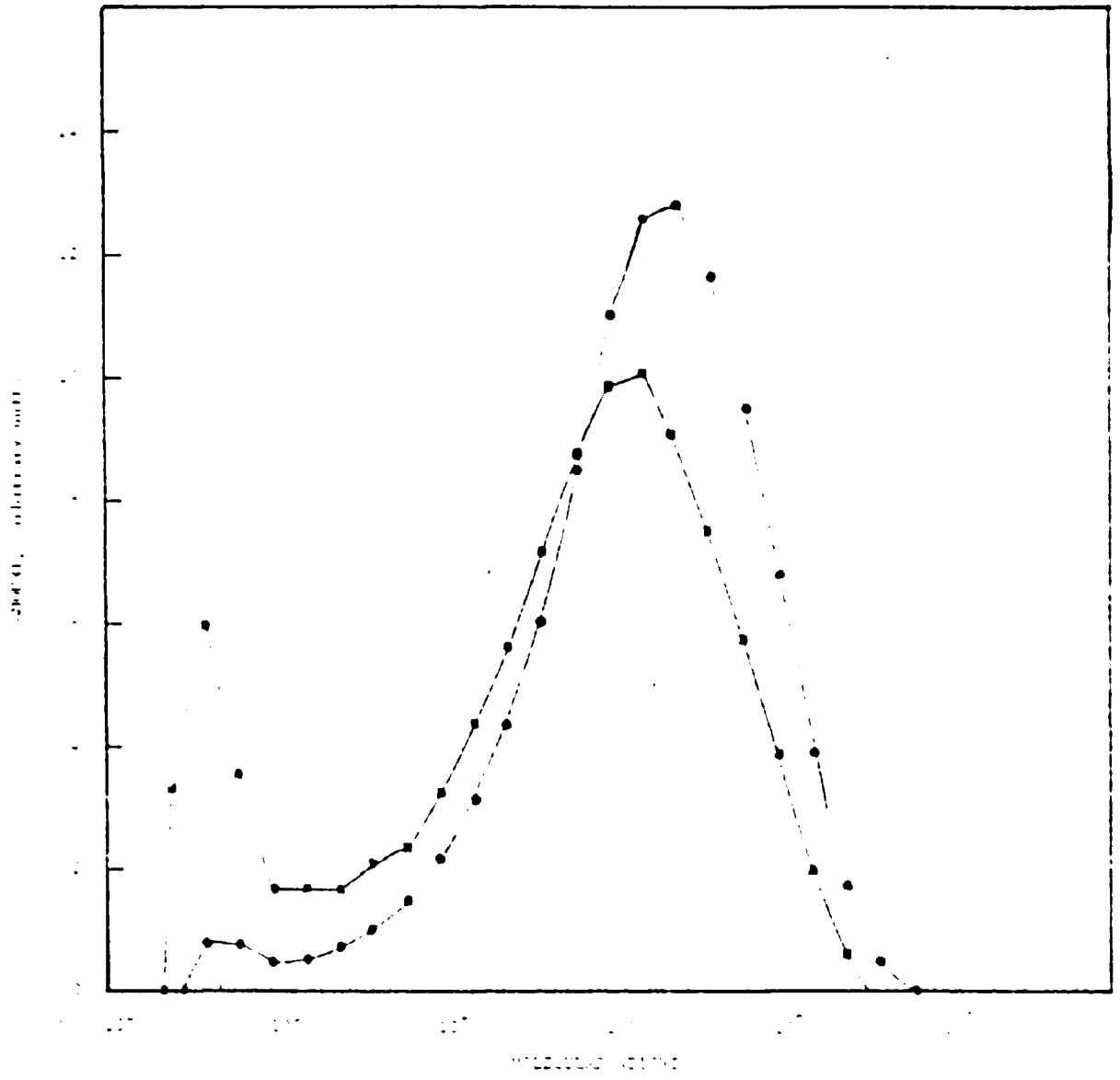

Figure III-A.2 Normalized chromatogram of SA-29 before (●) and after (■) ion exchange.

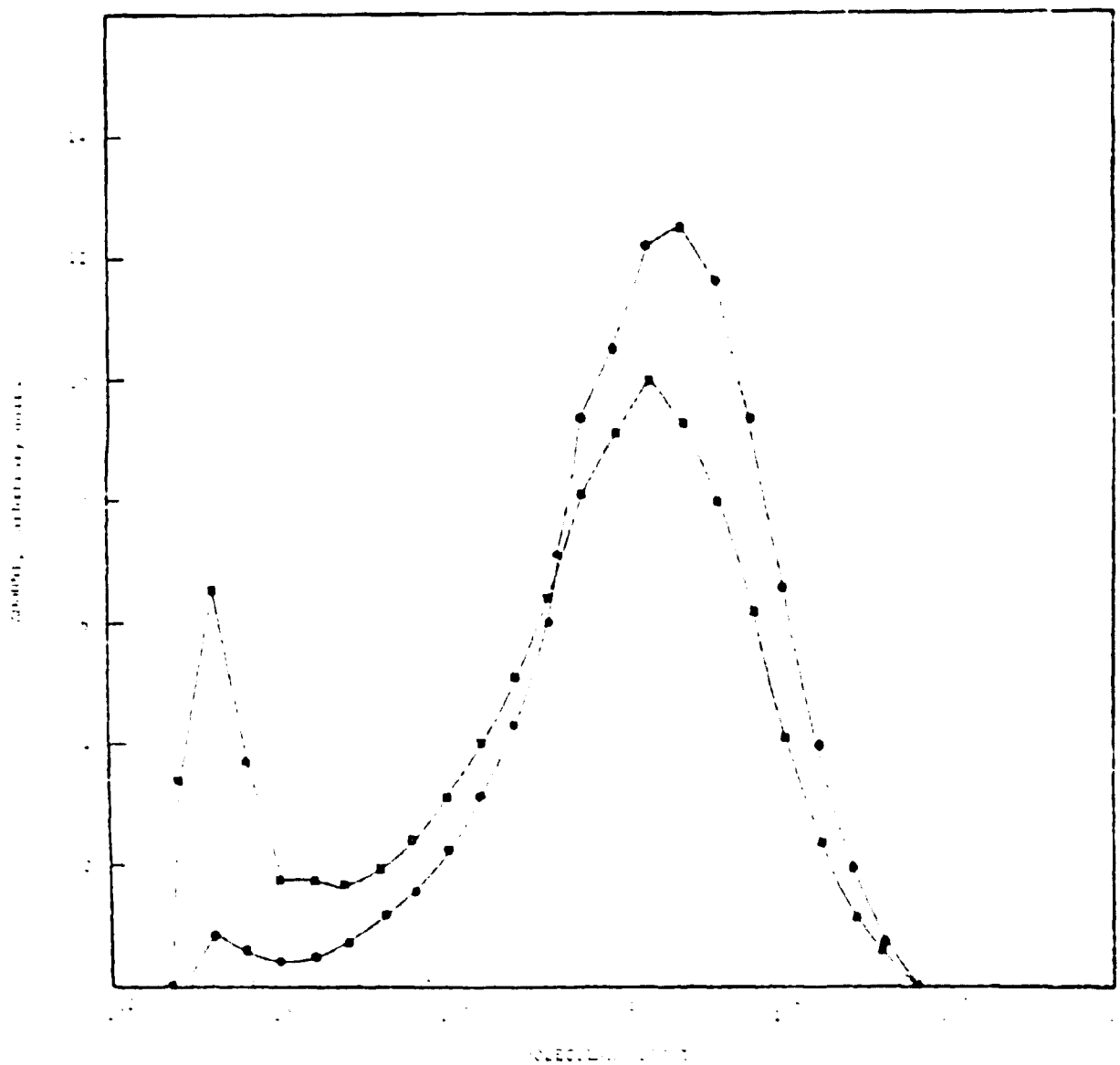

Figure III-A.3 Normalized chromatogram of SA-30 before (●) and after (■) ion exchange.

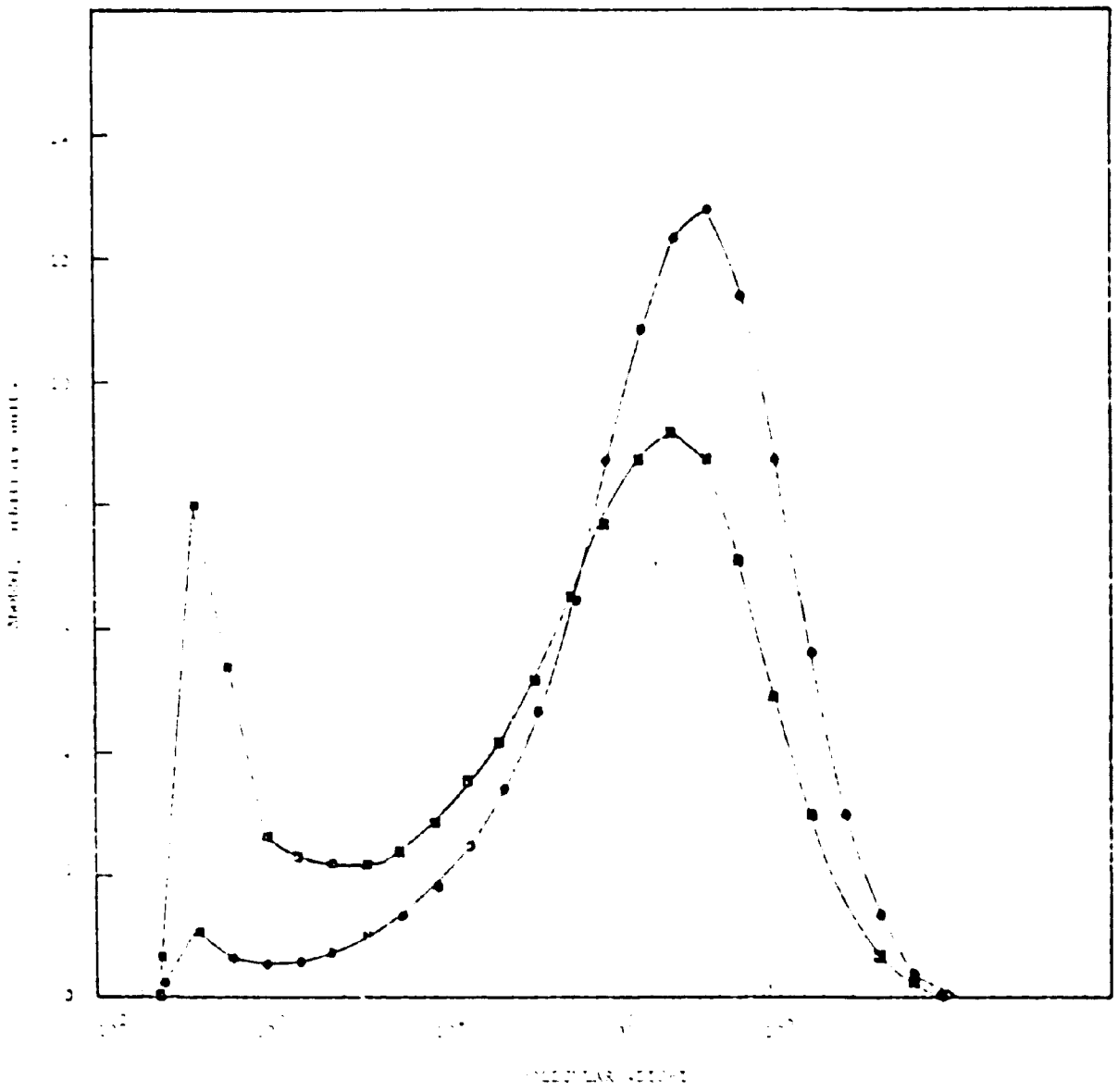

Figure III-A.4 Normalized chromatogram of SA-31 before (●) and after (■) ion exchange.

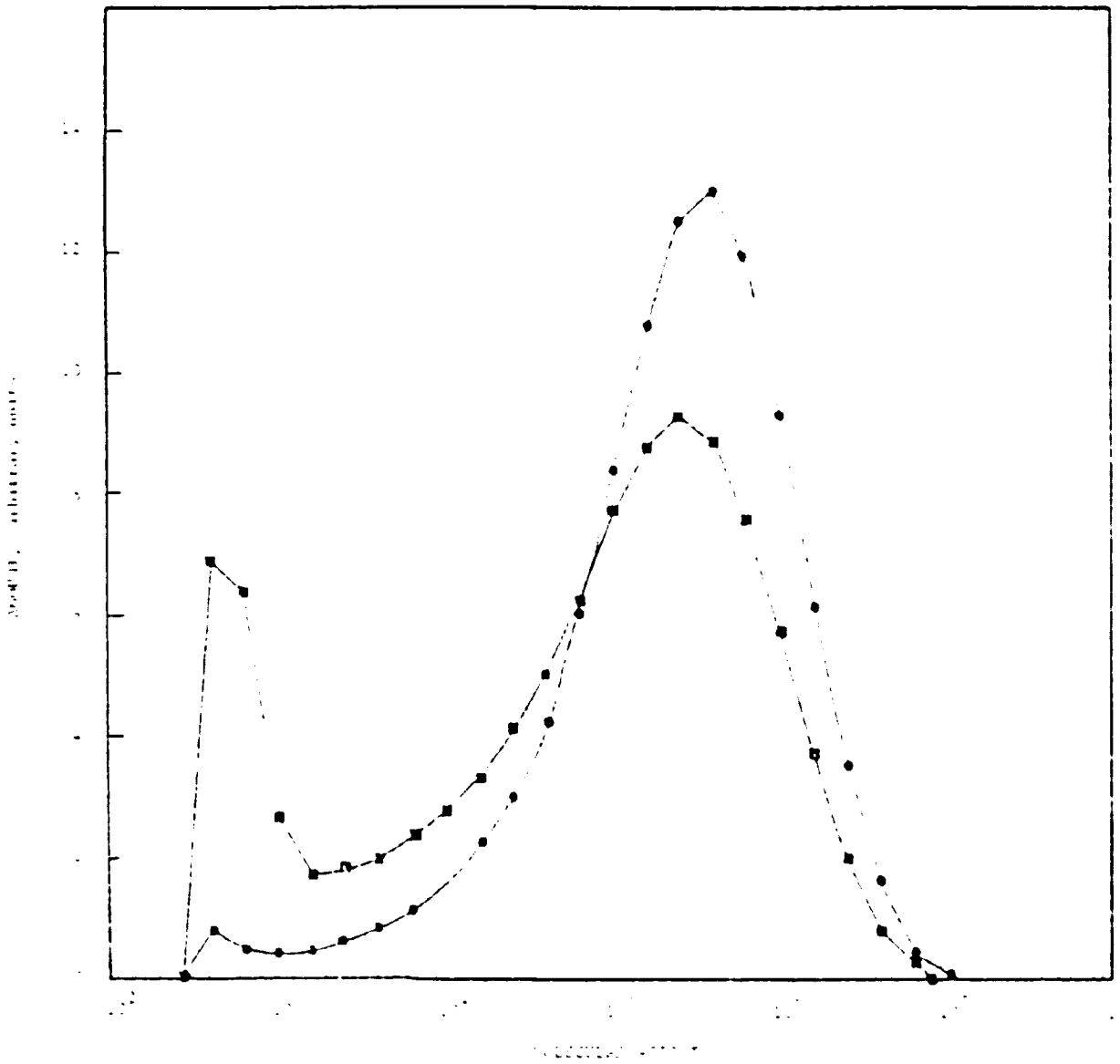

Figure III-A.5 Normalized chromatogram of SA-32 before (●) and after (■) ion exchange.

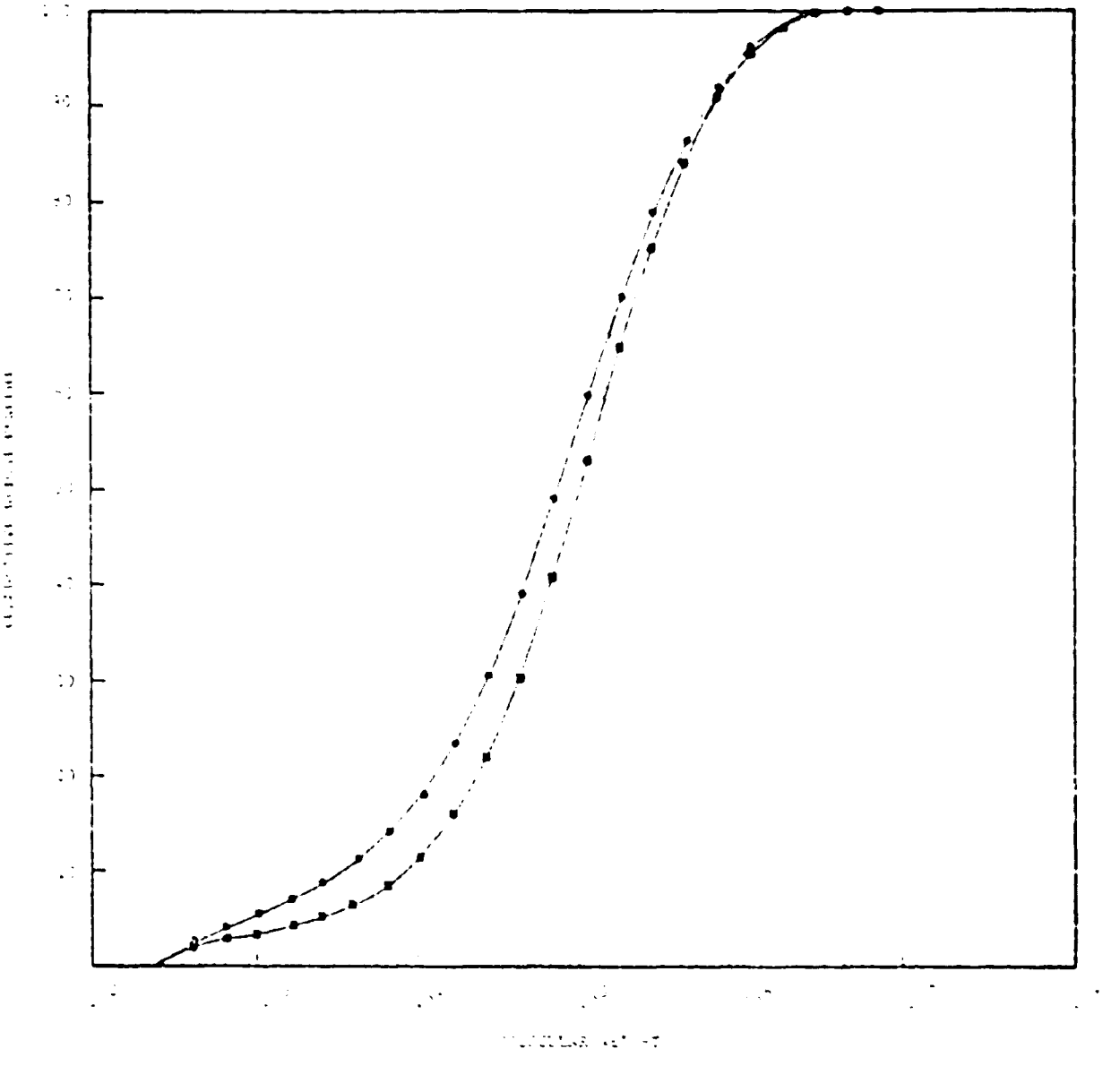

Figure III-A.6 Cumulative molecular weight distribution of SA-10 before (●) and after (■) ion exchange.

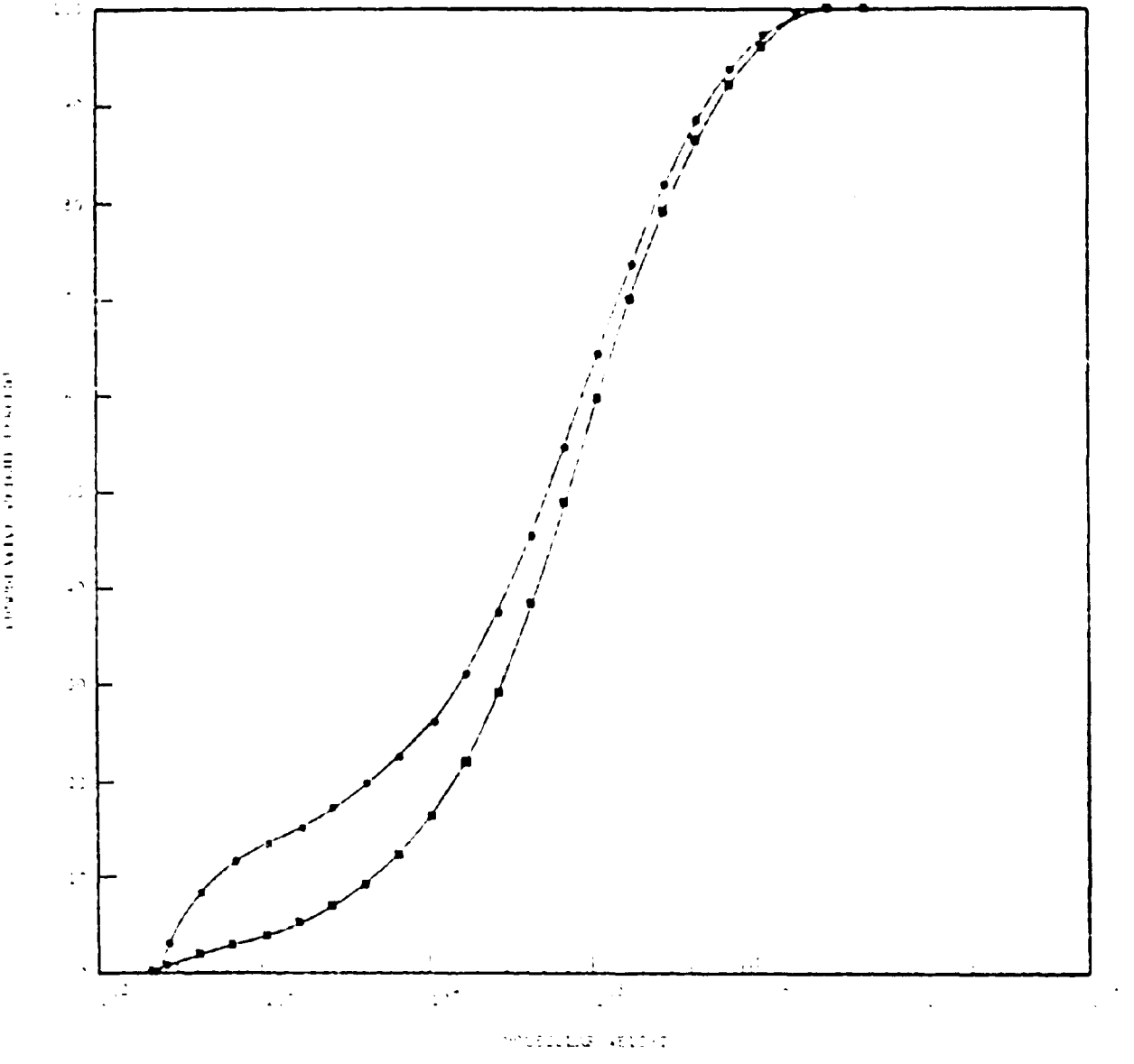

Figure III-A.7 Cumulative molecular weight distribution of SA-23 before (●) and after (■) ion exchange.

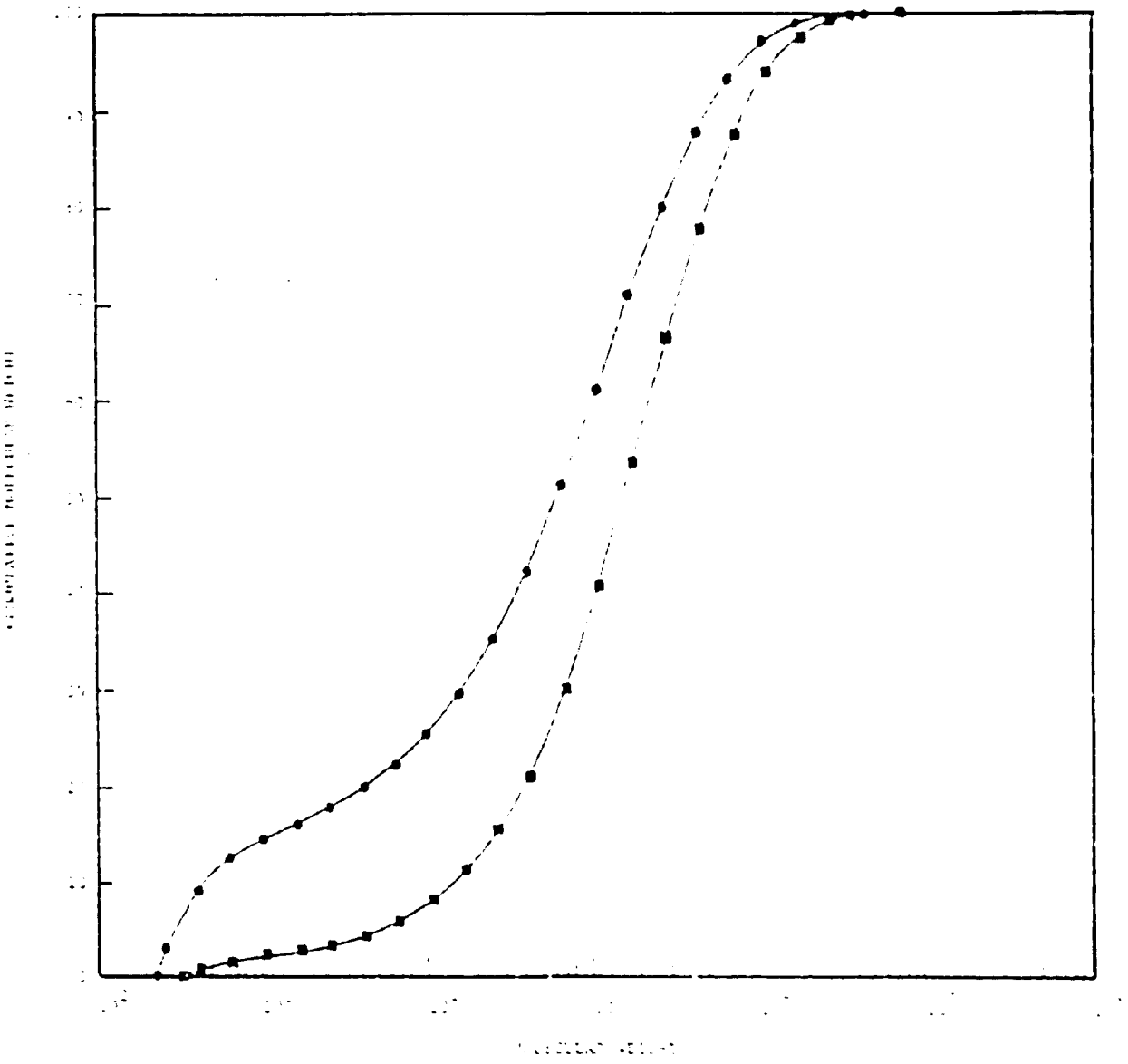

Figure III-A.8 Cumulative molecular weight distribution of SA-29 before (●) and after (■) ion exchange.

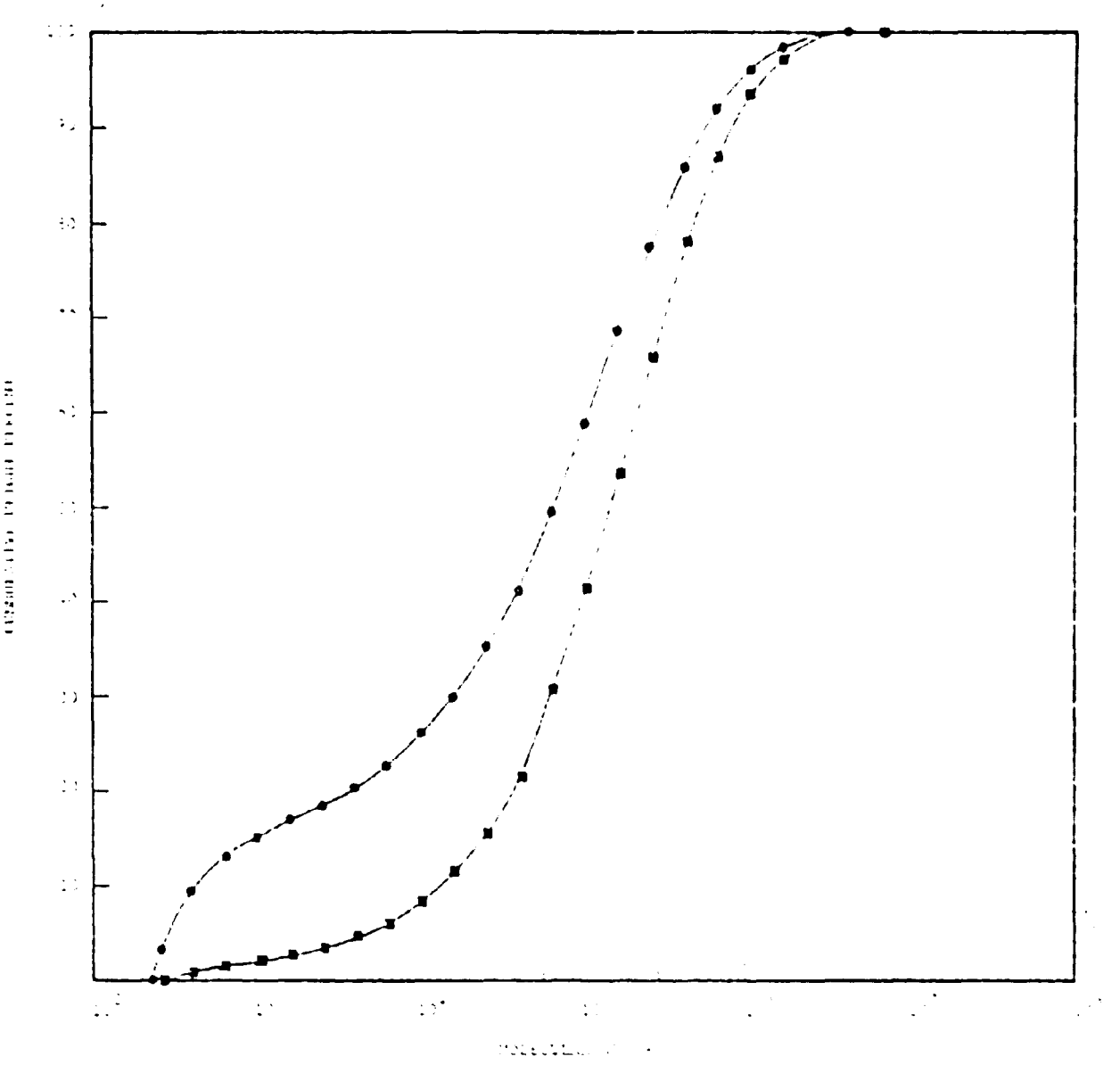

Figure III-A.9 Cumulative molecular weight distribution of SA-30 before (●) and after (■) ion exchange.

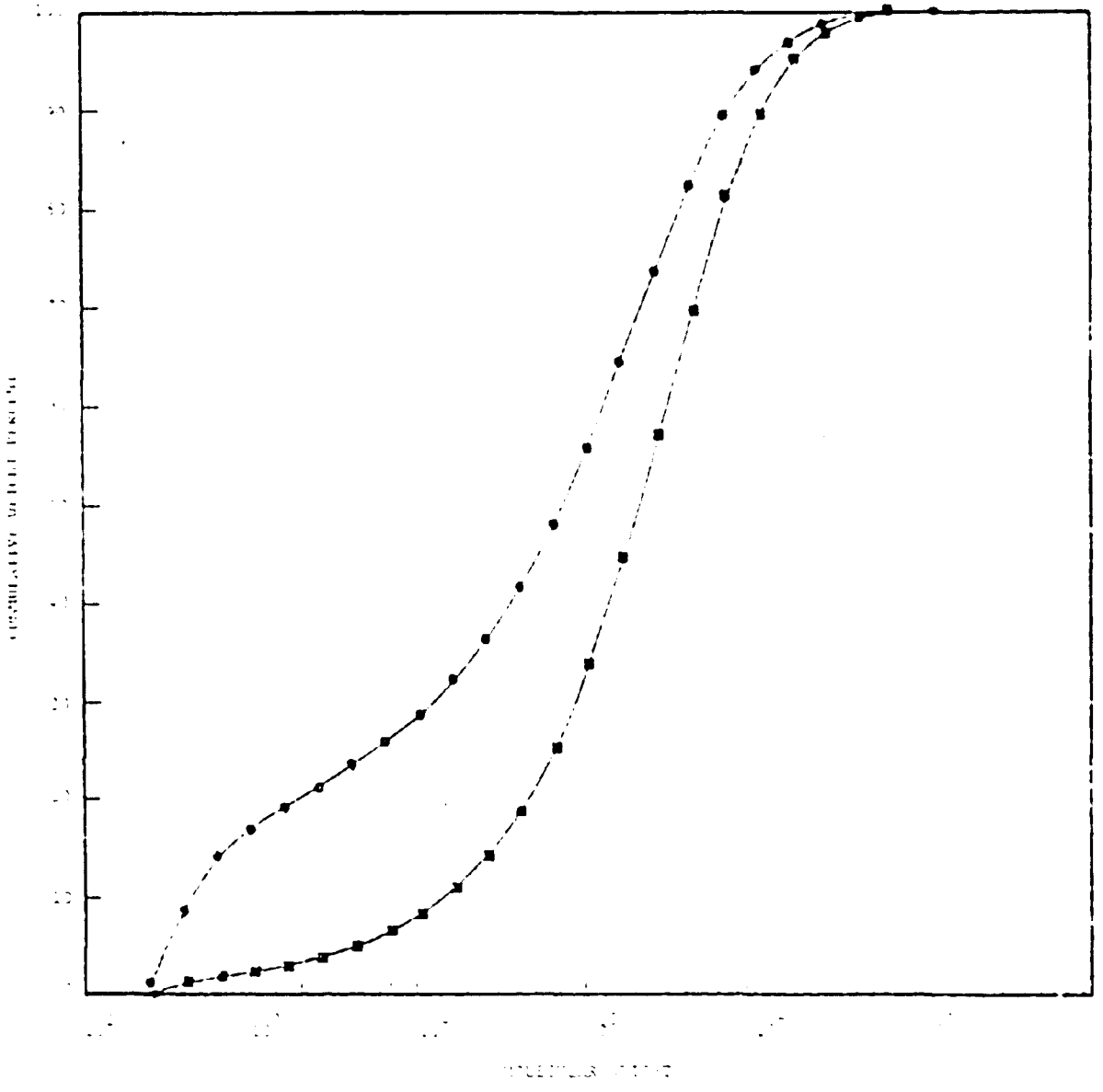

Figure III-A.10 Cumulative molecular weight distribution of SA-31 before (●) and after (■) ion exchange.

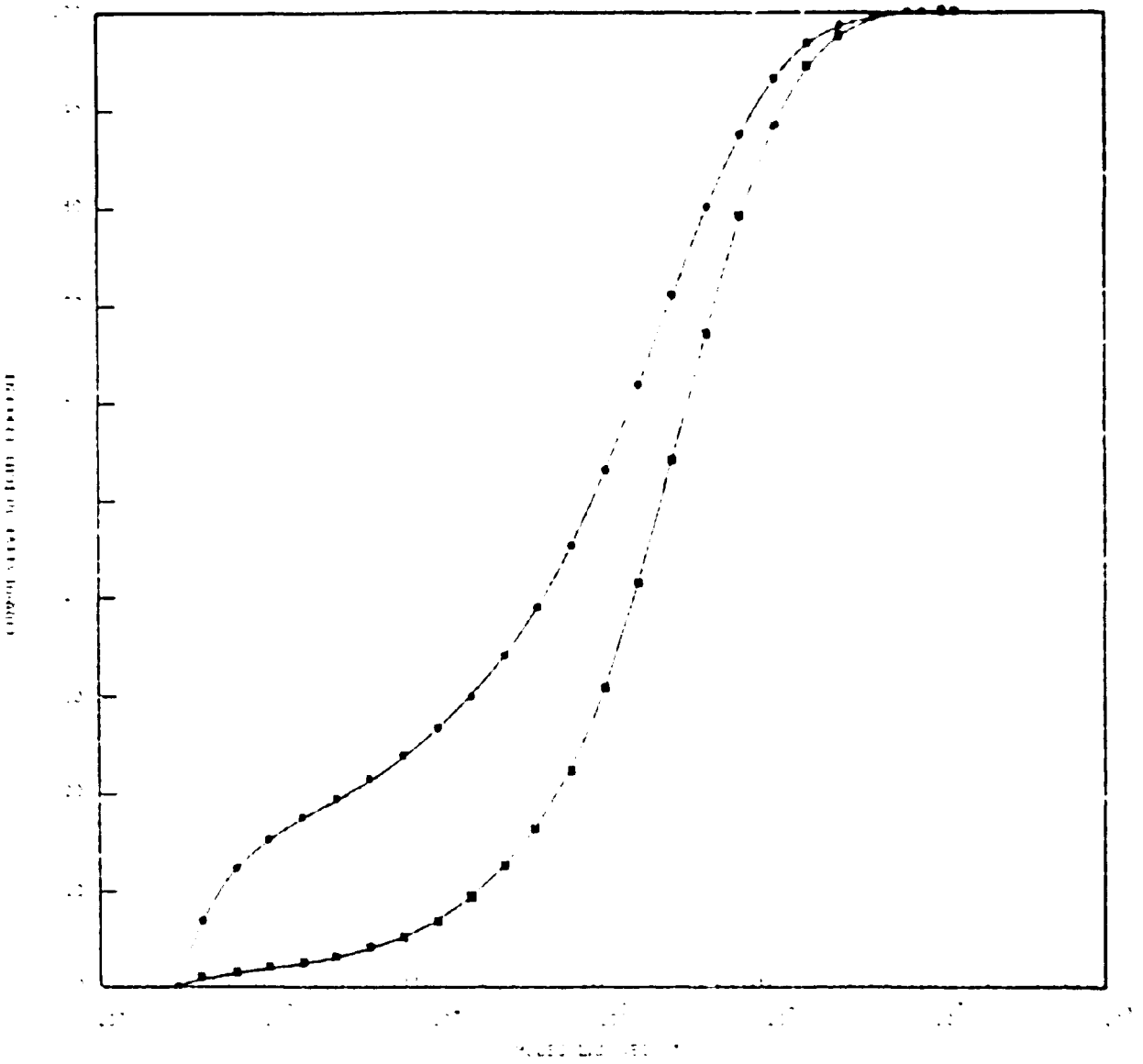

Figure III-A.11 Cumulative molecular weight distribution of SA-32 before (●) and after (■) ion exchange.

VITA

Richard Lewis Schild was born June 29, 1955 in Englewood, New Jersey. He is the oldest of three children born to Paul and Mae Schild. The author received his secondary education at Huntington High School in Huntington, Long Island. In 1977 he graduated with honors from Lehigh University with a B.S. in Chemical Engineering. Immediately afterwards he entered the graduate school under a University Fellowship and earned his Master of Science degree in Chemical Engineering in October 1978 from Lehigh. He is a member of the AIChE and participated in many activities at Lehigh including the Lehigh Outing Club and Lehigh Cycling Team.